Hydrogen production by steam reforming of bioethanol and
fusel oil over Ni/ZSM-5 nanosheet and Ni/SiC

Miss Porapak Suriya

จุฬาลงกรณ์มหาวิทยาลัย
CHULALONGKORN UNIVERSITY

A Dissertation Submitted in Partial Fulfillment of the Requirements
for the Degree of Doctor of Philosophy in Petrochemistry and Polymer
Science
Field of Study of Petrochemistry and Polymer Science
FACULTY OF SCIENCE
Chulalongkorn University
Academic Year 2022
Copyright of Chulalongkorn University

การผลิตไฮโดรเจนจากปฏิกิริยารีฟอร์มิงด้วยไอน้ำของไบโอเอทานอลและฟูเซลล์ออยล์บนตัวเร่ง
ปฏิกิริยานิกเกิล/ซีโอไลต์นาโนชีทและนิกเกิล/ซิลิกอนคาร์ไบด์

น.ส.ภรภัค สุริยะ

วิทยานิพนธ์นี้เป็นส่วนหนึ่งของการศึกษาตามหลักสูตรปริญญาวิทยาศาสตรดุษฎีบัณฑิต
สาขาวิชาปิโตรเคมีและวิทยาศาสตร์พอลิเมอร์ สาขาวิชาปิโตรเคมีและวิทยาศาสตร์พอลิเมอร์
คณะวิทยาศาสตร์ จุฬาลงกรณ์มหาวิทยาลัย
ปีการศึกษา 2565

Thesis Title   Hydrogen production by steam reforming of bioethanol and fusel oil over Ni/ZSM-5 nanosheet and Ni/SiC

By   Miss Porapak Suriya

Field of Study   Petrochemistry and Polymer Science

Thesis Advisor   Associate Professor PRASERT REUBROYCHAROEN

Thesis Co Advisor   Assistant Professor THANAKORN WASANAPIARNPONG

        Accepted by the FACULTY OF SCIENCE, Chulalongkorn University in Partial Fulfillment of the Requirement for the Doctor of Philosophy

                .... Dean of the FACULTY OF SCIENCE

        (Professor POLKIT SANGVANICH)

DISSERTATION COMMITTEE

                .... Chairman

        (Associate Professor Chanatip Samart)

                .... Thesis Advisor

        (Associate Professor PRASERT REUBROYCHAROEN)

                .... Thesis Co-Advisor

        (Assistant Professor THANAKORN WASANAPIARNPONG)

                .... Examiner

        (Professor NAPIDA HINCHIRANAN)

                .... Examiner

        (Assistant Professor DUANGAMOL TUNGASMITA)

                .... Examiner

        (Professor THARAPONG VITIDSANT)

ภรภัค สุริยะ : การผลิตไฮโดรเจนจากปฏิกิริยารีฟอร์มิงด้วยไอน้ำของไบโอเอทานอลและฟูเซลล์ออยล์บนตัวเร่งปฏิกิริยานิกเกิล/ซีโอไลต์นาโนชีทและนิกเกิล/ซิลิกอนคาร์ไบด์. (Hydrogen production by steam reforming of bioethanol and fusel oil over Ni/ZSM-5 nanosheet and Ni/SiC) อ.ที่ปรึกษาหลัก : รศ. ดร.ประเสริฐ เรียบร้อยเจริญ, อ.ที่ปรึกษาร่วม : ผศ. ดร.ธนากร วาสนาเพียรพงศ์

    งานวิจัยนี้ศึกษาการผลิตไฮโดรเจนจากปฏิกิริยารีฟอร์มิงด้วยไอน้ำของแอลกอฮอล์ชีวภาพบนตัวเร่งปฏิกิริยานิกเกิล งานวิจัยนี้ถูกแบ่งออกเป็นสองส่วน โดยในส่วนแรกของงานวิจัยเป็นเรื่องของตัวเร่งปฏิกิริยานิกเกิลบนตัวรองรับซิลิกอนคาร์ไบด์ซึ่งถูกเตรียมเพื่อใช้ในปฏิกิริยารีฟอร์มิงด้วยไอน้ำของฟูเซลล์ออยล์ในการผลิตไฮโดรเจน ตัวรองรับซิลิกอนคาร์ไบด์ถูกสังเคราะห์จากปฏิกิริยาไพโรไลซิสของข้าวเปลือกภายใต้อุณหภูมิสูงถึง 1500 องศาเซลเซียส ซิลิกอนคาร์ไบด์ที่เกิดขึ้นเป็นแบบเบตาเฟส ซึ่งมีพื้นที่ผิวสูงและช่วยลดปริมาณการเกิดคาร์บอนในระหว่างเร่งปฏิกิริยาเมื่อเทียบกับตัวรองรับซิลิกอนคาร์ไบด์ถูกสังเคราะห์จากปฏิกิริยาไพโรไลซิสของข้าวเปลือกภายใต้อุณหภูมิอื่นๆ เนื่องจากซิลิกอนคาร์ไบด์แบบเบตาเฟสมีสมบัติในการนำความร้อนได้ดีและยังทนความร้อนได้สูง ในส่วนของการศึกษาด้านประสิทธิภาพในการเร่งปฏิกิริยาพบว่าตัวเร่งนิกเกิลบนตัวรองรับซิลิกอนคาร์ไบด์ซึ่งถูกไพโรไลซิสที่อุณหภูมิ 1500 องศาเซลเซียส มีความสามารถในการเปลี่ยนแปลงฟูเซลล์ออยล์ร้อยละ 90 และสามารถผลิตไฮโดรเจนได้ร้อยละ 29% ขณะเร่งปฏิกิริยารีฟอร์มิงด้วยไอน้ำของฟูเซลล์ออยล์ที่อุณหภูมิ 700 องศาเซลเซียส เป็นเวลา 300 นาที อย่างไรก็ตาม มีข้อจำกัดบางประการสำหรับปฏิกิริยารีฟอร์มิงด้วยไอน้ำของฟูเซลล์ออยล์ เนื่องจากฟูเซลล์ออยล์เป็นแอลกอฮอล์ชนิดผสมทำให้เกิดความซับซ้อนของปฏิกิริยาเคมีเมื่อนำไปทำปฏิกิริยารีฟอร์มิงด้วยไอน้ำ ดังนั้นเพื่อปรับปรุงประสิทธิภาพของปฏิกิริยารีฟอร์มิงด้วยไอน้ำเพื่อผลิตไฮโดรเจน ในงานวิจัยนี้สนใจที่จะพัฒนาตัวเร่งปฏิกิริยานิกเกิล ซึ่งซีโอไลต์นาโนชีทชนิด ZSM-5 ถูกพิจารณาในการใช้เป็นตัวรองรับสำหรับตัวเร่งปฏิกิริยานิกเกิล เนื่องจากมีสมบัติของความเป็นรูพรุนทำให้พื้นที่ผิวสูงและทนความร้อนได้ดี โดยตัวเร่งปฏิกิริยานิกเกิลบนตัวรองรับซีโอไลต์นาโนชีทชนิด ZSM-5 ถูกนำไปใช้สำหรับปฏิกิริยารีฟอร์มิงด้วยไอน้ำของไบโอเอทานอลแทนฟูเซลล์ออยล์ เนื่องจากกลไกการเกิดปฏิกิริยารีฟอร์มิงด้วยไอน้ำของไบโอเอทานอลถูกศึกษาและวิจัยอย่างกว้างขวาง ทำให้เกิดการศึกษา เข้าใจข้อมูลเชิงลึก และสามารถใช้ข้อมูลที่ได้พัฒนาประสิทธิภาพของตัวเร่งปฏิกิริยาต่อไปได้ ดังนั้นในส่วนถัดมาของงานวิจัยนั้นจึงเกี่ยวข้องกับตัวเร่งปฏิกิริยานิกเกิลบนตัวรองรับซีโอไลต์นาโนชีทชนิด ZSM-5 ที่ถูกสังเคราะห์พร้อมกันด้วยวิธี in-situ ภายใต้อุณหภูมิและความดัน นอกจากนี้ยังมีการใช้เอทิลีนไดเอมีนซึ่งเป็นสารลดแรงตึงผิวช่วยทำให้นิกเกิลมีเสถียรภาพขณะถูกสังเคราะห์ไปพร้อมกับตัวรองรับ จากผลการทดลองพบว่าตัวเร่งปฏิกิริยานิกเกิลบนตัวรองรับซีโอไลต์นาโนชีทชนิด ZSM-5 มีความสามารถในการผลิตไฮโดรเจนร้อยละ 65 และมีการเปลี่ยนแปลงเอทานอลที่ร้อยละ 88 และหลังจากผ่านการเร่งปฏิกิริยารีฟอร์มิงด้วยไอน้ำของไบโอเอทานอลที่อุณหภูมิ 550 °C นานเป็นเวลา 48 ชั่วโมง พบว่ามีคาร์บอนเกิดขึ้นเพียงร้อยละ 17 ซึ่งมีประสิทธิภาพในการเร่งปฏิกิริยาสูงกว่าเมื่อเทียบกับตัวเร่งปฏิกิริยานิกเกิลบนตัวรองรับซีโอไลต์นาโนชีทชนิด ZSM-5 แบบชุบเปียก เพราะซีโอไลต์นาโนชีทชนิด ZSM-5 ซึ่งเป็นแบบสองมิติ มีสมบัติในการช่วยลดปริมาณคาร์บอนเนื่องจากระยะแพร่ในการเกิดปฏิกิริยาลดลงทำให้โมเลกุลมีโอกาสในการเกิดปฏิกิริยามากขึ้น นอกจากนี้วิธีการสังเคราะห์ตัวเร่งแบบ in-situ ส่งผลทำให้อนุภาคนิกเกิลมีขนาดเล็กและยังถูกห่อหุ้มอย่างดี ในระหว่างชั้นของแผ่นลามิเนตที่เชื่อมซ้อนกันของตัวรองรับซีโอไลต์นาโนชีทชนิด ZSM-5 ซึ่งช่วยป้องกันการรวมตัวกันของอนุภาคนิกเกิลและช่วยลดปริมาณคาร์บอนขณะเร่งปฏิกิริยาซึ่งเป็นสาเหตุที่ทำให้ตัวเร่งปฏิกิริยาเสียสภาพ

สาขาวิชา	ปิโตรเคมีและวิทยาศาสตร์พอลิเมอร์	ลายมือชื่อนิสิต ....
ปีการศึกษา	2565	ลายมือชื่อ อ.ที่ปรึกษาหลัก ....
		ลายมือชื่อ อ.ที่ปรึกษาร่วม ....

6271026023 : MAJOR PETROCHEMISTRY AND POLYMER SCIENCE

KEYWOR
D:
hydrogen production, ZSM-5 nanosheet, in-situ catalyst, bio-alcohol steam reforming, Pyrolysis of rice husk

Porapak Suriya : Hydrogen production by steam reforming of bioethanol and fusel oil over Ni/ZSM-5 nanosheet and Ni/SiC. Advisor: Assoc. Prof. PRASERT REUBROYCHAROEN Co-advisor: Asst. Prof. THANAKORN WASANAPIARNPONG

In this research, hydrogen production is performed by steam reforming of bio-alcohol over Ni-based catalysts. First section of the study, Ni/SiC catalyst was synthesized and used in steam reforming of fusel oil (FSR). The SiC support was prepared by pyrolysis of rice husk at 1500 °C to obtain β-SiC phase, which benefit to reduce the carbon formation due to its good thermal conductivity and durability. The Ni/SiC1500 indicated 90% of fusel oil gas conversion and 29% of hydrogen yield during a 300 min of steam reforming of fusel oil at 700 °C, hence presenting a good performance, and remaining stable in the steam reforming test. However, there were some restrictions in FSR catalytic performances. This is because fusel oil is a mixed alcohol, suggesting the complexity of reactions when applying to a steam reforming reaction. To improve the catalytic performances in terms of catalyst development, two-dimension ZSM-5 nanosheet was considered as a catalyst support for Ni catalysts due to its high surface area, porous structure properties, and thermal stability. Moreover, Ni/ZSM-5 nanosheet was applied to bioethanol steam reforming (ESR) instead of FSR because the reaction mechanism of ESR has been widely considered in the previous literature for many years and it provides insights into the catalyst development. Hence, the second part of the research investigates on ESR over Ni/ZSM-5 nanosheet. Ni/ZSM-5 nanosheet (in-situ) catalyst was successfully synthesized by hydrothermal process, using ethylenediamine as surfactant directing agent for nickel stabilizing precursor. The catalyst presented 65% of H_2 yield, 88% of ethanol conversion and only 17wt% of coke deposition under steam reforming of bioethanol at 550 °C, compared to impregnated catalyst. This was because two-dimension ZSM-5 nanosheet benefits to reduce the carbon formation due to the decrease in surface diffusion barriers. Moreover, *in-situ* method presented well encapsulated small size of nickel particles in the interconnected lamellar layers of ZSM-5 nanosheet to prevent nickel sinter and coke, hence giving an excellent catalytic performance, and maintaining a 48 h of longevity during the steam reforming of bioethanol.

Field of Study:	Petrochemistry and Polymer Science	Student's Signature
		....
Academic Year:	2022	Advisor's Signature
		....
		Co-advisor's Signature
		....

ACKNOWLEDGEMENTS

TABLE OF CONTENTS

Page

จุฬาลงกรณ์มหาวิทยาลัย

CHULALONGKORN UNIVERSITY

LIST OF FIGURES

LIST OF TABLES

จุฬาลงกรณ์มหาวิทยาลัย

CHULALONGKORN UNIVERSITY

CHAPTER 1
INTRODUCTION

Hydrogen (H_2) energy has been recognized as an alternative energy source. It is a direct source of clean energy and has applications in food industries, petrochemical refineries, cutting/welding, metallurgy, etc. Hydrogen is commercially produced by the electrolysis of water, reforming of natural gas, and gasification of coal. Almost 50% of hydrogen production is from natural gas or light oil fraction by steam reforming. However, the use of petroleum-based feedstock causes the effects of unsustainable and undesirable greenhouse gases, whereas hydrogen produces a clean form of energy with water as a by-product. Thus, hydrogen can be a clean energy carrier if the technologies associated with it are clean. To reduce the pollution gases [1-3], the alternative pathway for producing hydrogen is steam reforming of alcohol.

Bioethanol and fusel oil are attended to use as resources for hydrogen production via steam reforming in this work. Bioethanol is an interesting renewable alcohol source for hydrogen production since it is a clean reagent derived from biomass, which is widely around the world at a relatively low cost. Nowadays, bioethanol is mainly produced from the fermentation process of biomaterials, for example, corn grains, sugar cane, wheat straw, and other starch-rich materials [4, 5]. The steam reforming of bioethanol (ESR) process is one of the low-cost methods for hydrogen production. Industrial ethanol production causes a large number of by-products, called fusel oil. Fusel oil is a mixture of C_2-C_5 alcohols, and it has been considered a low-value reagent to produce solvents, extractants, energy resources, and medicinal products. However, it can also be used as a cheap and renewable source to produce hydrogen via steam reforming of fusel oil (FSR).

The metal active site on catalysts, used in steam reforming reactions, are divided into two groups: noble metal catalysts (e.g., Rh, Ru, Pt, and Pd) [6-8] and non-noble metal catalysts (e.g., Ni, Cu, and Co) [9-11]. Although noble-metal catalysts present good catalytic performances in steam reforming reactions, their usage in the catalytic reaction is undesirable because of their high cost. Therefore, the non-noble metal catalytic system is most interesting in steam reforming reactions since their cost is cheaper than those noble metal catalysts.

Nickel-based catalyst is particularly attractive non-metal catalysts, which have been widely used in steam reforming reaction because of their ability in breaking C−C, C−H, and C−O bond and their lower cost if compared with noble metals [12]. Nickel catalysts are basically prepared by the impregnation method on porous supports. Although they exhibit good catalytic performances towards high hydrogen selectivity in steam reforming reactions, the nickel metals over the external surface on porous supports would be agglomerated during catalysis. This leads to catalyst deactivation and carbon formation, bringing a decrease in catalytic performances.

To improve the catalytic performance of steam reforming, the catalyst supports play an important role in reducing nickel sinter and coke. In this work, silicon carbide (SiC) and ZSM-5 nanosheet are used for preparing nickel catalyst supports.

Silicon carbide (SiC) supports in this work were prepared from rice husk. Rice husk is an abundant biomass material, approximately composed of 40-50% of cellulose, 25-30% of hemicellulose, 18-20% of lignin, 10-14% of mineral ash, and 8-10% of water [13]. However, rice husk ash consists of 80-90% of silica (SiO_2) [14]. The components in rice husk, such as cellulose and silica, can be formed SiC by pyrolysis at 1300-1500 °C under inert gas purging [15]. For the pyrolyzed rice husk over 1700 °C, the obtained product is the α-SiC phase and more stable than that of $β$-SiC. However, the $β$-SiC is more attractive in this research because it is more active with the metal active sites and their surface area is also higher, compared to α-SiC. The $β$-SiC presents good thermal conductivity and high endurance properties, decreasing the hot spots on the catalyst surface during the reaction at high temperatures [16]. These properties reduce the amount of coke, blocking the active sites of catalysts and enhancing catalytic performances. Therefore, $β$-SiC from rice husk is appropriately used for catalyst supports [17-20].

ZSM-5 is a hierarchical porous material, known as an aluminosilicate zeolite. It has been widely used for the isomerization, alkylation, and aromatization of hydrocarbons in the petrochemical industry [21-23]. However, ZSM-5 composes of regularly stacked lamellas with a thickness of one unit, and it causes slow molecular transport in microporous systems due to the three-dimension structure. Therefore, two-dimension ZSM-5 or ZSM-5 nanosheet (Z-NS) has gained more extensive

attention, due to its excellent properties as high accessibility of active centres on the surface with reduced diffusion resistance and the improvement of molecular transport [24, 25]. These abilities could be beneficial to the catalytic performance of nickel catalysts.
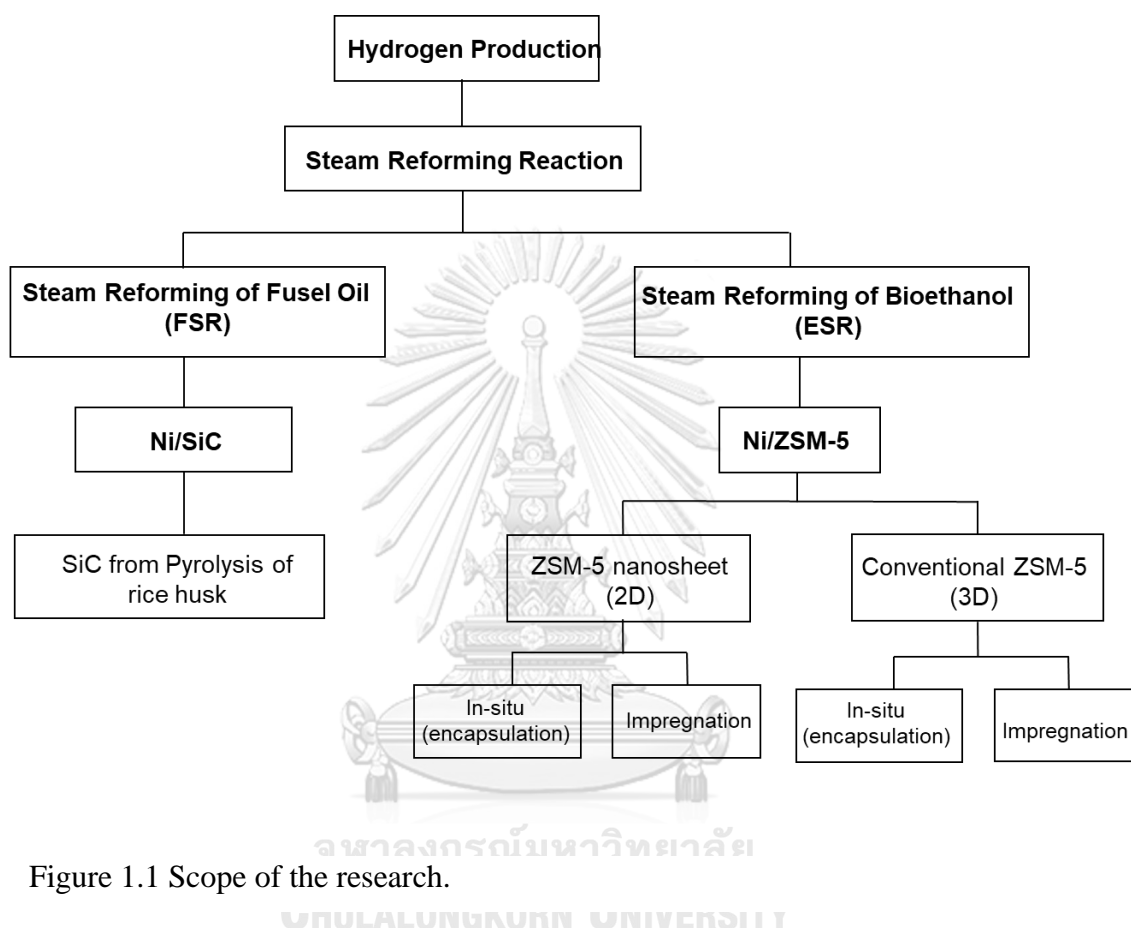
Figure 1.1 Scope of the research.

In this work, FSR over Ni/SiC catalyst were firstly investigated, however, there were some restrictions in catalytic performances. This is because fusel oil is a mixed alcohol, suggesting the complexity of reactions when applying to a steam reforming reaction. To improve the catalytic performances in terms of catalyst development, two-dimension ZSM-5 nanosheet was considered as a catalyst support for Ni catalysts due to its high surface area, porous structure properties, and thermal stability. Moreover, Ni/ZSM-5 nanosheet was applied to ESR instead of FSR because the reaction mechanism of ESR has been widely considered in the previous literature for many years and it provides insights into the further catalyst development.

This research is then divided to two main parts regarding hydrogen production via steam reforming as shown in Figure 1.1. The first part is hydrogen production by FSR over Ni/SiC. The SiC support was prepared by pyrolysis of rice husk. The influence of temperatures (1300, 1500, and 1700°C) on the morphology and crystalline phase of SiC was discussed. The properties of the prepared supports and catalysts were characterized by XRD, BET, H_2-TPR, SEM-EDX, FESEM, and TGA techniques. The catalytic performance of the Ni on pyrolyzed rice husk support on FSR was studied at 700°C and compared with Ni on commercial SiC (Ni/SiC-com).

The second part is ESR over Ni/ZSM-5 nanosheet catalysts. This part aims to investigate hydrogen production and improve catalytic performance via ESR over Ni on different ZSM-5 supports between ZSM-5 nanosheet (Z-NS) and conventional ZSM-5 (Z-CON) with a similar Si/Al ratio of 100. The catalysts were fabricated by two different methods, employed for catalyst synthesis, that is, *in-situ* (IN) and wet impregnation method (IMP). The prepared Ni catalysts were defined as Ni/Z-NS-IN and Ni/Z-NS-IMP, Ni/Z-CON-IN, and Ni/Z-CON-IMP. The effects of different ZSM-5 support and the preparation methods on the catalytic performance of Ni/ZSM-5 catalysts were further investigated in detail.

1.1 Scope of this work

1.1.1 Hydrogen production by FSR over Ni/SiC

1. Synthesis of silicon carbide (SiC) from pyrolysis of rice husk at high temperatures.

2. Study on the influence of temperatures (1300 °C, 1500 °C, and 1700 °C) on the pyrolysis of rice husk to investigate the morphology and chemical properties

3. Preparation of nickel on SiC by wet impregnation method

4. Study on catalytic performances toward hydrogen yield and fusel oil conversion.

1.1.2   Hydrogen production by ESR over Ni/ZSM-5 nanosheet

1. Synthesis of two-dimension ZSM-5 nanosheet (Z-NS) and three-dimension conventional ZSM-5 (Z-CON) by the hydrothermal process with the same ratio of Si/Al.

2. Preparation of nickel catalyst by two different methods; *in-situ* and impregnation, applied to both Z-NS and Z-CON.

3. Characterization of ZSM-5 supports and the prepared nickel catalysts to investigate the different properties of the chemical surface, porosity, thermal decomposition, and morphology.

4. Study catalytic performances of nickel catalysts in steam reforming of bioethanol (ESR) in a fixed bed reactor toward hydrogen yield, ethanol conversion, and stability test.

1.2 Objectives

1.2.1   Hydrogen production by FSR over Ni/SiC

1. To utilize bio-waste materials, which are rice husk and fusel oil, as catalyst support and a resource for steam reforming reactions.

2. To study the influence of temperatures (1300 °C, 1500 °C, and 1700 °C) on the pyrolysis of rice husk to investigate the morphology and chemical properties.

3. To investigate hydrogen production and improve catalytic performance via FSR over a Ni/SiC catalyst

1.2.2   Hydrogen production by ESR over Ni/ZSM-5 nanosheet

1. To investigate hydrogen production and improve catalytic performance via ESR over Ni on different ZSM-5 supports between ZSM-5 nanosheet (Z-NS) and conventional ZSM-5 (Z-CON) with a similar Si/Al ratio of 100.

2. To study the insight properties of the catalyst, fabricated by two different methods, which are *in-situ* (IN) and wet impregnation method (IMP).

CHAPTER 2
THEORICAL BACKGROUND AND LITERATURES

2.1 Hydrogen gas

Hydrogen (H_2) energy has been recognized as an alternative energy source for the future. It becomes an attractive energy option for transportation and electrical applications. Hydrogen energy can be used in vehicles, in houses, for portable power, and in many more applications [26]. Hydrogen can be produced from a variety of resources, such as fossil resources (natural gas and light oil fraction) and renewable resources (biomaterial and water). However, H_2 production from petroleum-based feedstock causes the effects of unsustainable and undesirable greenhouse gases. To reduce the pollution gases, the alternative pathway for producing H_2 is steam reforming of bio-alcohol.

2.2 Steam reforming of fusel oil (FSR)

Fusel oil is a by-product obtained during bioethanol production. Fusel oil is composed of a mixture of C_2-C_5 alcohols, which are 66.7, 12.5, 4.26, 3.43, 0.7, and 12% by weight of isoamyl alcohol isobutanol, propanol, ethanol, butanol, and water, respectively [27]. It can be described as a clear yellow liquid with a strong smell as shown in Figure 2.1.

Figure 2.1 A photograph of fusel oil.

A thousand liter of ethanol production produces five liters of fusel oil as a by-product. In some countries where bioethanol is produced on a large scale, by-product utilization has become an important issue in making the global process less polluting

and more useful. Fusel oil has been considered a low-value material that is only burned to produce energy. However, it can be used as a cheap and renewable source to produce H_2 by steam reforming reaction [27].

$$C_{4.35}H_{10.71}O + 7.7H_2O \longrightarrow 13.05H_2 + 4.35CO_2 \qquad (2.1)$$

The steam reforming reaction (SRR) is an endothermic reaction. The overall reaction is shown in Eq. (2.1). The process consists of 3 steps: (i) synthesis of gas production, (ii) water gas shift, and (iii) gas purification, as shown in Eq. (2.2) -(2.4), respectively:

$$C_nH_m + nH_2O + heat \longrightarrow nCO + (n+m/2)H_2 \qquad (2.2)$$
$$CO + H_2O \longrightarrow CO_2 + H_2 \qquad (2.3)$$
$$CO + 3H_2 \longrightarrow CH_4 + H_2O + heat \qquad (2.4)$$

Among these intermediate products, carbon dioxide (CO_2) is converted to carbon monoxide (CO) via reverse water gas shift (WGS) reaction, Eq. (2.5), while methane (CH_4) produced H_2 through SRR, as indicated in Eq. (2.7) and (2.8). According to the composition of fusel oil as a biomass and mixed C_2-C_5 alcohol, SRR of fusel oil can produce carbon formation via Boudouard reaction and thermal deposition of methane as shown in Eq. (2.11) and (2.12), respectively. Due to the carbon deposition, the catalyst could be deactivated by decreasing active sites and H_2 yield.

Reverse WGS reaction	$H_2 + CO_2 \longrightarrow CO + H_2O$	(2.5)
WGS reaction	$CO + H_2O \longrightarrow CO_2 + H_2$	(2.6)
Methanation	$CO + 3H_2 \longrightarrow CH_4 + H_2O + heat$	(2.7)
	$CO_2 + 4H_2 \longrightarrow CH_4 + 2H_2O$	(2.8)
SRR of methane	$CH_4 + 2H_2O \longrightarrow CO + 3H_2$	(2.9)
	$CH_4 + 2H_2O \longrightarrow CO_2 + 4H_2$	(2.10)
Boudouard reaction	$2CO \longrightarrow C + CO_2$	(2.11)
Thermal deposition of methane	$CH_4 \longrightarrow C + 2H_2$	(2.12)
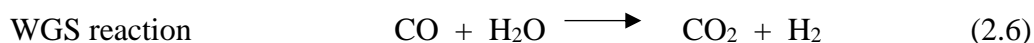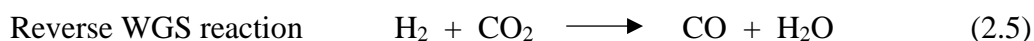
2.3 Steam reforming of bioethanol (ESR)

Bioethanol has been produced by about 60% from sugarcane and 40% from other crops. Figure 2.2 showed that the United States and Brazil remain the two largest producers of bioethanol, followed by the European Union and China. The world bioethanol production market is expected to grow further [28].
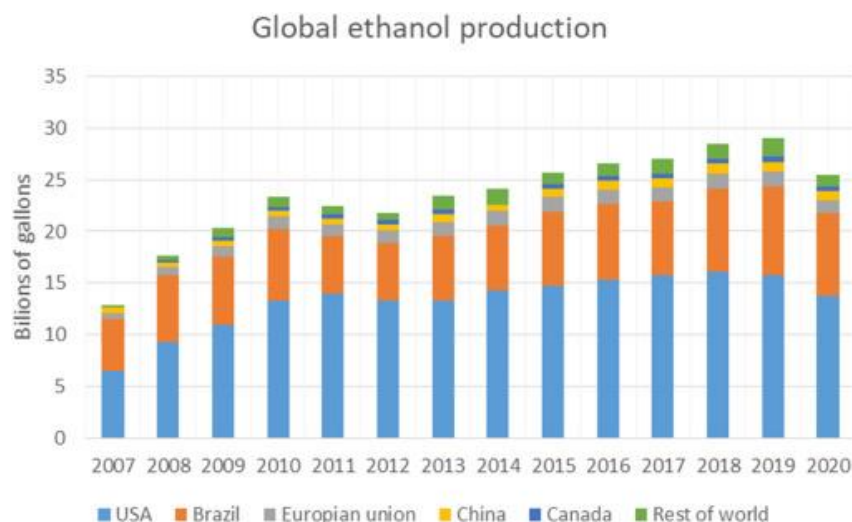
Figure 2.2 A schematic diagram of global ethanol production by countries between 2007 and 2020 [28]

According to the huge scale of bioethanol production, it has been considered one of the alternative resources to produce H_2 by steam reforming reaction. The steam reforming of ethanol (ESR) process is one of the low-cost methods for hydrogen production [29, 30].

Many studies have investigated the ESR using Ni, Co, and noble metal catalysts. An effective catalyst for hydrogen production from ESR must dissociate the C-C bond at low temperatures, including maintaining the CO concentration low, and remaining stable during catalysis. The overall ESR reaction for hydrogen production is given below in Eq. (2.13).

$$CH_3CH_2OH + 3H_2O \rightarrow 2CO_2 + 6H_2 \qquad (2.13)$$
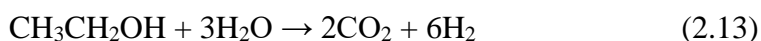
The ESR is an endothermic process. The possible reactions taking place in ESR could be summarized as shown in Eq. (2.14)-(2.26) [31].

Ethanol steam reforming

$$C_2H_5OH + 3H_2O \Leftrightarrow 2CO_2 + 6H_2 \qquad (2.14)$$

$$C_2H_5OH + H_2O \Leftrightarrow 2CO + 4H_2 \qquad (2.15)$$

Ethanol dehydrogenation

$$C_2H_5OH \Leftrightarrow CH_3CHO + H_2 \qquad (2.16)$$

Methane formation

$$2CO + 2H_2 \Leftrightarrow CH_4 + CO_2 \qquad (2.17)$$

$$CO + 3H_2 \Leftrightarrow CH_4 + H_2O \qquad (2.18)$$

$$CH_3CHO \Leftrightarrow CH_4 + CO \qquad (2.19)$$

Water gas shift

$$CO + H_2O \Leftrightarrow CO_2 + H_2 \qquad (2.20)$$

Oxidation

$$CH_3CH_2OH \Leftrightarrow CH_3COOH + 2H_2 \qquad (2.21)$$
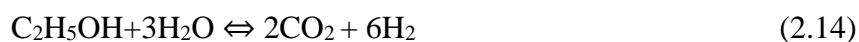
Acetic acid steam reforming

$$CH_3COOH + 2H_2O \Leftrightarrow 2CO_2 + 4H_2 \qquad (2.22)$$

Carbon formation

$$CH_4 \Leftrightarrow C + 2H_2 \qquad (2.23)$$

$$2CO \Leftrightarrow C + CO_2 \qquad (2.24)$$

$$H_2 + CO \Leftrightarrow C + H_2O \qquad (2.25)$$

$$CO_2 + 2H_2 \Leftrightarrow C + 2H_2O \qquad (2.26)$$

2.3.1 Proposed reaction scheme of ethanol steam reforming over metal catalysts

The reaction mechanism of ethanol steam reforming (ESR) has been widely considered in the previous literature for many years. The different reaction pathways for ESR are presented in Figure 2.3. Several pathways are considered in the ESR reaction: (i) dehydrogenation of ethanol, (ii) cleavage of the C-C bond of C_2 intermediates to produce CO and CH_4, and (iii) steam reforming of C_1 products to produce more hydrogen.

The ESR reaction can also proceed through two main pathways: (i) dehydration to produce ethylene (C_2H_4), (ii) dehydrogenation to produce acetaldehyde (CH_3CHO) as shown in Figure 2.4. Both C_2H_4 and CH_3CHO can interact further

with steam to generate CO_2 and methane (CH_4) and it could be dehydrogenated to perform carbon deposits. To effectively produce hydrogen, the undesired by-products such as CO, CH_4, C_2H_4, and carbon deposits must be reduced [32].
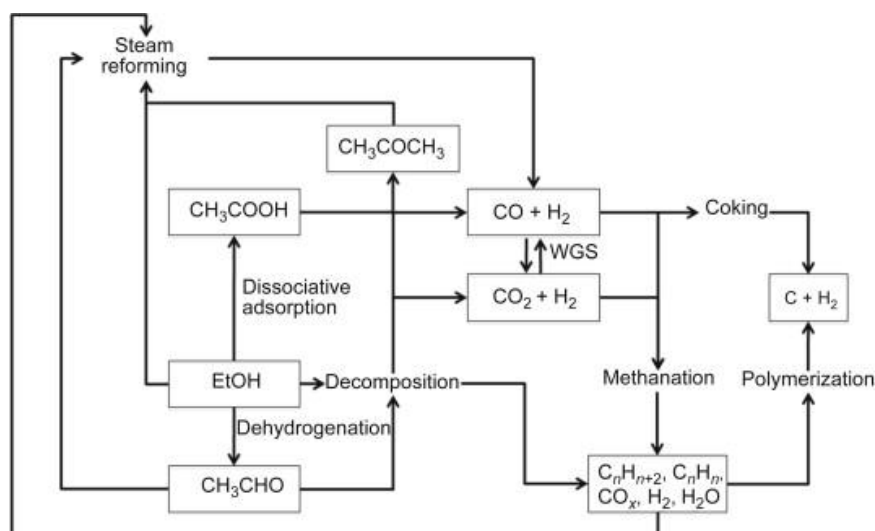
Figure 2.3 The possible reaction scheme of ethanol steam reforming over metal catalysts [32].
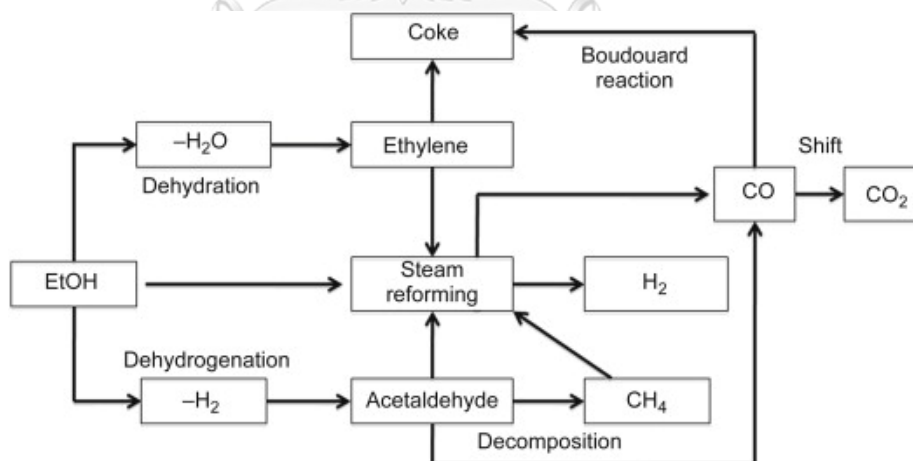
Figure 2.4 Pathways for the steam reforming of ethanol over bifunctional catalysts [32].

2.4 Ni-based catalysts

    2.4.1   The ability of Nickel catalyst in steam reforming reaction

        There are several catalysts, including transition metals (Ni, Co, Cu, and Fe) and noble metals (Pt, Pd, Ru, and Rh), have been used in steam reforming reactions as mentioned before. Ni-based catalyst is a particularly attractive transition/non-metal catalysts, which have been widely used in the ESR because of their ability in breaking C−C, C−H, and C−O bond. Moreover, Ni-based catalysts can be industrially produced at a low cost, compared to noble metals.

        Ni-based catalyst has been widely deposited onto alumina supports because of their capability of tolerating reactive circumstances. However, due to the alumina acid sites, hence this supports favors carbon deposition, leading to catalyst deactivation as shown in Figure 2.5 [33]. Furthermore, the nickel particles have a tendency to sinter during the ESR reaction. Additionally, acid sites on alumina favor the dehydrogenation of ethanol into ethylene rather than the dehydrogenation into acetaldehyde. Therefore, the sintering of nickel particles and alumina acidity simply cause carbon deposits, which deactivate the catalyst. There are several ways to prevent such circumstances such as adding a promoter, modifying catalyst morphology, and preparing catalysts by metal encapsulation.
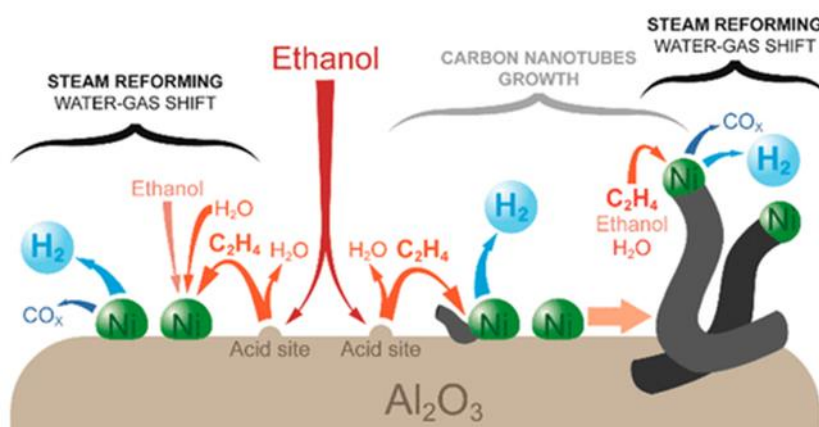
Figure 2.5 Schematic reaction of steam reforming over Ni on alumina support [34].

2.4.2 Carbon deposition

Many reactions are contributed to carbon formation in ESR, including (i) ethanol dehydration, producing ethylene, (ii) thermal decomposition of methane, (iii) Boudouard reaction, and (iv) methane and ethylene decomposition. These proposed reactions can further perform carbon deposition. The carbon deposition rate depends on the reaction conditions, including the catalyst. For example, the Boudouard reaction favors producing coking at low reaction temperatures, while the decomposition of hydrocarbon favors at high temperatures.

According to the previous research [35], there were three main types of carbon deposition produced from Ni-based catalysts during the steam reforming process: amorphous, filamentous, and encapsulating carbon as shown in Figure 2.6. The carbon that is the most damaging to the dispersion of Ni is the filament or whisker carbon. Because the carbon atoms are soluble in the metal lattice, hence this form of carbon is uniquely found in Ni and Co catalysts. The growth of filamentous carbon is believed to occur by the diffusion of adsorbed carbon atoms through large Ni crystallites. (>7 nm) and condense at the base, raising the Ni particle off the surface, resulting in the formation of the whisker. The amorphous carbon is found at low temperatures between 200-500 °C, whereas the carbon filament is formed at high temperatures.
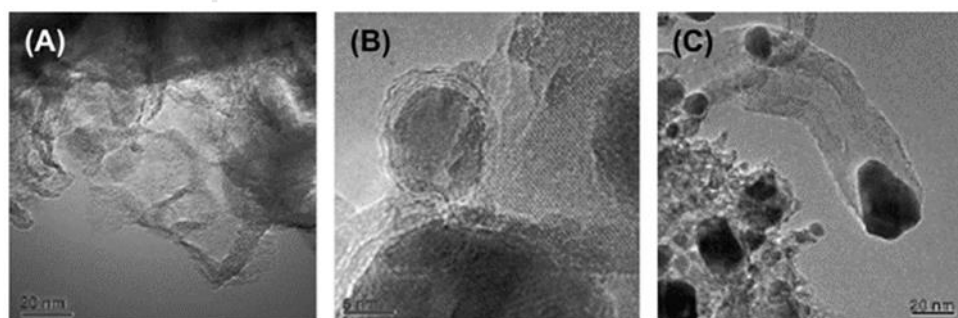
Figure 2.6 SEM images of different types of carbon formation over a Ni/MgAl$_2$O$_4$ catalyst (A) amorphous, (B) encapsulating, and (C) filamentous carbon [35].

2.4.3 Nickel sinter

Metal sintering is one of the important keys, leading to the deactivation of catalysts. The Ni sintering is considered to become a significant deactivation cause at high temperatures between 600–700 °C in Ni catalysts, depending on the catalyst structure, the reaction conditions, and metal-support interactions. The presence of high temperature could induce significant sintering. The catalyst preparation method plays an important role in determining catalytic activity and stability during the steam reforming catalysis due to the preparation method can accompany the Ni particle sizes. Hence, the proper preparation method should be provided to form the small metal particle sizes with uniform dispersion. Moreover, the metal-support interaction should be strong enough to stabilize small particles during catalysis [36].

Figure 2.7 [37] demonstrated TEM images corresponding to the fresh catalyst and spent catalysts at a time on stream, at 50, 75, 90, and 100 min (Figure 2.7b–e). The round, darkest, and most sharply defined areas in the TEM images are Ni^0 particles. The distribution of Ni particle size for fresh and spent catalysts is depicted in Figure 2.8. The distribution of Ni particle sizes turns higher and broader when increase of time on stream. The Ni sintering leads to bigger and more ununiformly particle sizes.
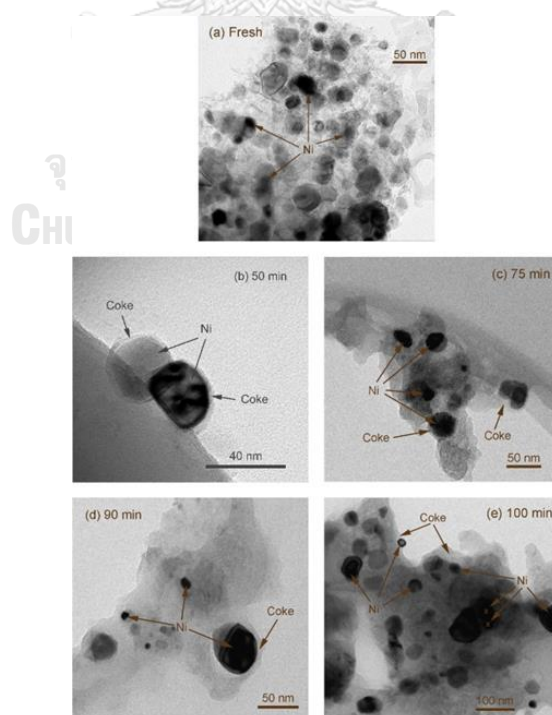
Figure 2.7 TEM images of the fresh catalyst (a) and spent at different time on stream of 50 min (b), 75 min (c), 90 min (d) and 100 min (e) [37].
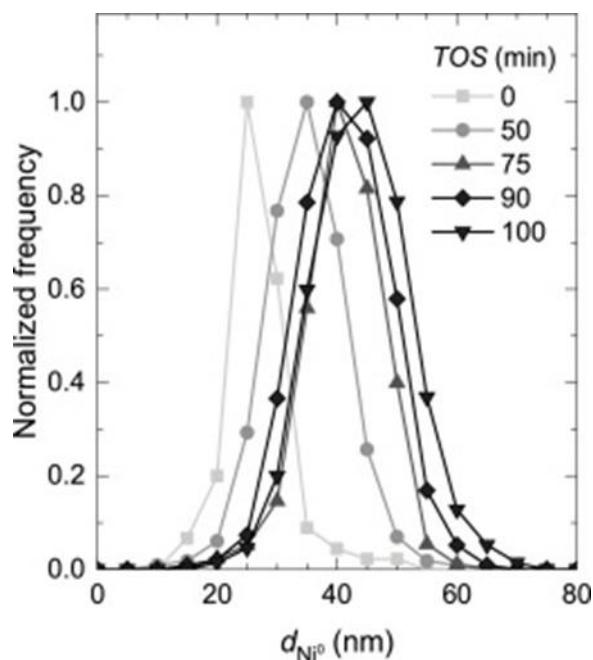
Figure 2.8 The distribution of Ni^0 particle size of the fresh and spent catalyst, based on TEM images, after steam reforming reaction [37].

2.5 Catalyst preparation

The catalytic activity of Ni-based catalyst in ESR reaction is influenced by the catalyst preparation methods. In general, there are several techniques of catalyst preparation method, used for preparing Ni-based catalysts, for example, impregnation, deposition-precipitation, strong electrostatic adsorption, co-precipitation, and metal encapsulation.

2.5.1 Metal encapsulation

The catalyst deactivation is generally observed as a result of metal sintering and structural deformation. However, the problems increasing upon metal agglomeration or metal loss have become more challenging to solve. The conventional methods of introducing metals into supports, such as impregnation, co-precipitation, and deposition–precipitation, have been studied and have still experienced those problems. Hence, metal encapsulation into the support structure has been considered the most believable approach for reducing catalytic deactivation issues.

The metal encapsulation can confine the size and shape of metal particles within the support structure and inhibit their aggregation and further growth due to the confinement effects immobilizing metal particles. The throughout pore network performs the mass transfer more efficiently during the catalysis.

Xu *et al*, 2018 [38] studied the encapsulation strategies for metal nanoparticles (NPs) within the mesoporous zeolite. The encapsulation of metal NPs inside the porous zeolites can be mainly divided into two classes of strategies: a post-synthetic process and a one-step (*in-situ*) process. The post-synthetic strategy can be referred to the introduction of metal NPs after the complete zeolitic structural framework. In contrast, the one-step (*in-situ*) method needs the co-crystallization of zeolites and metallic precursors.

2.5.1.1 Post-synthetic metal encapsulation

The post-synthetic strategy is widely used to introduce metal NPs into porous zeolite structures as it does not restrict the types of zeolite frameworks. The process can be reached by soaking the zeolite supports in soluble metal precursors. The pore channels inside zeolites provide the area for the NPs metal loading. The diffusion of metal precursors is usually accelerated in the mesopores, but it is difficult to enter the structures of zeolites where most of them only load on the external surface. Most of the studies for the preparation of zeolite-encapsulated metal NPs catalysts apply soluble metal precursors or a wetness impregnation method. In this process, metal species can easily diffuse into the inner structure and load in the pores after the elimination of solvent.

2.5.1.2 One-step (*in-situ*) metal encapsulation

The metal precursors can be loaded into the zeolite intra-structure through the one-pot hydrothermal synthetic process as shown in Figure 2.9 and Figure 2.10. In this strategy, the soluble metallic precursors were firstly mixed with the synthetic zeolite gel, which contains structural-directing agents (SDA), silica-alumina resources, deionized water, and sodium hydroxide. The mixture was then conducted at a high temperature for the crystallization of zeolites. The metal-encapsulated products were further calcined to eliminate the organic species.
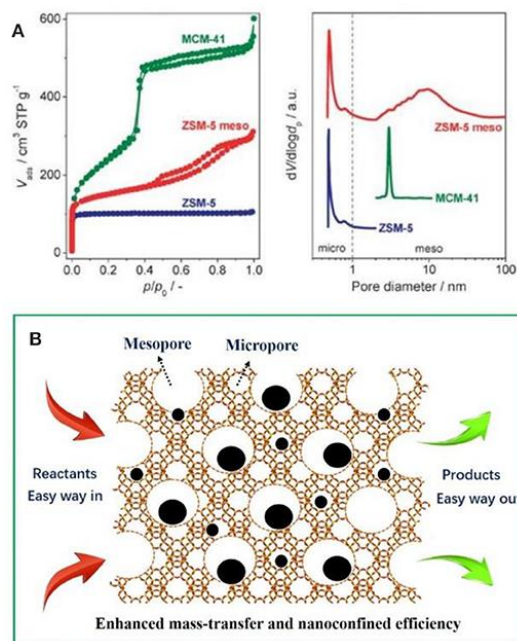
Figure 2.9 (A) Adsorption-desorption isotherms and pore size distributions of porous solids with different diameter (B) Schematic representation of the mesoporous zeolites-encapsulated metal NP catalysts [39].
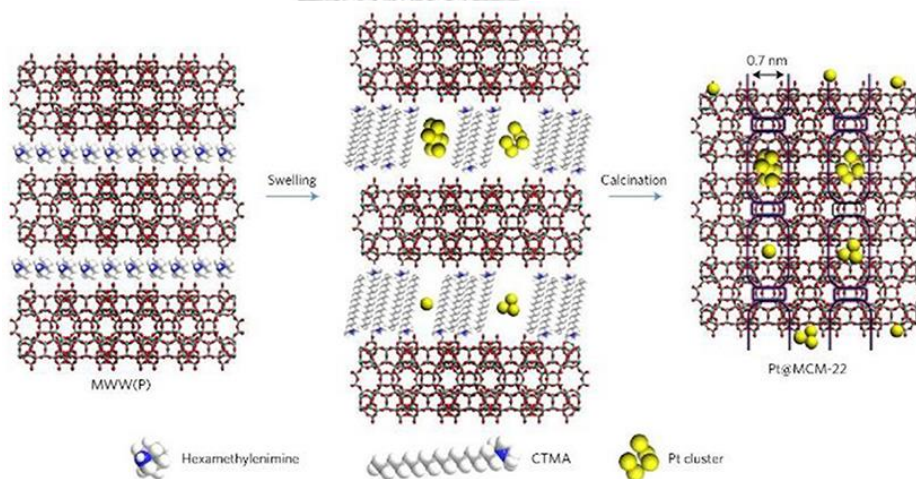
Figure 2.10 Schematics of the encapsulated Pt@MCM-22 [40].

2.5.2 Impregnation

Impregnation is the simplest and least expensive method. Impregnation can be termed wet or dry, depending on the volume of impregnating solution, whether it is equal to the pore volume of the catalyst support. For the preparation of silica supported metal catalysts, the impregnation process is frequently employed.

When using a dry impregnation method (as known as incipient wetness impregnation), a substantial amount of metal complex-containing solution is applied to the support to effectively wet it. Wet impregnation involves adding more metal solution than the pore volume of support material. The metal is attracted to the support through the interaction of physical adsorption.

The impregnation method requires three steps of preparation. Firstly, a metal precursor salt, such as nickel (II) nitrate hexahydrate, is first dissolved in deionized water and added drop by drop to the support while being constantly stirred. Then, the mixture is dried in an oven overnight to eliminate water. The catalyst is then reduced to its catalytically active state by calcining it at the appropriate temperature in the atmosphere to remove the metal ligands. Although the impregnation approach can create small metal particles, it is challenging to achieve a narrow particle size distribution. The type of precursor, rate of temperature increase, and temperature of calcination are the factors that might have an influence on the properties of the catalyst that is produced [41].

2.5.3 Strong electrostatic adsorption (SEA)

Strong electrostatic adsorption (SEA) [42] is a catalyst preparation method, based on the electrostatic attraction of oppositely charged particles. The principal consideration of the SEA method is that ions only adsorb on the oxide surface of the catalyst when it is charged. If the oxide surface of the catalyst is positively charged, then it can adsorb anions. Furthermore, ions could not adsorb at the point of zero charge (PZC) of metal oxides due to the catalyst surface is neutral. PZC can be determined by pH titrations.

2.5.4 Deposition-precipitation (DP)

Deposition precipitation (DP) [43] relates to the precipitation of a metal precursor onto a suspended support material through a change of pH, temperature, and evaporation, so that metal compounds can be formed with low soluble ability. DP method can be performed in the presence of existing support, and the concentration of the new compound increases gradually. It is possible to achieve precipitation on the existing support because adding the support to the solution either lowers the surface free energy of small nuclei or stabilizes the precipitate, lowering the energy barrier for nucleation. Basically, the DP method was developed to prepare catalysts with metal loadings greater than those obtained by impregnation, which is limited by solubility.

2.5.5 Co-precipitation

The salt of catalyst support and active metal are mixed and dissolved with a basic solution of sodium hydroxide (NaOH) or potassium hydroxide (KOH). The hydroxide precipitation of catalyst support and the active metal is produced. Then, the precipitate is filtrated, washed, dried, and calcined. Sodium carbonate (Na_2CO_3) and potassium carbonate (K_2CO_3) are used to change pH during the process of preparation, while carbonate (H_2CO_3) and NaOH can stabilize the pH. To avoid undesired nucleation events and different growth patterns, temperatures and concentration have to be considered.

The different catalyst preparation methods can be seen in Figure 2.11. There was gold catalyst prepared by different methods [44].
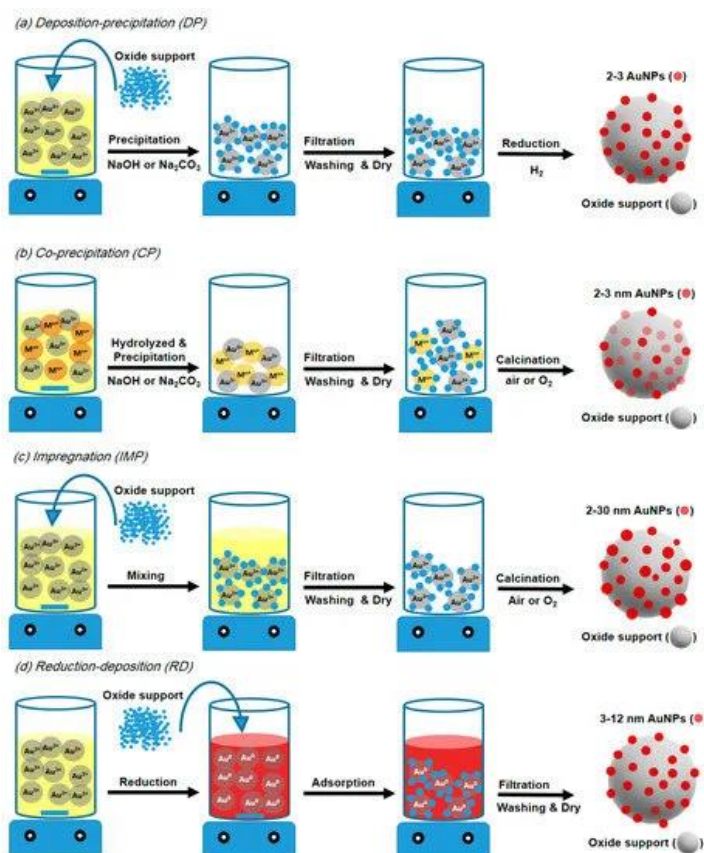
Figure 2.11 Gold catalyst with different preparation methods [44].

2.6 Catalyst supports

The catalyst supports are played an important role during catalysis, which is because the support could decrease the sintering of active metal and affect the reaction pathways under a high temperature. Hence, the catalyst supports should provide the properties against carbon formation: (i) high surface area, (ii) strong interaction between metal-support, (iii) good heat/mass transfer to enhance metal dispersion and stabilize metal particle size.

2.6.1 Rice husk

Rice husk (RH) is a natural by-product recovered from the rice grains after the rice milling process. The casing of rice husk is generally composed of 20% lignin, 20% hemicellulose, 30% cellulose, 10% of mineral ash, and impurities, while over 90% of mineral ash consisted of silica (SiO_2) as shown in Table 2.1. When the rice husk was burned by controlled thermal decomposition, it becomes the residue into ashes.

Rice husk is claimed as an organic waste product that becomes a major concern regarding disposal issues. Therefore, several attempts have been made to reuse rice husk and minimize its waste. Rice husk ash is considered using as an additive cementing material in the construction industry. As an admixture, rice husk ash creates a high-strength concrete with a lighter weight, and the cement with rice husk ash produces low-cost. Moreover, rice husk has been used as a sorbent material, especially to absorb heavy metals in industrial wastewater. Furthermore, rice husk has been considered to pretreat and use as catalyst support due to the components in rice husk, such as cellulose and silica, which can be formed SiC by the pyrolysis process [14].
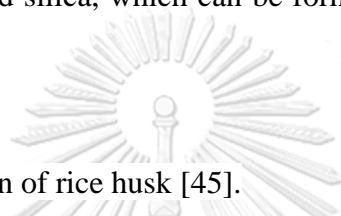
Table 2.1 The composition of rice husk [45].

Composition	Percentage
Cellulose	31.12
Hemicellulose	22.48
Lignin	22.34
Mineral ash	13.87
Water	7.86
Extractives	2.33
Chemical analysis of mineral ash	
SiO_2	93.19
K_2O	3.84
MgO	0.87
Al_2O_3	0.78
CaO	0.74
Fe_2O_3	0.58

2.6.2 Silicon carbide

Silicon carbide (SiC) is one of the non-oxide materials, used in many applications due to its properties such as hardness and mechanical stability, and good thermal conductivity. SiC can be used in the semiconducting field, it is also used for products such as bulletproof vests, ceramic materials, crucibles, and car clutches.

Furthermore, the surface area toward porous character makes it becomes an alternative catalyst support.

SiC is a tetrahedral structure. The carbon atom is linked to three Si atoms. SiC is polymorphic with the ability to crystallization in different ways as shown in Table 2.2. Due to the nature of polymorphism, there is a sequence of consecutive atoms, which will arrange in one direction. According to this feature, the silicon carbide atomic arrangements can be crystallized in several different ways, depending on the seed orientation as shown in Figure 2.12. SiC seed orientation is divided into two types according to the structure: α-SiC (6H-SiC) and β-SiC (3C-SiC). The stacking of atoms in a crystal depends on a surrounding factor when crystallization takes place. To form a SiC crystal, both temperature and pressure are applied to induce the atoms in the sequence. When applying the temperature below 1700 °C, SiC is crystallized to form β-SiC with cubic zinc-blende, but when the temperature is above 1700 °C, the crystal structure is formed α-SiC with the hexagonal crystal structure. These different seed orientations cause different physical and chemical properties of SiC [16]. The β-SiC is more attractive in some research fields because it is more active with the metal and its surface area is also higher, compared to α-SiC.
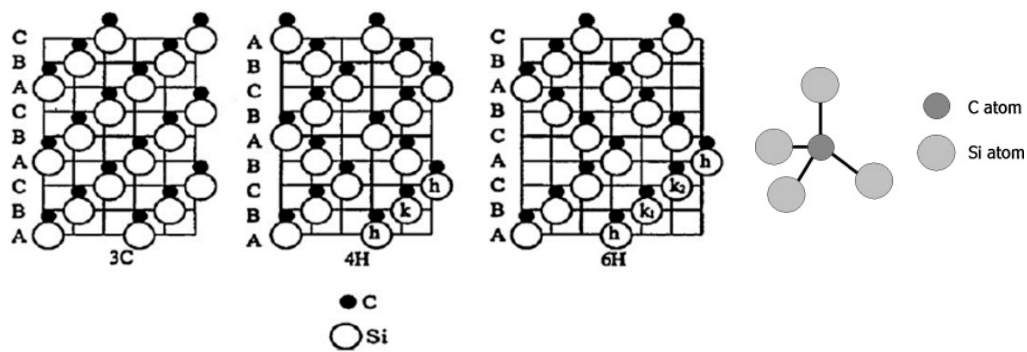
Figure 2.12 The crystal orientation of SiC: α-SiC (6H-SiC) and β-SiC (3C-SiC) and SiC tetrahedral structure [16].

Table 2.2 SiC structural crystalizing properties [46].

Polytype	3C (β)	4H	6H (α)
Crystal structure	Zinc blende (cubic)	Hexagonal	Hexagonal
Lattice constants (A°)	4.3596	3.0730; 10.053	3.0810; 15.12
Density (g/cm³)	3.21	3.21	3.21
Bandgap (eV)	2.36	3.23	3.05
Bulk modulus (GPa)	250	220	220
Thermal conductivity (W m⁻¹K⁻¹)	360	370	490

SiC is commercially produced through the Acheson process, based on the carbothermal reduction of SiO_2 by carbon in an electric arc furnace. However, the Acheson process consumes excessive energy, for example, a long reaction period, and high cost. The SiC product from this process is in the α-SiC form due to it is difficult to control the structure at high temperatures (2500 °C) [47].

2.6.2.1 Silicon carbide from rice husk

Due to the limitations of the Acheson process as mentioned before, there has been a lot of studies done on low-cost, renewable sources of silicon carbide. Rice husk has emerged as one of these attractive possibilities. The advantage of employing rice husk as a raw material is that it is inexpensive because it is typically abandoned.

SiC synthesis from rice husk was done in two steps [15]. The rice husk was first carbonized. The carbonization of rice husk was performed at different temperatures, ranging from 270 to 650 °C. The pyrolysis was then performed at a high temperature between 1200-1700°C under inert gas purging. SiC production from rice husk takes place at lower temperatures than processes involving solid quartz and graphite (1200 to 2000 °C) as mentioned above. The chemical equation between silica and carbon in the composition of rice husk was shown in Eq. (2.27) - (2.29).

$$SiO_{2(s)} + 3C_{(s)} \longrightarrow SiC_{(s)} + 2CO_{(g)} \qquad (2.27)$$

$$SiO_{2(s)} + 2C_{(s)} \longrightarrow Si_{(s)} + 2CO_{(g)} \qquad (2.28)$$

$$SiO_{2(s)} + C_{(s)} \longrightarrow SiO_{(g)} + CO_{(g)} \qquad (2.29)$$

2.6.3 Conventional ZSM-5

ZSM-5 is a hierarchical porous material, known as an aluminosilicate zeolite, and it is widely used in the catalytic cracking of hydrocarbon. Moreover, ZSM-5 is attractive in the field of steam reforming as catalyst support due to its high surface area, microporous structure properties, and thermal stability. However, the microporous structure exists in conventional ZSM-5 zeolite, and the diffusion efficiency of the molecule is low. The large reactant molecules are difficult to diffuse in micropores. This leads to carbon deposition, blocking the pore channels. The length of the diffusion pathway in conventional ZSM-5 zeolite is long, which interrupts the diffusion of the molecule resulting in a low catalytic performance [48]. Figure 2.13 exhibited that the metal particles were deposited into the conventional ZSM-5 support as a catalyst. It could deactivate quickly during catalysis due to its three-dimension structure, resulting in simple porous structures, strong acid sites, and a long diffusion pathway as mentioned above. Therefore, many investigations have been carried out to overcome these restrictions, such as the preparation of zeolite with special morphology, hierarchical zeolite, zeolite nanosheet, and compound modification.
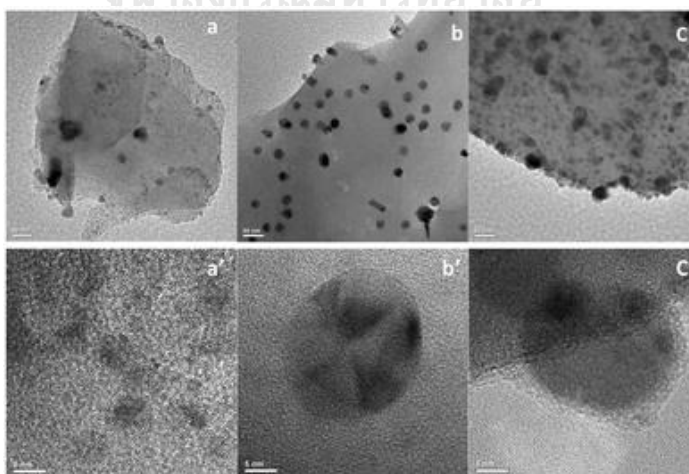
Figure 2.13 TEM images of (a, a′) 5% Ni/ZSM-5 catalysts; (b, b′) 17% Ni/ZSM-5; and (c, c′) 17% Ni/ZSM-5-DP catalysts. (Ni particles counted at 100 for analysis) [49].

2.6.4 ZSM-5 nanosheet

ZSM-5 nanosheet has gained more extensive attention, due to its two-dimension structure, resulting in excellent properties such as high accessibility of active centres on the surface with reduced diffusion resistance and the improvement of molecular transport. The zeolite nanosheet contained both microporous and mesoporous structures, which promoted the diffusion of reactant molecules. In addition, the ZSM-5 nanosheets consist of very thin lamellar layers (Figure 2.14), which reduced the diffusion lengths and improved the catalytic performance as well as a long lifetime. Besides, the nanosheet zeolite could be used as an excellent catalyst supporter for loading metal nanoparticles and it can also be applied to the catalytic reaction. The metal nanoparticles could uniformly disperse within the zeolite structure and prevent the metal sinter. While for the conventional ZSM-5, the metal particles are only loaded on the external surface, and it is easy to sinter resulting in the drop of BET surface area and the pore channel blockage. The disadvantages of the zeolite nanosheet are the duration of the synthesis process. The whole synthetic process is usually more than 5 days, consuming time, and energy in industrial manufacture. Hence, developing a time-saving method to prepare the nanosheet zeolite is significant [48].
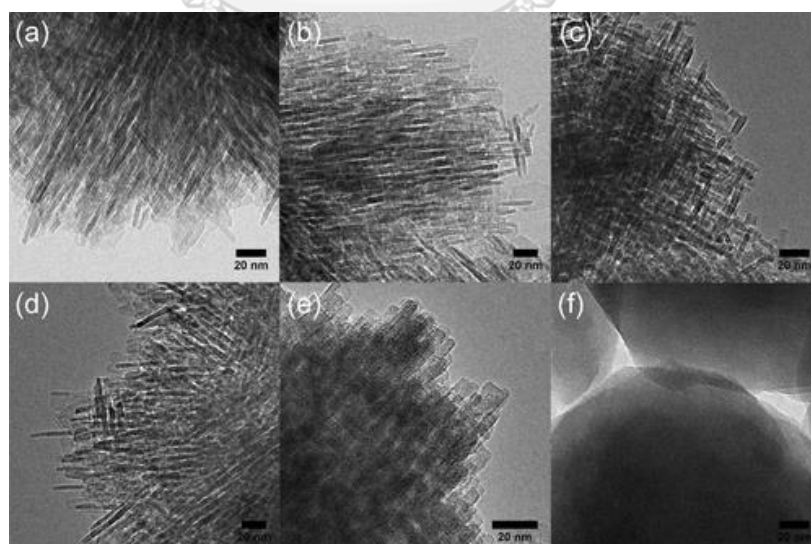
Figure 2.14 TEM images of the Fe/ZSM-5 zeolites nanosheet prepared at a Si/Fe of 360 [50].

2.7   Relevant literature reviews

Zhang *et al*, 2012 [51] have successfully prepared self-pillared nanosheets by the one-step hydrothermal process of crystal growth with tetra(n-butyl) phosphonium hydroxide solution (TBPOH) as a surfactant directing agent (SDA). The thickness of prepared nanosheets was only 2 nm, suggesting a short diffusion pathway and high surface area. This leads to promoting the reaction of large molecules.

Wetchasat *et al,* 2021 [25] have successfully synthesized the ultra-small Pt-NPs, distributed over hierarchical zeolite nanosheet surfaces by a one-step hydrothermal process using ethylenediaminetetraacetic acid (EDTA) as a ligand stabilizing agent. Moreover, the 0.6%Pt-NPs on zeolite surfaces were applied as a catalyst for the hydrodeoxygenation of 4-propyl phenol. The catalyst revealed an excellent catalytic performance, almost 100% of cycloalkane product can be obtained.

Kumar *et al*, 2019 [52] prepared Ni/ZSM-5 and Co/ZSM-5 by wet impregnation method to investigate the catalytic performance under ESR. They found that the 10% Ni/ZSM-5 catalyst produced 72% hydrogen selectivity at 600 °C, suggesting that Ni is a more stable catalyst as compared to Co/ZSM-5 support. However, C_2H_4 was found main undesirable product at 600 °C. This study indicated that a 10% Ni/ZSM-5 catalyst can be used as low-cost catalyst for hydrogen production.

Cimenler *et al*, 2017 [53] studied hydrocarbon steam reforming using zeolite encapsulated Ni-based catalyst. The nickel catalyst was prepared by encapsulation of nickel with a silicalite-1 (pore size 0.44–0.55 nm) zeolite. The findings showed that $1.6\%Ni/1.2wt\%Mg/Ce_{0.6}Zr_{0.4}O_2$ steam reforming composite catalyst was synthesized by a physical coating technique. Steam reforming of CH_4 and C_7H_8 at 800°C on the composite Ni catalyst demonstrated that the catalyst showed 10 h of time on stream while the non-encapsulated catalyst deactivated.

Davidson *et al*, 2014 [54] studied hydrogen production via steam reforming of alcohols and sugar alcohols over various kinds of catalysts. The $Ni/CeO_2-Al_2O_3$ is one of the effective catalysts, prepared by the impregnation method. It revealed good catalytic performance. Moreover, the $Ni/CeO_2-Al_2O_3$ catalyst showed conversion of ethanol at 95%, while the H_2 yield is around 60%. There was also carbon formation in the process while the reaction proceeded at 500°C.

Jiang *et al,* 2014 [55] synthesized silicon carbide/porous carbon (SiC-PC) hybrids materials with high specific surface areas via a facile evaporation-induced assembly approach combined with a thermal treatment in the presence of TEOS as a bifunctional agent. Then, platinum particles (20 wt%) were loaded onto the SiC-PC hybrid as Pt/SiC-PC by a borohydride reduction method in alkaline media. These Pt/SiC-PC have great potential as high-performance catalyst supports for fuel cell electrocatalysts.

Wang *et al,* 2015 [56] investigated catalytic steam reforming of n-propanol over ruthenium (Ru) and ruthenium nickel (Ru/Ni) bimetallic catalysts supported on ceria-alumina oxides with different ceria loading (0-10% CeO_2 wt/wt) which were prepared by wetness impregnation method. Steam reforming activity was tested in a fixed bed tubular flow reactor at 450 or 500ºC using a feed of n-propanol/water mixture. They found that catalysts with 3 wt% Ru, 10 wt% Ni and 3 or 10 wt % ceria were very reactive and stable at both 450 and 500ºC with high selective to H_2 (60%). When the reaction was proceeding, the selectivity and yield products decreased after 5 hours due to carbon deposition covered on the metal active sites.

Prasongthum *et al,* 2017 [57] synthesized carbon nanotubes-silica fibrous composite (CNTs-SF) by the steam reforming of ethanol over a Ni/silica fiber catalyst prepared by electrospinning technique. The reaction performance of the NiCNTs-SF catalysts was investigated and compared with the Ni/silica fiber (NiSF) and Ni/silica porous (NiSP) catalysts. The effect of temperatures on the ethanol conversion and product distribution was studied in the range of 300 and 500 °C. They found that the NiCNTs-SF catalyst (10 wt% loading of Ni) exhibited the best performance in terms of stability and high activity at the lower reaction temperature. The catalyst showed almost 100% of ethanol conversion and 50% of H_2 product yield.

Mhadmhan *et al,* 2018 [58] investigated the performance of the Ni/SF catalysts for hydrogen production from ethanol steam reforming at various conditions in comparison with a conventional Ni/silica porous (Ni/SP) catalyst. The catalysts were prepared by three different preparation techniques: impregnation (IM), deposition precipitation (DP), and strong electrostatic adsorption (SEA). The Ni/SF-SEA catalyst was found to exhibit the highest ESR catalytic activity at 600°C in terms of giving the highest H_2 yield of 65%.

Sumrunronnasak *et al,* 2020 [59] successfully synthesized $CeCoO_x$ mixed-oxide catalysts with different Ce/Co ratios. The catalyst was applied to steam reforming of fusel oil for hydrogen production. 60%Ce ($Ce_{0.6}Co_{0.4}O_x$) presented excellent catalytic performance, 60% of fusel oil was converted, 21% of hydrogen was produced, and the catalyst remained stable for 300 minutes, indicating that the presence of Ce^{3+} and active oxygen in $CeCoO_x$ catalysts encouraged oxygen mobility and reduced coking.

Olivares *et al,* 2018 [60] synthesized $Ni/MgAl_2O_4–CeO_2$ catalysts. The catalysts were used over ethanol steam reforming and were prepared using different impregnation media (ethanol or water) and Ni precursors (nitrate or acetate). The best catalytic behavior was found over the catalyst prepared from an ethanolic solution of $Ni(NO_3)_2$. The $Ni/MgAl_2O_4–CeO_2$ catalysts showed high selectivity to H_2, the highest CO formation, and an amount of deposited carbon of 14% after 6 h in reaction.

Ogo *et al,* 2020 [61] studied Co-based and Ni-based catalysts used for ethanol steam reforming catalysts because of their high activity and low cost. They investigated various kinds of catalysts, for example, Ni/Mg-Attapulgite, Ni/CeO_2-MgO, Ni-Co/MCM-41, and $Ni-Co/CeO_2$. This catalyst showed almost 100% of ethanol conversion and over 60% of H_2 product yield. However, these non-noble transition metal catalysts present severe difficulties including the deactivation of activity by the formation of coke.

Makornpan *et al,* 2014 [62] fabricated silicon carbide from rice husk. The silicon carbide (SiC) ceramics were prepared by *in-situ* bonding of rice husk under a carbothermal reduction reaction. The carbonized rice husk was pretreated with acid to eliminate the impurities. The sample was then mixed with Si metal powder and was pyrolyzed at high temperatures in Ar or N_2 atmosphere separately to compare the structural differences. SiC phase was found in pyrolyzed rice husks. Cristobalite was formed under the Ar atmosphere pyrolysis process while silicon oxynitride was found when pyrolyzed in a N_2 atmosphere at lower than 1500 °C. Silicon carbide whisker is the main phase on the surface of pyrolyzed rice husk. Increasing pyrolysis temperatures reduced the size and amount of the silicon carbide whisker but increased the silicon carbide particle. Increasing the pyrolysis temperature to 1700 °C led to the porosity decrease due to the sintering process.

Krishnarao *et al,* 1998 [63] studied the pyrolysis of raw rice husks directly in a graphite resistance heating furnace at a temperature between 1100-1400 °C in a nitrogen atmosphere. The SiC can be obtained without applying a catalyst. Increasing the pressure during the pyrolysis reduced the formation of SiC whiskers. However, pyrolysis of rice husk in a nitrogen atmosphere resulted in SiC whiskers forming.

CHAPTER 3
RESEARCH EXPERIMENT

The experimental works are divided into two main sections due to the different both resources and catalyst supports.

3.1 Hydrogen production by FSR over Ni/SiC

3.1.1 Materials

Fusel oil composed of 68.19, 20.07, 8.02, 4.13, and 0.01 % by weight of isoamyl alcohol, iso-butanol, propan-1-ol, ethanol, and water, respectively, was commercially available from KTIS Bioethanol Co. Ltd. (KTBE). The fusel oil had a density of 0.8152 g/cm^3 at 25°C and a molecular weight of 78.91 g/mol. The Rice husk obtained from the Sukhothai rice mill was used as a precursor to synthesize SiC. Silicon carbide (SiC), commercial grade, was purchased from DU B-1, Showa Denko, Japan. Nickel nitrate hexahydrate ($Ni(NO_3)_2.6H_2O$) was purchased from Sigma-Aldrich. 36.5-38% Hydrochloric acid (HCl) was purchased from J.T Baker. 99% purity of nitrogen gas (N_2), hydrogen gas (H_2), argon gas (Ar), and air-zero gas (O_2) were purchased from Bangkok Industrial Gas Co., LTD.

3.1.2 Preparation of SiC from rice husk

Rice husk (RH) was washed with DI water for removing the dirt and dried at 110°C overnight. After that, it was carbonized at 300°C for 2 h under the atmosphere and grounded into powder (RH300). Then, the RH300 was washed and stirred by 0.1 M HCl at room temperature for 12 h to remove the alkali oxide, then washed and filtrated by DI water several times until the filtrate reached pH 7 and dried at 110°C overnight (RH300H). The RH300H was pyrolyzed by a furnace at 1300, 1500, and 1700°C (heating rate 10°C/min) under Ar purging (1 L/min) to obtain SiC1300, SiC1500, and SiC1700, respectively. The commercial SiC (SiC-com) was also used for catalyst support to compare the catalyst performance in steam reforming of fusel oil. The whole process is shown in Figure 3.1.
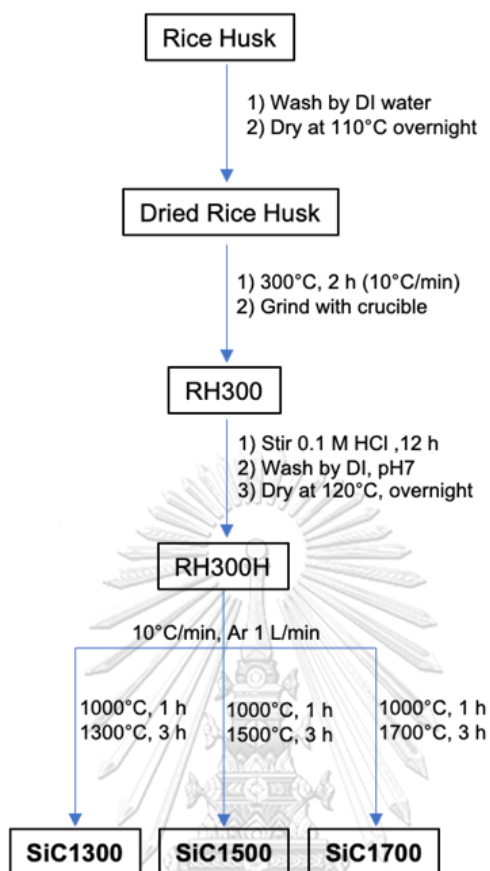
Figure 3.1 Preparation of SiC from rice husk from pyrolysis process.

3.1.3 Preparation of nickel catalysts

Catalysts (Ni/SiC1300, Ni/SiC1500, Ni/SiC1700, Ni/SiC-com) were prepared by an excess solution impregnation method as follows: $Ni(NO_3)_2.6H_2O$ and DI water were mixed and homogenized. After that, the support was put into the solution and stirred at 50°C for 3 h until it dried. Then, the dried mixture was dehydrated at 110°C overnight and calcined at 700°C for 3 h.

3.1.4 Catalyst characterization

X-ray diffraction (XRD) was performed to examine the crystal structure, and particle size of catalysts at room temperature in a Bruker D8 Advance equipped with Cu-Kα radiation. The profile was scanned in the 2-degree (2θ) range of 5°- 80° at 0.02 steps. Similarly, the XRD phases of SiC, pyrolyzed from rice husk, were detected via the same instrument.

The weight percentage of metal on support was measured using energy dispersive X-ray analysis (EDX) from FESEM-EDX (7610F). The weight percentage of the element of rice husk before and after pyrolysis was measured via the same method.

The specific surface areas and pore size of the catalyst sample were measured in ASAP 2020 at liquid nitrogen temperature (-196°C). Prior to analysis, the catalysts were degassed at 200 °C for 2 h. The specific surface area was estimated by Brunauer-Emmett-Teller (BET) equation, the pore volume and the average pore diameter were calculated by the Barrett-Joyner-Halenda (BJH) method.

Temperature-programmed reduction (H_2-TPR) was carried out by a Micromeristics TPD/TPR 2920 system to analyse the reduction of the metal oxidation state. The catalyst sample was pre-treated with nitrogen flow at 100°C for 30 min to remove a trace of water. After that, the catalyst was exposed to reduce in $5\%H_2/N_2$ while the temperature was increased up to 900 °C at the rate of 10 °C/min.

The morphology was obtained using a Field Emission Scanning Electron Microscope and Energy Dispersive X-Ray Spectrometer (FESEM-EDS) of JEOL JSM-7610F, Oxford X-Max 20 model. Similarly, the morphology of rice husks before and after pyrolysis was detected through the same method.

Thermogravimetric analysis was carried out in a TGA/DSC 1 (Mettler Toledo) instrument at a heating rate of 10°C/min from 30 to 1000 °C to estimate the amount of coke on the spent catalyst.

3.1.5 Catalytic activity evaluation

The catalytic performance of the prepared catalysts in the FSR was examined in a fixed-bed reactor containing 200 mg of catalyst at 700 °C. Before FSR, the catalyst was reduced *in-situ* under $5\%H_2/N_2$ at 700 °C for 1 h. Then a mixture of DI water and fusel oil with a molar ratio (S/C) of 5 was fed into the reactor through the pump (0.04 ml/min) under N_2 flow at 45 ml/min. The effluent gases were trapped and cooled via an ice trap to condense the liquid product and unreacted fusel oil. The effluent gas from a fixed-bed reactor was detected online by gas chromatography. The gas products were analysed by thermal conductivity detector (TCD) and flame ionization detector (FID) with Porapak Q column. The results were reported in terms

of fusel oil gas conversion, selectivity of gas products, and hydrogen yield, defined as follows: Eq. (3.1)-(3.3).

$$X(Fusel) = \frac{Fin - Fout}{Fin} \, x \, 100 \tag{3.1}$$

Where *X(Fusel)* is fusel oil gas conversion, F_{in} is the molar flow rate of fusel oil inlet, and F_{out} is the molar flow rate of fusel oil outlet.

$$S(i) = \frac{Fci}{Fcout} \, x \, 100 \tag{3.2}$$

Where *S(i)* is the selectivity of each gas product, Fc_i is the molar flow rate of the carbon-containing species (i) in the gas products, including CO, CO_2, CH_4, C_2H_4, and C_2H_6, and Fc_{out} is the molar flow rate of C atom total in the gas outlet.

$$Y(H2) = \frac{molH2produce - molFusel \; oil \; converted}{4.35/13.05} \, x \, 100 \tag{3.3}$$

Where *Y(H₂)* is percentage of hydrogen yield, *molH₂ produced* is mole of hydrogen gas, and *molFusel oil converted* is mole of converted fusel oil.
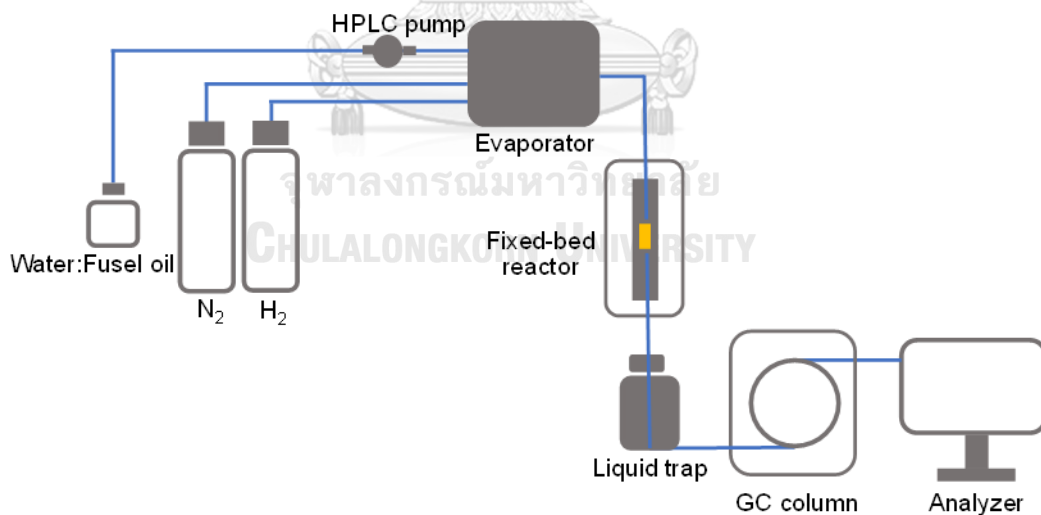
Figure 3.2 Schematic of steam reforming of fusel oil over Ni/SiC catalysts.

3.2   Hydrogen production by ESR over Ni/ZSM-5 nanosheet

3.2.1 Materials

The two-dimension ZSM-5 nanosheet (Z-NS) was successfully synthesized by hydrothermal process. Tetraethyl orthosilicate (TEOS: ≥99.0%, Sigma-Aldrich) was used as a silica source and was mixed with tetrabutylammonium hydroxide (TBAOH: 40% in aqueous solution, Sigma Aldrich), used as a structure directing agent (SDA). Aluminium isopropoxide (NaAlO$_2$: ≥98.0%, Sigma-Aldrich) was used as an alumina source. Sodium hydroxide (NaOH: Sigma-Aldrich) and ethylenediamine (99%, Sigma-Aldrich) were used as a mineralizer and a stabilizing agent, respectively. Nickel nitrate hexahydrate (Ni(NO$_3$)$_2$.6H$_2$O: ≥98% Sigma-Aldrich) was used as a nickel source for catalysts. The conventional ZSM-5 (Z-CON) support was synthesized with a similar process but using tetrapropylammonium hydroxide solution (TPAOH: 40% in aqueous solution, Sigma-Aldrich) as an SDA.

3.2.2 Preparation of ZSM-5 supports

3.2.2.1   ZSM-5 nanosheet

The ZSM-5 nanosheet (Z-NS) was synthesized by a hydrothermal process. The ratio of Si/Al was 100. 8.4 g of TEOS, 8.1 g of TBAOH, and 0.086 g of Al isopropoxide were mixed first, then added 0.02 g of a basic solution of NaOH. After that, the mixture was stirred at room temperature for 15 h, then it was heated up to 130 °C for 48 h by using an autoclave for the crystallization process. Then, the autoclave was cooled down to room temperature, and the Z-NS gel was washed with DI water by using the centrifuge, and it was dried at 110 °C overnight. The dried powder was calcined at 550 °C for 5 h by using the heating rate of 2 °C/min.

3.2.2.2 Conventional ZSM-5

The conventional ZSM-5 (Z-CON) was synthesized by mixing 3.5 g of TEOS and 2.02 g of TPAOH and 0.041 g of Sodium aluminate, then adding 0.07 g of a basic solution of NaOH. The crystallization process was heated at 180 °C for 72 h in the autoclave, then the obtained Z-CON gel was washed with DI water by using the centrifuge, and it was dried at 110 °C overnight. The dried powder was calcined at 650 °C for 8 h by using the heating rate of 5 °C/min.

3.2.3 Preparation of nickel catalyst

3.2.3.1 *In-situ* method

To synthesize Ni on Z-NS under the *in-situ* method, 8.4 g of TEOS and 8.1 g of TBAOH, and 0.086 g of Al isopropoxide were mixed, then added 0.02 g of a basic solution of NaOH. After that, the mixture was stirred at room temperature for 15 h. The solution of $[Ni(NH_2CH_2CH_2NH_2)_3](NO_3)_2$ was prepared by mixing 0.25 g of ethylenediamine, 1.17 ml of DI water, and 0.38 g of $Ni(NO_3)_2.6H_2O$, then homogenizing the solution and dropwise into the Z-NS solution. Next, the mixture was further stirred for 1 hour. Then, the crystallization and calcination conditions were similar to Z-NS. The obtained catalyst was named Ni/Z-NS-IN.

To synthesize Ni on Z-CON under the *in-situ* method, there were the same processes with a synthesis of Z-CON and the solution of $[Ni(NH_2CH_2CH_2NH_2)_3](NO_3)_2$ was added before the crystallization process. The obtained catalyst was named Ni/Z-CON-IN.

3.2.3.2 Wet impregnation method

The Z-NS support was used as catalyst support, mixed with the nickel nitrate solution at 3wt% of Ni loading. After that, the mixture was stirred at 60 °C for 2 h until it dried, then it was dried at 110 °C overnight. The dried powder was calcined at 550 °C for 5 h by using the heating rate of 2 °C/min. The obtained catalysts were called Ni/Z-NS-IMP.

The Z-CON support was also used as a support for Ni catalysts, prepared by the same wet impregnation method. The obtained catalyst was defined as Ni/Z-CON-IMP.

3.2.4 Catalyst characterization

The prepared catalysts were characterized by X-ray diffraction (XRD), X-ray photoelectron spectroscopy (XPS), H_2 temperature-programmed reduction (H_2-TPR), NH_3 temperature-programmed desorption (NH_3-TPD), thermogravimetric analysis (TGA), scanning transmission electron microscopy (STEM), N_2 adsorption-desorption inductively coupled plasma-optical emission spectrometry (ICP-OES), energy dispersive X-ray analysis (EDX). *In-situ* diffuse reflectance infrared Fourier transform spectroscopy (*in-situ* DRIFTS).

3.2.5 Catalytic performance

The prepared catalysts, used in a fixed-bed reactor, were pelletized and sieved to obtain a size between 250-425 microns. Before doing the ESR, the fresh catalysts were reduced to form nickel metals by flowing 5% H_2/Ar at 500°C for 1 h. The ratio of Steam/Carbon at 8/1 was used to investigate the catalytic performance of all catalysts. The absolute ethanol at 0°C and steam water at 55°C were purged by Argon gas at flow rates of 65.7 ml/min and 27.5 ml/min, respectively, through the reactor, which was packed with 50 mg of a fixed-bed nickel catalyst. The steam reforming reaction of ethanol was carried at different temperatures; 300, 400, 500, and 600 °C to produce the H_2 production. For the longevity test, the ESR was set up at 550 °C for 48 h. All gas products were detected by GC-online. The results were reported in terms of EtOH gas conversion, selectivity of gas products, and hydrogen yield, defined as follows: Eq. (3.4)-(3.6).

$$X(EtOH) = \frac{F(in) - F(out)}{F(in)} \, x \, 100 \tag{3.4}$$

Where X(EtOH) is EtOH gas conversion, F(in) is the molar flow rate of EtOH inlet, and F(out) is the molar flow rate of EtOH outlet.

$$S(i) = \frac{Fc(i)}{\Sigma Fc(out)} \, x \, 100 \tag{3.5}$$

Where S(i) is the selectivity of each gas product, Fc(i)is the molar flow rate of the carbon-containing species (i) in the gas products, including CO, CO_2, CH_4, CH_3CHO, and C_2H_4 and $\Sigma Fc(out)$ is the summation of molar flow rate of C gas products in the gas outlet.

$$Y(Hydrogen) = \frac{mole(Hydrogen)}{6 \times mole(EtOH)} \, x \, 100 \tag{3.6}$$

Where Y(Hydrogen) is percentage of hydrogen yield, mole(Hydrogen) is the molar flow rate of produced hydrogen, and mole(EtOH) is the molar flow rate of converted EtOH.
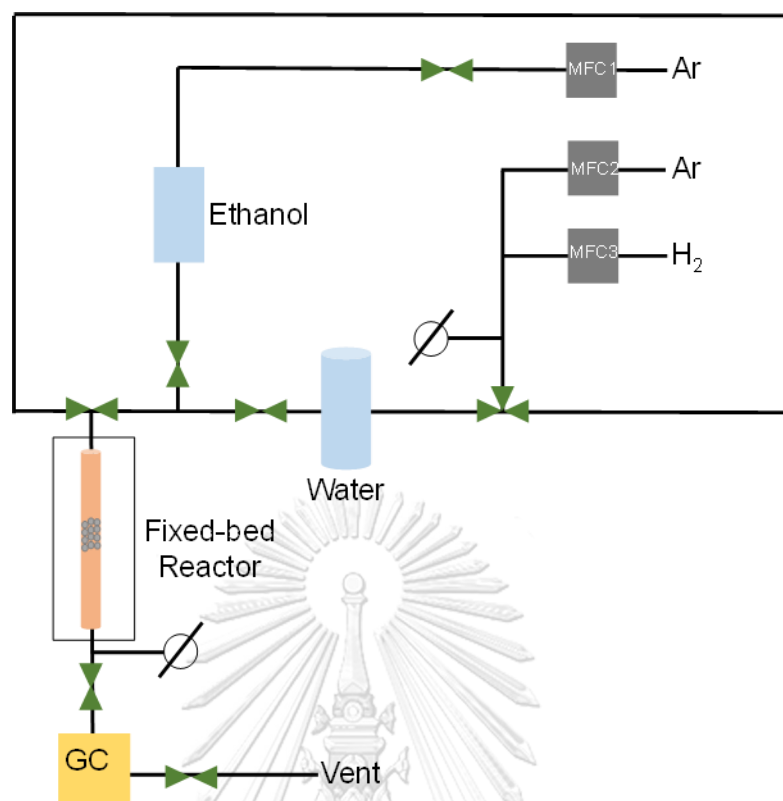
Figure 3.3 Schematic of steam reforming of ethanol over Ni/ZSM-5 nanosheet catalysts.

CHAPTER 4
RESULTS AND DISCUSSION

The study in this chapter is distributed into two sections as mentioned before. The first section is hydrogen production by FSR over Ni/SiC and the second section is hydrogen production by ESR over Ni/ZSM-5 nanosheet. The catalyst preparation methods, the characterizations of prepared catalysts, and catalytic performances will be investigated. Furthermore, the spent catalysts after the steam reforming reaction will also be studied on carbon formation and nickel sinter.

4.1 Hydrogen production by FSR over Ni/SiC

4.1.1 Characterization of rice husk and as-prepared catalysts

4.1.1.1 Morphology and elemental composition of rice husk

The morphology and the composition of RH before and after pyrolysis at different temperatures were shown in Figure 4.1 and Table 4.1, respectively. Before the pyrolysis process, natural RH (Figure 4.1a) showed rough surfaces of cellulose and lignin, which mainly consisted of C, O, Si at 65.33, 31.93, and 2.19 wt%, respectively, and 0.55 wt% of some other metal impurities (Al, Mg, and K). After carbonization at 300 °C for 2 h, noted as RH300 (in Figure 4.1b), the surface of RH300 was less rough, compared to RH. The components of RH300 showed less amount of C at 32.8 wt%, while Si and O, increased to 19.11 and 44.95 wt%, respectively, and 3.14 wt% of other metal impurities (Al, Mg, K, P, Ca, and Mn) appeared after celluloses and lignin were carbonized. Then, RH300 was treated with 0.1 M HCl for 12 h, named RH300H, to eliminate the metal impurities. The morphological surface of RH300H in Figure 4.1c was smoother than that of RH300 due to the loss of metal impurities after acid treatment, similar to the composition of RH300H, showing that 20.20 wt% of C, 48.54 wt% of O, and 30.99 wt% of Si were the main components, which were the remained SiO_2 and cellulose. After pyrolysis of RH300H at high temperatures (1300, 1500, 1700 °C), noted as SiC1300, SiC1500, and SiC1700, respectively, SiO_2 was reacted with cellulose to form SiC as it showed only Si and C components, and the small amount of Al from natural RH structure remained in the structure, while the commercial SiC (SiC-com) exhibited SiC without

Al. However, the FESEM image of SiC1300 in Figure 4.1d showed an unchanged morphological surface, while that of SiC1500 in Figure 4.1e, illustrated SiC rod structures with a diameter of 80 nm, as whisker forms. With the Further increasing temperature at 1700 °C, the diameter of SiC1700 in Figure 4.1f as rod structures continuously increased from 80 nm to 200 nm as the SiC whisker forms were sintered. A similar result has been obtained by Pereira *et al, 2020* [15].
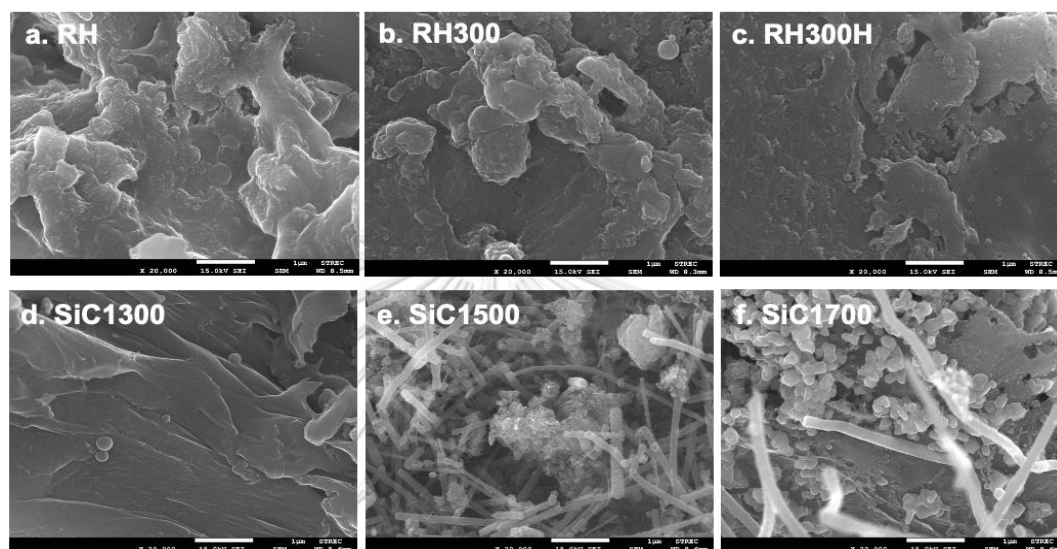
Figure 4.1 FESEM images of a. RH, b. RH300, c. RH300H, d. SiC1300, e. SiC1500, f. SiC1700.

Table 4.1 The composition of RH before, after pyrolysis and after loading Ni determined by SEM-EDS.

Samples	The composition (wt%)								
	C	Si	O	Al	Mg	K	P	Ca	Mn
RH	65.33	2.19	31.93	0.23	0.07	0.25	-	-	-
RH300	32.80	19.11	44.95	0.27	0.46	0.40	0.68	1.08	0.25
RH300H	20.20	30.99	48.54	0.26	-	-	-	-	-
SiC1300	50.21	49.22	-	0.57	-	-	-	-	-
SiC1500	56.48	42.25	-	1.27	-	-	-	-	-
SiC1700	56.30	43.09	-	0.61	-	-	-	-	-
SiC-com	49.30	50.70	-	-	-	-	-	-	-

4.1.1.2 Chemical composition of SiC supports and catalysts

Figure 4.2 exhibited an XRD pattern of all supports and catalysts: (a) SiC1300, (b) SiC1500, (c) SiC1700, (d) SiC-com, and (e) Ni/SiC1500. SiC-com consists of both *β*-SiC and α-SiC phases. The *β*-SiC phase showed 2*θ* peaks at 35.6°, 41.6°, 60°, and 71.8°, while that of the α-SiC phase showed 34.2°, 38.2°, 45.5°, 55°, and 66°, similar to the previous work, reported by Yi *et al, 2013* [64]. Stein *et al, 1993* [65] have suggested that the phase of the SiC structure depends on seed orientation. In this work, the *β*-SiC phase was obtained by pyrolysis below 1700 °C. However, the α-SiC phase was formed over 1700 °C. Pyrolysis of RH at 1300 °C shows that it was completely amorphous with no significant crystalline phases. This may have been caused by the coarse nature of the starting materials, where the surface area of the RH was not sufficient for chemical reactions to proceed at this temperature and the pyrolysis duration was only 3 h. The XRD patterns of SiC1500 and SiC1700 showed their 2θ peaks of the *β*-SiC phase at 35.6°, 60°, and 71.8°, respectively. The NiO phases of all Ni/SiC catalysts were observed at 36.9°, 43°, and 62.6°, corresponding to the crystal plane of (1 0 0), (2 0 0), and (2 2 0), respectively. This finding was also reported by Hu *et al, 2007* [66].
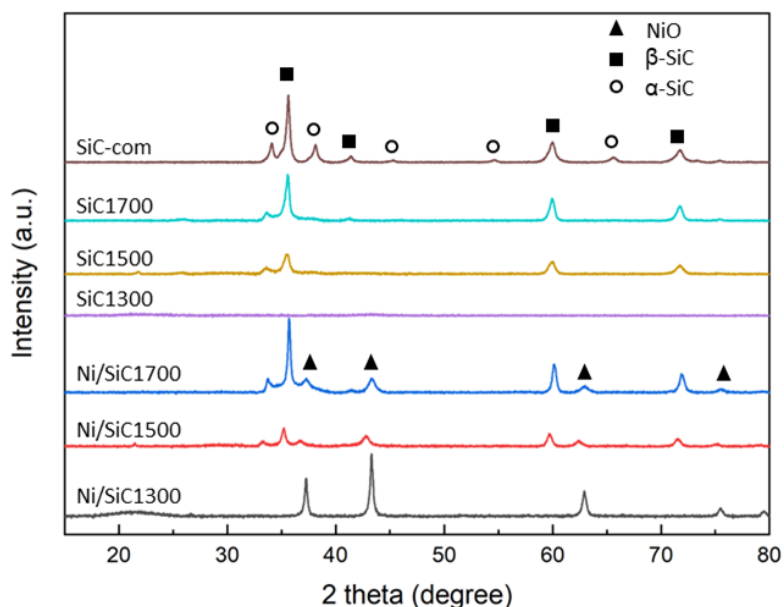
Figure 4.2 XRD patterns of SiC supports and after loading 10 wt% of Ni.

Representative TPR spectra of the catalysts were shown in Figure 4.3. There were two ranges of H_2-TPR for NiO reduction to form Ni. Firstly, the presence of peaks over 300-500 °C (α-NiO region) showed weak interaction between NiO and supports. In the cases of Ni on pyrolyzed RH supports, which are Ni/SiC1300, Ni/SiC1500, and Ni/SiC1700, H_2-TPR peaks in α-NiO region shifted towards higher temperatures at 470 °C, 490 °C, and 440 °C, respectively, compared to that of Ni on SiC-com at 400 °C, due to the smaller NiO particles, as evidenced by SEM analyses in Figure 4.5. Secondly, the β-NiO region over 500-800 °C showed that NiO strongly interacted with SiC supports. The peaks in the second range (β-NiO) of Ni/SiC1500, and Ni/SiC1700 were at high temperatures, which were 700 °C and 730 °C, respectively, because the small Ni particles strongly reacted with porous structures of SiC, and the peaks were broad because the rest of the carbon in the pores of RH may decompose during the reduction. The H_2-TPR discussion can be referred to our earlier research study by Reubroycharoen *et al, 2010* [67].
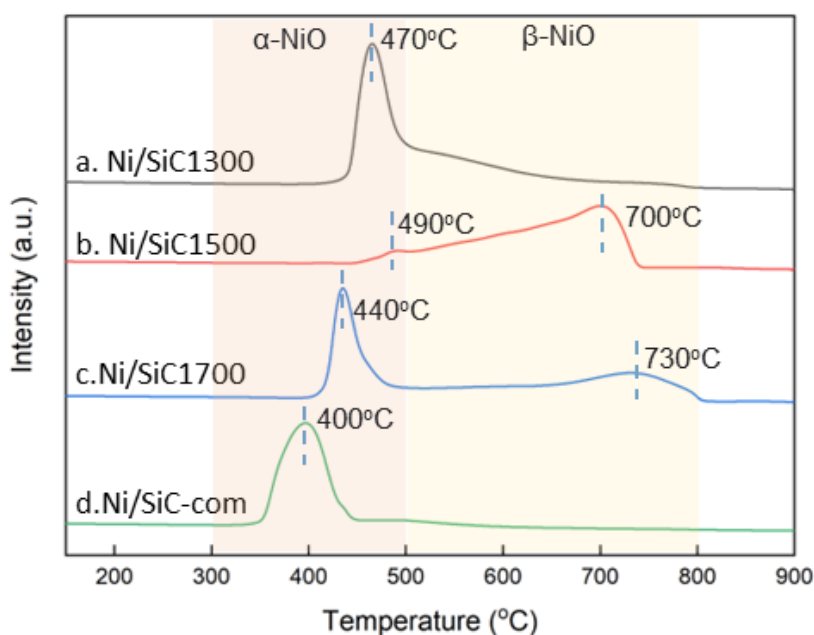
Figure 4.3 H_2-TPR profiles of fresh Ni/SiC catalysts.

4.1.1.3 Surface area and porosity

The nitrogen adsorption-desorption technique was used to determine N_2 adsorption-desorption isotherm, BET surface area, pore size, and pore volume of the

supports and catalysts, with the results shown in Table 4.2 and Figure 4.4. The surface area of the SiC-com showed a relatively smallest BET surface area and pore volume due to its non-porous material. Similarly, the N_2 adsorption-desorption isotherm of the SiC1300 support was linear with a relative pressure of P/P_0 of 0 and had a small BET surface area and pore volume, showing that the support was a non-porous structure due to uncomplete pyrolysis. The SiC1500 support noticeably showed type IV isotherms with hysteresis loop, suggesting a porous material as reported by Touhami *et al* 2017 [68]. The surface area of the SiC-com showed a relatively smallest BET surface area (5.83 m^3/g) and zero pore volume due to its non-porous material. Similarly, the N_2 adsorption-desorption isotherm of the SiC1300 support had a small BET surface area (19.20 m^3/g) and a small pore volume (0.03 cm^3/g), showing that the support was a non-porous structure. In contrast, the surface area of SiC1500 exhibited markedly larger than that of the SiC-com. The BET surface area and pore volume of SiC1500 were 64.79 m^2/g and 0.13 cm^3/g, respectively, because the impurities were decomposed and silica reacted with carbon, forming β-SiC during pyrolysis. The β-SiC as whisker forms showed the rod structures, and they caused higher surface area as confirmed by FESEM images in Figure 4.1e. However, once the temperature of pyrolysis was as high as 1700 °C, the BET surface area and pore volume decreased to 25.48 m^2/g and 0.04 cm^3/g, respectively. This was due to the β-SiC as whisker forms were sintered and SiC grains were getting bigger. The results indicated that the optimum pyrolysis temperature of RH was 1500 °C to retain the higher surface area.

The 10wt% of Ni was loaded to SiC supports, confirmed by SEM-EDS mapping as shown in Figure 4.6 and Table 4.2. After loading Ni, the isotherms remained type IV isotherms with a hysteresis loop, suggesting a porous material. The BET surface areas of 10%Ni/SiC1300, 10%Ni/SiC1500, and 10%Ni/SiC1700 increased to 27.07, 83.72, and 31.80 m^2/g, respectively, due to Ni particles were distributed on the SiC support surfaces and some particles may possess inside the pores. However, SiC-com support was a non-porous material, as mentioned before. Therefore, the BET surface area of 10%Ni/SiC-com decreased to 4.47 m^2/g after Ni impregnation because Ni particles on the surface area were easily sintered without pores.

Table 4.2 Physical properties of supports and catalysts.

Samples	S_{bet_a} (m^2/g)	Vp_b (cm^3/g)	Pore size$_c$ (Å)	Ni loading$_d$ (%wt)	Ni particle sizes (nm)
SiC1300	19.20	0.03	56.62	-	-
SiC1500	64.79	0.13	77.69	-	-
SiC1700	25.48	0.04	65.42	-	-
SiC-com	5.93	0.00	-	-	-
10%Ni/SiC1300	27.07	0.05	69.22	9.72	23.6
10%Ni/SiC1500	83.72	0.16	76.17	9.52	12.4
10%Ni/SiC1700	31.80	0.06	78.49	10.73	13.7
10%Ni/SiC-com	4.47	0.01	7.99	10.15	40.3

a; BET surface area from Brunauer-Emmett-Teller equation, b; Total pore-volume weas calculated from the Barret-Joyner-Halenda (BJH) equation, c; Average pore diameter was calculated from the Barret-Joyner-Halenda (BJH) equation, and d; The amount of Ni loading was detected from SEM-EDS mapping.
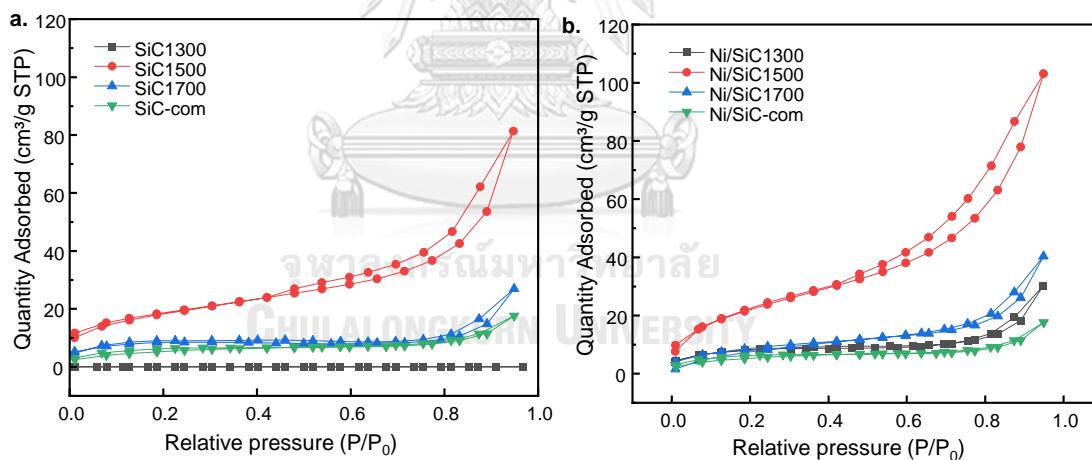
Figure 4.4 N$_2$ adsorption–desorption isotherm of the SiC supports after pyrolysis.

4.1.1.4 Morphology of catalysts and distributions of Ni particle sizes

The surface areas of SiC1300 and SiC-com were smaller than those of SiC1500 and SiC1700, as shown in Table 4.2. The lower surface area caused Ni particles to have less interaction area with SiC supports, and the Ni particles agglomerated themselves when they were at a high concentration of nickel nitrate solution. This causes Ni particle sizes of 10%Ni/SiC1300 and 10%Ni/SiC-com were

larger than that of 10%Ni/SiC1500 and 10%Ni/SiC1700 as shown in the histograms in Figure 4.5. To compare Ni particle sizes from the largest to smallest, there were 10%Ni/SiC-com > 10%Ni/SiC1300 > 10%Ni/SiC1700 > 10%Ni/SiC1500, which were 40.3 > 23.6 > 13.7 > 12.4 nm, respectively, as shown in Table 4.2. The 10%Ni/SiC1500 and 10%Ni/SiC1700 showed more uniform Ni particle size distribution, compared to that of 10%Ni/SiC1300 and 10Ni/SiC-com. The Ni particle size distributions were analyzed from the ImageJ software (N=100). There were also weak interactions between Ni and SiC surfaces from the wetness impregnation method. Therefore, after calcination at 700 °C, some Ni particles were released from the SiC surfaces, and the rest of the Ni particles were aggregated, mildly affecting the dispersion of Ni particles. These results are in agreement with those obtained by Kim *et al, 2012* [69].
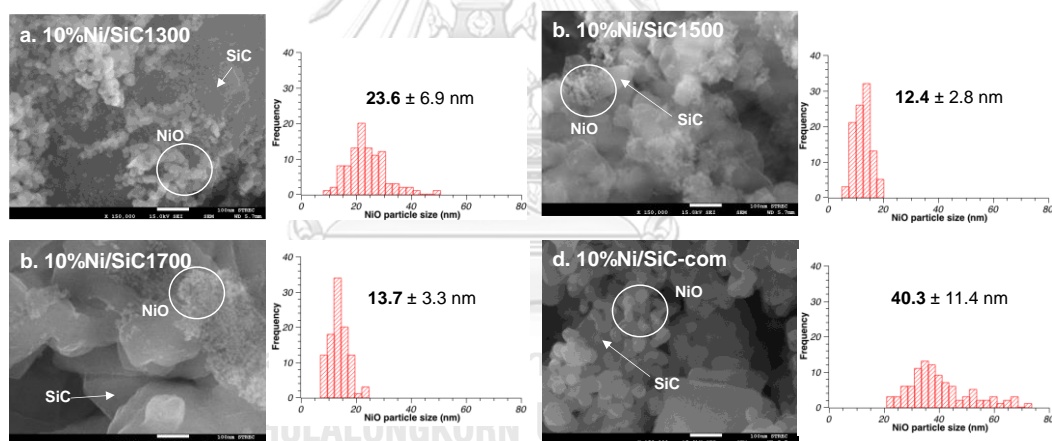
Figure 4.5 FESEM images of calcinated catalysts and their NiO size distribution: a. 10%Ni/SiC1300, b. 10%Ni/SiC1500, c. 10%Ni/SiC1700, and d. 10%Ni/SiC-com.
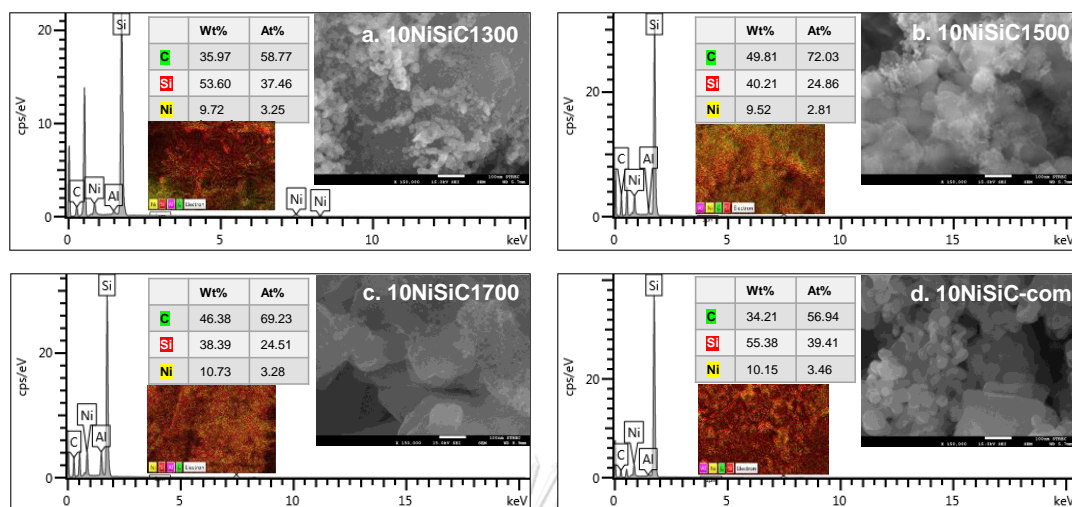
Figure 4.6 SEM-EDS mapping of as-prepared Ni/SiC catalysts.

4.1.2 Catalytic performance

The catalytic performance of prepared catalysts was investigated with different parameters, which were Ni loading amounts, reaction temperatures, steam/carbon molar ratios, and feed rate, to optimize the catalytic activity of FSR. In this research, Ni/SiC1500 was applied to study the effect of each parameter.

4.1.2.1 The influence of Ni loading amount

Figure 4.7 illustrated the gas conversion of fusel oil, hydrogen yield, and product distribution of Ni/SiC1500 with different Ni loading amounts at 700 °C, S/C of 9. It was observed that loading 5wt% of Ni on catalyst support exhibited only 26% of fusel oil conversion and 4% of hydrogen yield. This was because the percentage of Ni active sites may be too low. The 10wt%Ni on catalyst support showed fusel oil conversion at 93% and hydrogen yield at 36%, while those of 15wt% presented at 82% and 32%, respectively. This was probably due to an increase in metal loading may lead to metal agglomeration, causing the decrease in metal active sites. The product distribution of 10wt%Ni and 15wt%Ni displayed higher selectivity of CO and CO_2 but smaller, CH_4 and C_2H_4, compared to those of 5wt%. This supported the C-C and C-H cleavage bonding of nickel properties. From these results, loading Ni at 10wt% was considered for catalysts.

Figure 4.7 Gas conversion of fusel oil, hydrogen yield, and product distribution of Ni/SiC1500 with different Ni loading amounts. The reaction conditions; 700 °C, S/C of 9/1, feed rate at 0.04 ml/min.

4.1.2.2 The influence of reaction temperatures

Figure 4.8 showed the catalytic performances in FSR toward gas conversion of fusel oil, hydrogen yield, and product distribution of Ni/SiC1500 with different reaction temperatures ranging from 600-800°C. The FSR at low temperatures, 600 and 650 °C, showed the low gas conversion of fusel oil and low hydrogen yield at approximately 20% and 10%, respectively. When the temperature reached 700 °C, the gas conversion of fusel oil increased to 93% and the hydrogen yield also rose to 34%. However, when further increased temperature to 750 °C, the catalyst exhibited lower gas conversion of fusel oil and hydrogen yield at 77% and 22%, respectively. Similarly, the catalyst revealed 65% of gas conversion of fusel oil and 16% hydrogen yield at 800 °C. According to the composition of fusel oil as a biomaterial base and mixed alcohol, FSR produces carbon formation via the Boudouard reaction and thermal deposition of methane at high temperatures. Due to the coking, the catalyst is deactivated by decreasing active sites, and it leads to reduce the yield of H_2 production. Hence, performing the FSR at 700 °C could be the suitable reaction temperature to produce hydrogen yield.

Figure 4.8 Gas conversion of fusel oil, hydrogen yield, and product distribution of Ni/SiC1500 with different temperatures at 600-800 °C. The reaction conditions; 10wt%Ni loading, S/C of 9, W/F of 15 $g_{catalyst}.h/mol^{-1}$.

4.1.2.3 The influence of steam/carbon molar ratio

The influence of the S/C molar ratio on the catalytic performance of steam reforming reaction Ni/SiC1500 was studied at 700 °C with the different S/C ratios of 5, 9, 12, and 15 as shown in Figure 4.9. The highest fusel oil gas conversion of 93% and hydrogen yield of 34% was achieved at an S/C ratio of 9. It can be clearly seen that S/C of 15 produced a large amount of CO_2 but a small amount of CH_4. This was because an increase in S/C ratio promoted steam reforming of methane and WGS but not methanation. Although the product distributions of 9 and 12 were similar, the fusel conversion and hydrogen yield from S/C of 12 presented lower percentages. It can be concluded that high ratios of steam would be unfavorable for the hydrogen production in this study. Therefore, the S/C of 9 exhibited the highest hydrogen yield as well as fusel oil gas conversion.
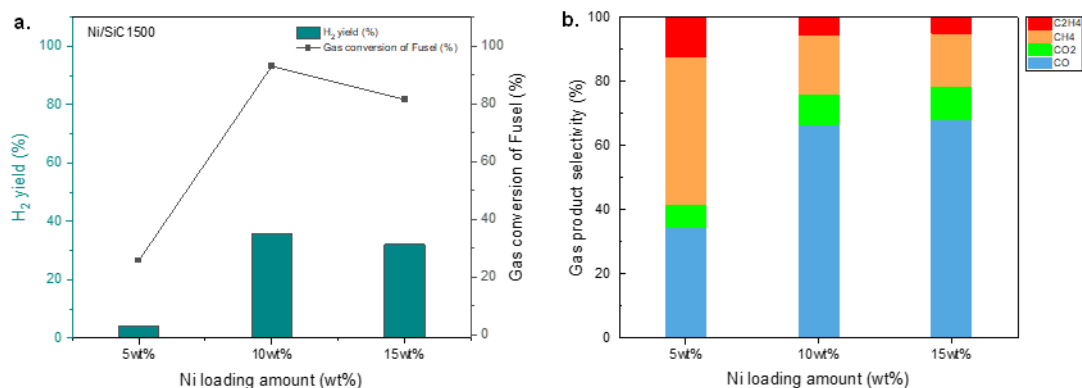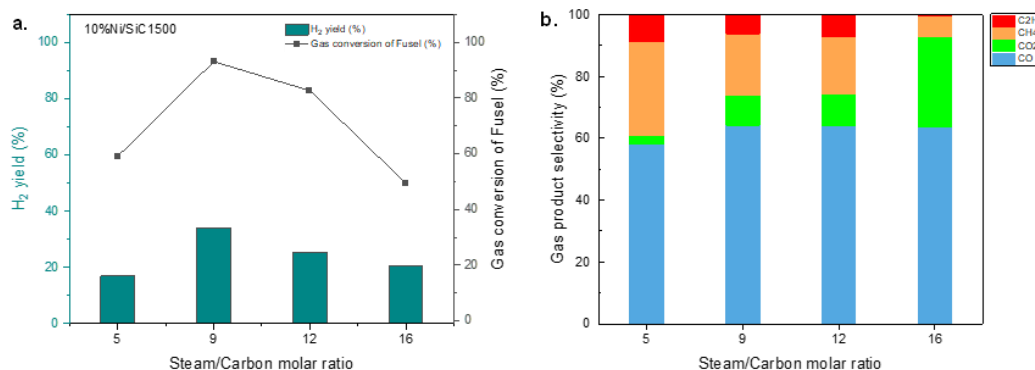
Figure 4.9 Gas conversion of fusel oil, hydrogen yield, and product distribution of Ni/SiC1500 with different S/C molar ratio. The reaction conditions; 700 °C, 10wt%Ni loading, W/F of 15 $g_{catalyst}$.h/mol^{-1}.

4.1.2.4 The influence of space time

The different W/F was varied by changing the feed flow rate. Figure 4.10 exhibited that at low space-time at 9 $g_{catalyst}$.h.mol^{-1}, the fusel oil gas conversion was very low, at 30%, because fusel oil and steam had high velocities when going through the active sites of the catalyst. This could be explained that the reactants had a short time to interact between their molecules. Then, at the space-time at 15 $g_{catalyst}$.h.mol^{-1}, the fusel oil gas conversion significantly increased to 92% due to the fact that a large W/F meant a longer time for interaction between fusel oil and steam. Therefore, steam reforming of methane was favored, resulting in a high hydrogen yield of 42% and 70% of CO selectivity. At the space time at 25 $g_{catalyst}$.h.mol^{-1}, the fusel oil gas conversion slightly dropped 88%, similar to hydrogen yield, decreasing to 22%. The long period of interaction between fusel oil and steam not only favored the steam reforming of methane to perform CO but also caused the Boudouard reaction and thermal deposition of methane, which lead to produce carbon deposition. Hence, the space-time at 9 $g_{catalyst}$.h.mol^{-1} presented good catalytic performances regarding hydrogen yield and fusel oil gas conversion.
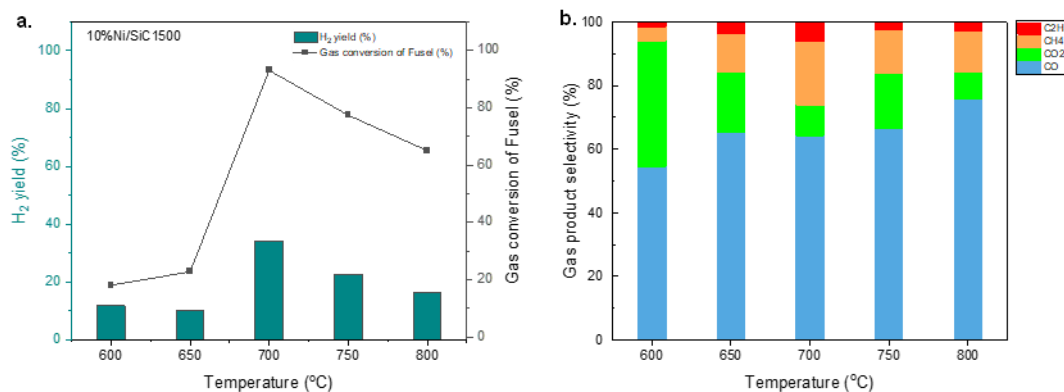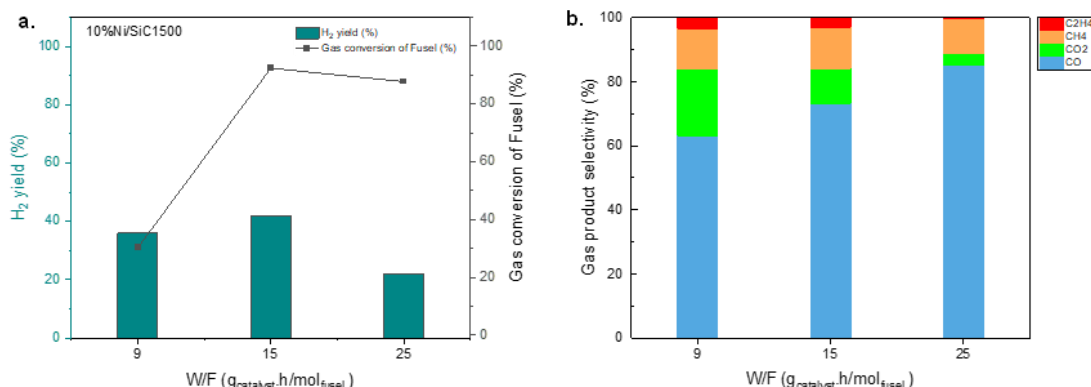
Figure 4.10 Gas conversion of fusel oil, hydrogen yield, and product distribution of Ni/SiC1500 with different W/F. The reaction conditions; 700 °C, 10wt%Ni loading, S/C of 9.

4.1.2.5 The influence of different SiC supports

The optimum conditions, which were 10wt%Ni loading, 700 °C, S/C of 9, and W/F of 15 $g_{catalyst}.h.mol^{-1}$, were applied to FSR over catalysts with different SiC supports, obtained from RH. The performances of the Ni/SiC catalysts on steam reforming of fusel oil were studied at an FSR reaction for 300 min. The gas conversion and hydrogen yield, obtained from each catalyst, are presented in Figure 4.11a and 4.11b. The fusel gas conversion obtained with all Ni/SiC catalysts reached an equilibrium state after 90 min of reaction. However, the steam reforming of fusel oil over 10%Ni/SiC1300 showed that the reaction was running for only 180 min because of the carbon formation blockage inside the reactor, so the gas reactants could not flow through. According to the XRD patterns in Figure 4.2, SiC1300 was not properly pyrolyzed to form SiC, this decreased property of heat transfer of SiC support and caused a large amount of coking. However, steam reforming of fusel oil over 10%Ni/SiC1500 presented good catalytic performances. After 90 min of reaction, the fusel oil gas conversion remained over 90% throughout 300 min and the hydrogen yield remained at 29%. It was because SiC1500 support was a β-SiC form, showing a good heat transfer and high thermal conductivity, which benefitted reducing coke formation during steam reforming. Noh *et al*, 2019 [70] also observed that Ni-based catalysts with modified supports containing SiC enhanced the thermal conductivity and coke formation resistance for effective hydrogen production by

steam reforming of methane. The catalytic activities of 10%Ni/SiC1700 showed fluctuated gas conversion, 58-87%, and hydrogen yield dropped from 56 to 25% during 300 min time on steam. The 10%Ni/SiC-com catalyst presented high gas conversion, 99% at 210 min of reaction, after that, it dramatically decreased to 46% at 300 min, similar to hydrogen yield, which gradually decreased from 62% at 90 min to 9% at 300 min of the FSR.

The selectivity of gas products also exhibited that CO was produced significantly as presented in Figure 4.11 (c, d, e, f). Both 10%Ni/SiC1500 and 10%Ni/SiC1700 presented similar selectivity of CO, about 50% for 300 min of FSR due to the reverse water gas shift and steam reforming of CH_4. These results further support the experimental work, performed by Le-Mai et al, 2022 [71].
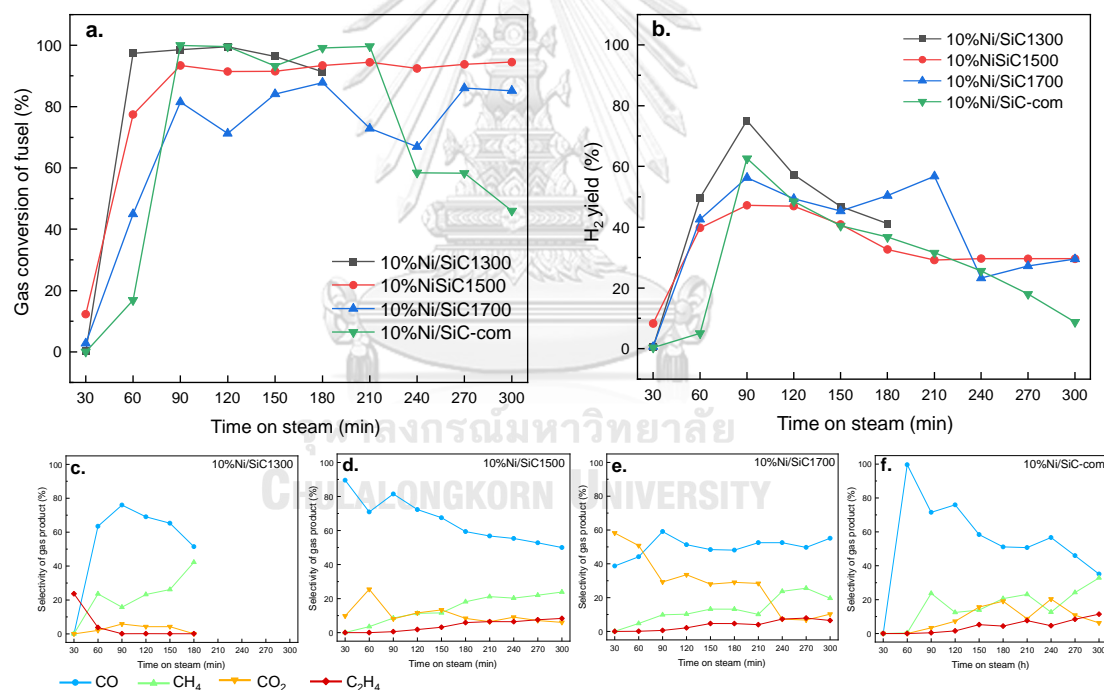
Figure 4.11 a. Gas conversion of fusel oil (%), b. Hydrogen yield (%), Selectivity of gas products (%) of c.10%Ni/SiC1300, d.10%Ni/SiC1500, e.10%Ni/SiC1700, f.10%Ni/SiC-com of all Ni/SiC catalysts (FSR at 700 °C for 300 min, S/C of 9, W/F of 15 $g_{catalyst}.h/mol^{-1}$).

4.1.3   Characterization of spent catalysts
4.1.3.1 Morphological and chemical properties

The FESEM images in Figure 4.12A presented morphologies of the spent catalyst after FSR at 700 °C for 300 min, showing the sintering of Ni and carbon formation. The XRD patterns of the spent catalysts are presented in Figure 4.12B. The diffraction peak at a 2θ of 26° was the carbon nanotubes (CNTs) as carbon formation on the surface of spent catalysts. The peaks, located at a 2θ of 44.5° and 52° for all spent catalysts, were assigned to metallic Ni, which may sinter during catalysis. The XRD peak positions were similar to the result, obtained by Łamacz *et al*, 2020 [72]. This evidence indicated that steam reforming of fusel oil over Ni/SiC generated coking formation in the form of CNTs, confirmed by XRD in Figure 4.12B.
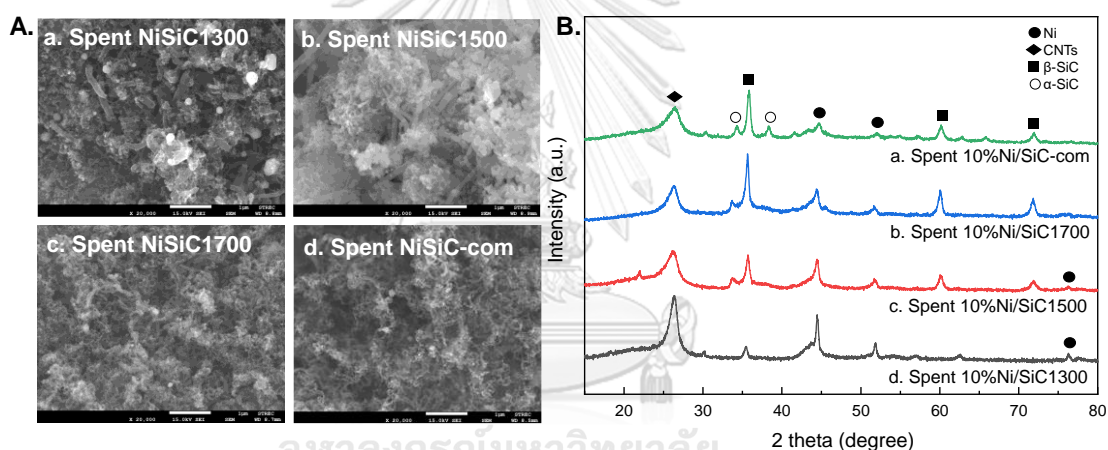
Figure 4.12 A. FESEM images and B. XRD patterns of spent catalysts after FSR at 700 °C for 300 min: a. spent 10%Ni/SiC1300, b. spent 10%Ni/SiC1500, c. spent 10%Ni/SiC1700, and d. spent 10 %Ni/SiC-com.

4.1.3.2 Carbon formation

The TGA profiles of the spent catalysts after 300 min running steam reforming of fusel oil showed the percentage of weight loss, and they were attributed to the combustion of coke deposition, shown in Figure 4.13. The spent 10%Ni/SiC1500 presented 44.3 wt%, the smallest amount of coke according to smallest %weight loss, followed by 62.8 wt% of the spent 10%Ni/SiC1700, while the amount of coking of the spent 10%Ni/SiC1300 and spent 10%Ni/SiC-com were larger and similar (at

about 75 wt%). The results suggested that less carbon deposited was formed on the 10%Ni/SiC1500 surfaces because β-SiC support enhances the thermal conductivity and coke formation resistance. This should be the reason why the gas conversion level after 90 min of reaction was unchanged and remained constant for all of the 300 min period on steam. Moreover, all spent catalysts presented a weight loss step in the temperature 600-700 °C, indicating the combustion of coke, which were filamentous carbon forms as presented in FESEM images in Figure 4.12A. Trane *et al, 2012* [31] also observed that filamentous carbons were from the decomposition of hydrocarbon between 500-700 °C.
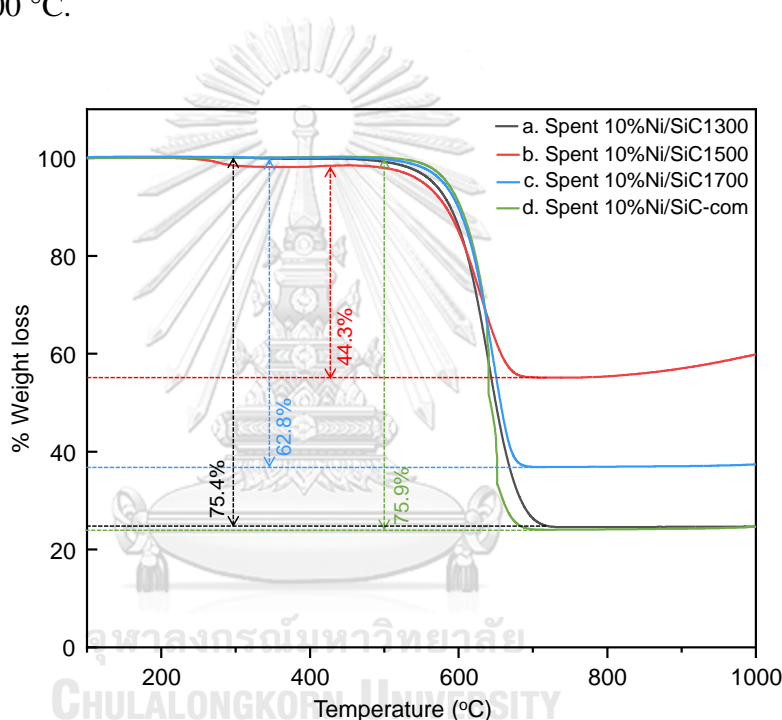
Figure 4.13 The TGA profiles of the spent Ni/SiC catalysts after FSR at 700 °C for 300 min; a. spent 10%Ni/SiC1300, b. spent 10%Ni/SiC1500, c. spent 10%Ni/SiC1700, and d. spent 10%Ni/SiC-com.

4.2 Hydrogen production by ESR over Ni/ZSM-5 nanosheet

4.2.1 Characterization of as-prepared catalyst

4.2.1.1 Chemical properties

The as-prepared Ni/ZSM-5 catalysts were characterized by the XRD technique to confirm the identification of as-prepared catalysts, and the results were displayed in Figure 4.14. The diffractions characteristic peaks of ZSM-5 were observed at 2θ of

8.1°, 9.0°, 14.1°, 15.0°, 23.3°, 24.2°, 24.6°, and 45.0° as reported by Pérez-Page *et al*, 2016 [73]. After loading Ni, the catalysts formed NiO due to the calcination in the air. The characteristic peaks of NiO were basically located at 37.2°, 43.3°, and 62.4°. These results agree with those obtained by Tang *et al*, 2014 [74].
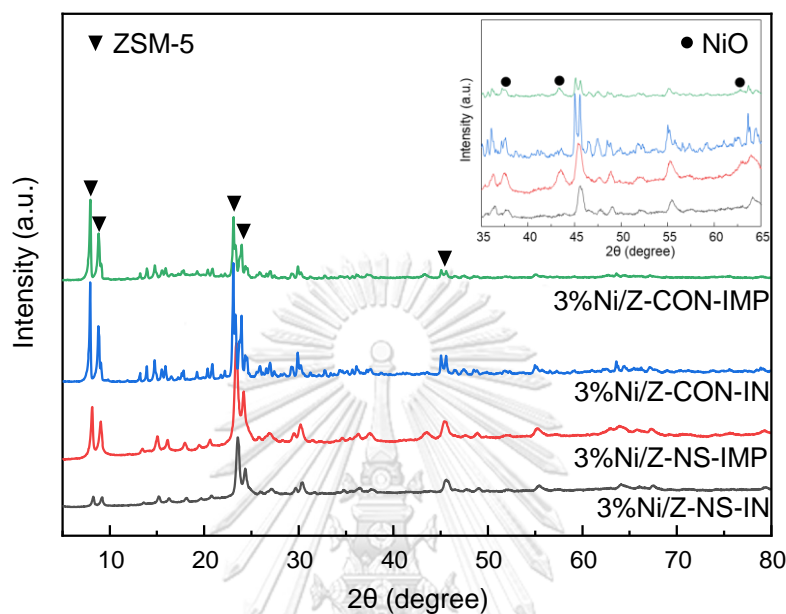
Figure 4.14 XRD pattern of calcinated Ni/ZSM-5 catalysts.

Figure 4.15 presented the chemical surface of Ni/ZSM-5 catalysts, prepared by different methods, using the XPS technique. The Ni/Z-NS-IN showed binding peaks indicated at 855.1, 861.2, 872.5, and 878.7 eV, corresponding to the Ni $2p_{3/2}$, satellite Ni $2p_{3/2}$, Ni $2p_{1/2}$, and satellite Ni $2p_{1/2}$, respectively, while those of Ni/Z-NS-IMP were at 853.2, 858.8, 870.6, and 876. eV. The binding energies of Ni/Z-NS-IN were a bit higher than those of Ni/Z-NS-IMP. Similarly, Ni/Z-CON-IN also showed a similar XPS pattern, Ni $2p_{3/2}$ and Ni $2p_{1/2}$ were shifted to higher binding energies, compared to those of Ni/Z-CON-IMP. It could be concluded that the *in-situ* catalyst reflects stronger metal-support interactions. Moreover, the agglomeration of NiO would rather take place in impregnation catalysts, leading to weaker interactions between metal and supports. However, the XPS patterns of all nickel catalysts towards the Ni 2p were attributed to Ni^{2+} in NiO on these fresh nickel catalysts. The results are in agreement with those obtained by Cui *et al*, 2020 [75]. In addition, Ni/Z-CON-IMP displayed the shoulder peaks of Ni $2p_{3/2}$ and Ni $2p_{1/2}$, corresponding to the Ni-OH species. This

could be because of the nickel incorporation into the ZSM-5 structure, forming Ni-OH-Si linkages as reported by Hu *et al*, 2018 [76].
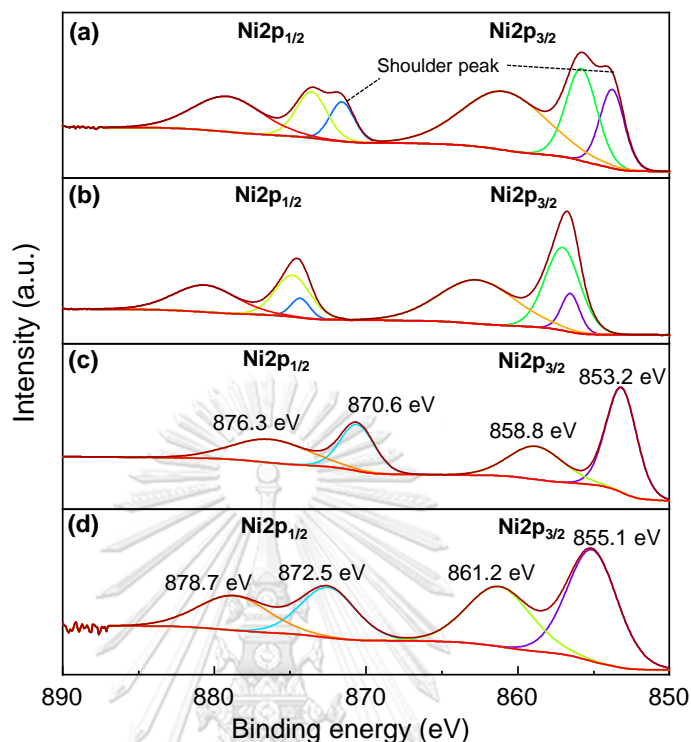
Figure 4.15 XPS spectra of different catalysts: (a) Ni/Z-CON-IMP, (b) Ni/Z-CON-IN, (c) Ni/Z-NS-IMP and (d) Ni/Z-NS-IN.

4.2.1.2 Metal-support interaction

The H_2-TPR was studied to investigate the metal-support interaction. The H_2-TPR spectra of the catalysts were shown in Figure 4.16a. There was for NiO reduction to form metal Ni, as shown in Eq. (4.1). Ni/Z-NS-IN and Ni/Z-NS-IMP exhibited the H_2-reduction temperature in α-NiO (300-500 °C) and β-NiO (500-650 °C) ranges, which were weak NiO and bulk NiO species, respectively, located outside the mesopore of ZSM-5 supports. They also showed the H_2-reduction in the range of γ-NiO (650-850 °C), suggesting that NiO species strongly interacted with ZSM-5 support inside the mesopore. Ni/Z-CON-IN exhibited a curve of the H_2-reduction temperature in the γ-NiO range due to encapsulated Ni particles in the Z-CON structure with strong interactions as confirmed by higher binding energies from XPS result in Figure 4.15. In contrast, Ni/Z-CON-IMP showed a curve in the α-NiO area according to weak NiO deposited on the Z-CON surface. Similar H_2-TPR results can

be referred to the previous research investigated by Sarkar *et al*, 2012 [77]. In this research, all catalysts performed the H_2-reduction at 500 °C to reduce both α-NiO and β-NiO, indicating the reduction of free and weak interaction of NiO species with the support. Table 4.3 reports the total amount of H_2-consumptions of Ni/Z-NS-IN (0.260 mmol/g), and Ni/Z-NS-IMP (0.218 mmol/g) are higher than that of Ni/Z-CON-IN (0.199 mmol/g), and Ni/Z-CON-IMP (0.134 mmol/g). This could be correlated with different mesopore volumes between Z-NS and Z-CON as the data shown in Table 4.4. Ni/Z-NS-IN and Ni/Z-NS-IMP had much larger amounts of mesopore volume, which causes a higher opportunity to reduce NiO species by consuming H_2, compared to Ni/Z-CON-IN and Ni/Z-CON-IMP.

Moreover, reducing a catalyst at a high temperature leads to nickel aggregation and loss of surface area. This also decreases catalytic performance in terms of hydrogen yield. Figure B1 (Appendix B) presented the influence of reducing the temperature at 400 °C, 500 °C, and 650 °C on ESR catalytic performances. The findings showed that reducing the catalyst at 500 °C gave 65% of the highest hydrogen yield at the reaction temperature at 600 °C while reducing the catalyst at 650 °C exhibited below 20% of hydrogen yield at the same reaction temperature.

$$NiO + H_2 \longrightarrow Ni° + H_2O \qquad (4.1)$$
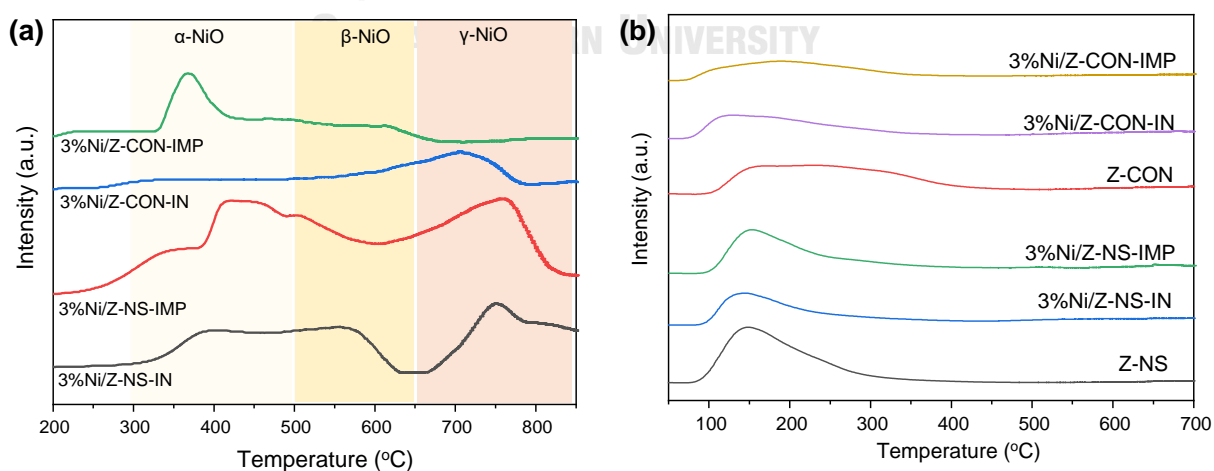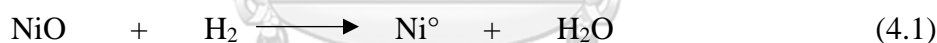
Figure 4.16 (a) H_2-TPR spectra and (b) NH_3-TPD profiles of Ni/ZSM-5 catalysts.

Table 4.3 The total amount of H_2 consumption and the total acid amount on ZSM-5 supports and their nickel catalysts

Catalysts	Total amount of H_2 consumption (mmol/g)	Total acid amount (mmol/g)
Z-NS	0.086	0.275
3%Ni/Z-NS-IN	0.260	0.153
3%Ni/Z-NS-IMP	0.218	0.163
Z-CON	0.021	0.254
3%Ni/Z-CON-IN	0.199	0.146
3%Ni/Z-CON-IMP	0.134	0.116
Z-COM-25	0.095	0.545
3%Ni/Z-COM-25	0.750	0.829

The acidic properties of supports and catalysts were studied by NH_3-TPD analysis as shown in Figure 4.16b and the total acid amounts were reported in Table 4.3. The NH_3-TPD profiles of Z-NS and their nickel catalysts indicated weak acid sites, located in the temperature range of 50-300 °C, which can be attributed to the Al content and the desorption of physisorbed NH_3 as reported by Hu *et al*, 2018 [76]. The total amounts of acid of Z-NS, Ni/Z-NS-IN, and Ni/Z-NS-IMP were 0.275 mmol/g, 0.153 mmol/g, and 0.163 mmol/g, respectively. The acid amounts were observed to have a lower amount of weak acidity after loading nickel, compared to that of bare Z-NS, it is probably due to the interaction of Ni with the silanol group of the support as Saini *et al*, 2022 [78] mentioned in their research. The Z-CON and their nickel catalysts indicated the NH_3-TPD profiles between 80-350 °C, representing weak acid sites due to the weak NH_3 adsorption. The total amounts of acid of Z-CON, Ni/Z-CON-IN, and Ni/Z-CON-IMP were 0.254 mmol/g, 0.146 mmol/g, and 0.116 mmol/g, respectively. The acid amount decreased after loading nickel, it could be the same phenomenon with Z-NS and their catalysts as previously mentioned. Moreover, Shetsiri *et al*, 2019 [79] studied the effect of catalyst acidity on the ESR. They found that the catalyst with strong acid sites can promote coke formation. Therefore, the strong acid sites are disadvantageous to producing hydrogen via ESR.

4.2.1.3 Thermal properties

TGA thermograms of the Z-NS, Z-CON, and their nickel catalysts were measured in the temperature range from 50 to 850 °C and the thermogravimetric curves are shown in Figure 4.17. The initial weight loss region below 200 °C were determined to be weakly physisorbed water interlayer molecules, which can mobile and freely bounded. The second range of 300-500 °C was attributed to strongly bonded water molecules of the interlayer structure. The result is in agreement with those obtained by Ayodel, 2017 [80]. From the TGA profiles, there were no essential weight loss peaks shown due to the ZSM-5 framework is thermally stable up to 930 °C. Pérez-Page *et al*, 2016 [73] observed that the phase transitions of zeolite would change when the temperature is above 1500 °C.
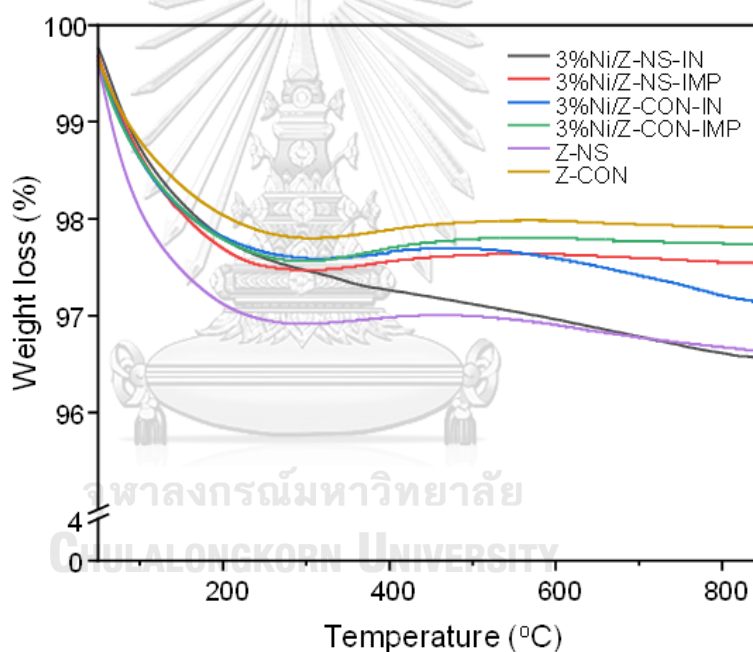
Figure 4.17 Thermal analysis of ZSM-5 supports and Ni/ZSM-5 catalysts.

4.2.1.4   Morphology and chemical composition

Figure 4.18 showed the morphology of different ZSM-5 supports and their nickel catalysts with the same amount of 3 wt% Ni loading, including Ni particle size distributions and a HAADF image. In Figure 4.18a, the Z-NS supports were formed by several thin sheets, grown in one direction and the size of the entire particle was about 200 nm. The thickness of each lamellar stacking, composed of ZSM-5 framework, was about 10-20 nm. In contrast, Z-CON had a sphere-shaped particle

with diameters in the range of 500-700 nm as shown in Figure 4.18d. TEM investigation clearly indicated that there is some correlation between the SDA molecular size. There were different SDAs, TBAOH, and TPAOH, used for the synthesis of Z-NS and Z-CON, respectively. The Z-NS was templated by the larger SDA, TBAOH, exhibiting larger pore size distributions as shown in Figure 4.20b. To synthesize Z-CON by using TPAOH, the processes required longer treatment and higher temperatures to induce substantial crystallinity as a sphere-shaped particle. The catalysts loaded a similar amount of Ni at 3wt%. To compare Ni particle sizes from the smallest to largest, there were Ni/Z-NS-IN < Ni/Z-NS-IMP < Ni/Z-CON-IMP, which were 5.6 < 7.8 < 31.7 nm, respectively. Although, the TEM image of Ni/Z-CON-IN indicated no Ni particles, the inserted HAADF image in Figure 4.18e proved that Ni particles distributed over the Z-CON. In addition, the Ni/Z-NS-IN and Ni/Z-NS-IMP showed more uniform Ni particle size distribution, compared to that of Ni/Z-CON-IMP. The Ni particle size distributions were analyzed from the ImageJ software (N=100).

The amount of Ni loading of all catalysts was proved by the ICP-OES technique, the catalysts were loaded Ni at 3wt% and the results showed the actual amount between 2.4-3.0 wt%, displayed in Table 4.4. Besides, the spatial distributions of O, Al, Si, and Ni elements on the prepared catalysts were further studied by the SEM-EDS element mapping analysis, as confirmed by Figure 4.19, the Ni active sites had successfully been loaded over all these catalysts. In addition, Figure 4.19c could be confirmed that the nickel particles had been efficiently encapsulated into the Z-CON, although there was no evidence of nickel on the TEM image of the Ni/Z-CON-IN catalyst.
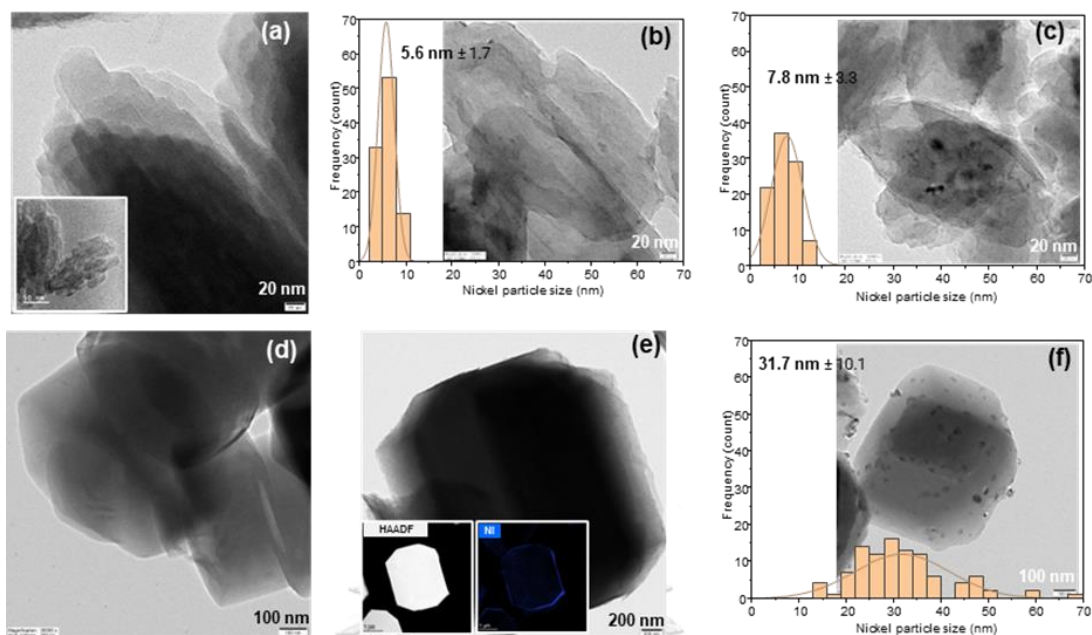
Figure 4.18 TEM images of ZSM-5 supports and prepared catalysts regarding Ni particle size distribution and HAADF: (a) Z-NS, (b) Z-CON, (c) 3%Ni/Z-NS-IN, (d) 3%Ni/Z-NS-IMP, (e) 3%Ni/Z-CON-IN and (f) 3%Ni/Z-CON-IMP.
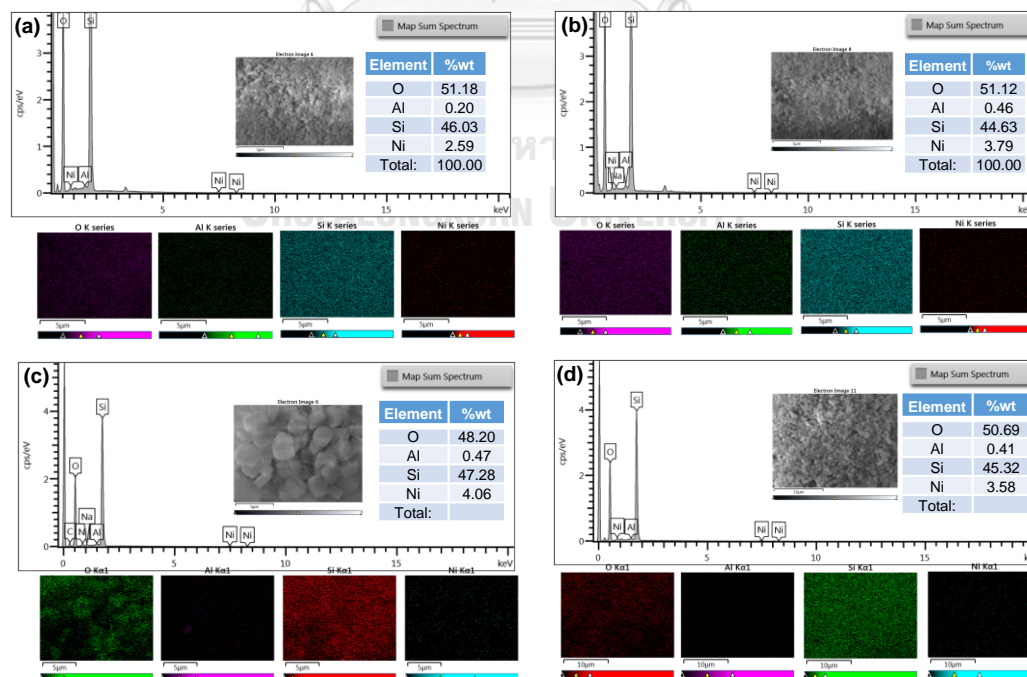
Figure 4.19 SEM-EDS mapping analysis of fresh catalysts: (a) 3%Ni/Z-NS-IN, (b) 3%Ni/Z-NS-IMP, (c) 3%Ni/Z-CON-IN and (d) 3%Ni/Z-CON-IMP.

4.2.1.5 Surface area and porosity

The N_2 adsorption-desorption technique was employed to determine the porosity of ZSM-5 supports and their nickel catalysts. The N_2 adsorption-desorption isotherms and pore size distributions are presented in Figure 4.20 and the pore properties are summarized in Table 4.4. As shown in Figure 4.20a, all the ZSM-5 supports and their nickel catalysts showed the inflection points of the catalysts at relative pressure from 0 to 0.1, indicating the fingerprint of a microporous structure. In addition, their adsorption-desorption isotherms revealed the type IV isotherms with the hysteresis loop, suggesting all the samples indicated that both micropore and mesopore exist in the structures as reported by Feng *et al*, 2019 [81].

The N_2 adsorption-desorption isotherms of their BET surface areas range from 320 m^2/g to 390 m^2/g, and their pore size distributions are in the range of 1.8-2.0 nm, displayed in Figure 4.20b. Although the pore size of these catalysts after loading nickel did not show significant change, it indicated that the catalyst structures did not shrink or collapse during the synthesis process and provided excellent thermal stability as previously mentioned on thermal decomposition in TGA profiles in Figure 4.17. In addition, the Z-NS, and their nickel catalysts; Ni/Z-NS-IN and Ni/Z-NS-IMP, had approximately half smaller external surface areas, compared to Z-CON and their nickel catalysts.

However, the adsorption-desorption isotherms of the Z-CON and their nickel catalysts; Ni/Z-CON-IN and Ni/Z-CON-IMP showed a hysteresis loop at a relative pressure from 0.1 to 1.0, suggesting that the mesopores were proved the capillary condensation of nitrogen in the mesoporous channels with multilayer adsorption. Their mesopore volume is very small (0.1 cm^3/g) due to the mesopores originating from voids between the aggregation of Z-CON particles as it can refer to the same results from Meng *et al*, 2017 [50]. Those of Z-NS support and their catalysts; Ni/Z-NS-IN and Ni/Z-NS-IMP indicated a remarkable hysteresis loop at a relative pressure, which typically was from 0.45 to 1.0, suggesting the existence of mesopores, which was derived from the interparticle voids between the stacked lamellas of nanosheet. These N_2 adsorption-desorption results of Z-NS are in agreement with the previous research by Kore *et al*, 2014 [82] and Feng *et al*, 2020 [83].
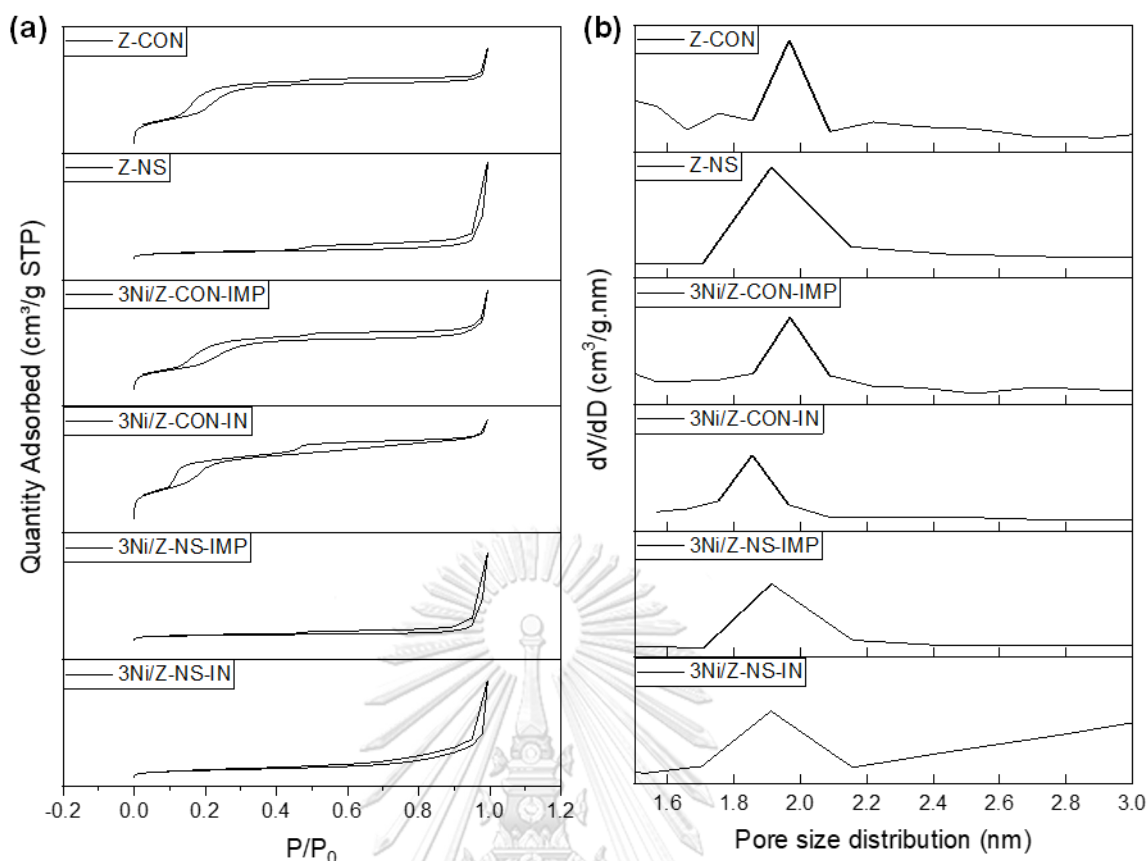
Figure 4.20 (a) N₂-adsorption-desorption isotherms, and (b) pore size distributions of ZSM-5 supports and their nickel catalysts.

Table 4.4 Physicochemical properties of ZSM-5 supports and catalysts.

Materials	$^{a}S_{BET}$ (m²/g)	$^{b}S_{ext}$ (m²/g)	$^{c}V_{total}$ (cm³/g)	$^{d}V_{micro}$ (cm³/g)	$^{e}V_{meso}$ (cm³/g)	^{f}Ni (wt%)
Z-NS	376	73	0.638	0.117	0.521	-
3%Ni/Z-NS-IN	322	72	0.514	0.097	0.417	3.04
3%Ni/Z-NS-IMP	330	47	0.570	0.108	0.462	2.62
Z-CON	385	154	0.200	0.088	0.112	-
3%Ni/Z-CON-IN	390	149	0.221	0.103	0.118	2.68
3%Ni/Z-CON-IMP	357	145	0.201	0.079	0.122	2.42

$^{a}S_{BET}$ is BET surface area (P/P₀ = 0.05−0.25)

$^{b}S_{ext}$ is the external surface area, determined according to the t-plot method

$^{c}V_{total}$ is the total pore volume calculated at P/P₀ = 0.99

$^{d}V_{micro}$ is the micropore volume calculated from t-plot method

$^{e}V_{meso}$ is the mesopore volume, calculated by using $V_{meso}=V_{total}-V_{micro}$ was calculated from N_2 uptake at a relative pressure (P/P₀) of 0.99

^{f}Ni is the amount of Ni loading, determined by using ICP-OES analysis

4.2.2 Catalytic performances

4.2.2.1 The influence of temperatures

The effect of temperatures of ESR on the EtOH conversion, H_2 yield, and gas product distribution of Ni/Z-NS-IN, Ni/Z-NS-IMP, Ni/Z-CON-IN, and Ni/Z-CON-IMP catalysts, studied in the range between 300 and 600 °C, as illustrated in Figure 4.21. When the temperature was increasing, the conversion of EtOH of all catalysts increased significantly. The EtOH conversions on the Ni/Z-NS-IN and Ni/Z-NS-IMP catalysts hit above 80% at 500 °C and reached 100% at 600 °C. In contrast, the complete EtOH conversion over the Ni/Z-CON-IN, and Ni/Z-CON-IMP catalysts could be accomplished at 500 °C and 400 °C, respectively. According to the H_2 yield, when the temperature was at 500 °C, the impregnated catalysts; Ni/Z-NS-IMP and Ni/Z-CON-IMP exhibited a higher H_2 yield, compared to those of *in-situ* catalysts; Ni/Z-NS-IN, and Ni/Z-CON-IN. This was because of the effect of catalyst preparation methods. The impregnated catalysts showed that Ni particles distributed on the external surface as shown in TEM images in Figure 4.18c and 4.18f and could actively interact under ESR at lower temperatures. When the temperature was up to 600 °C, the H_2 yields of all catalysts were about 60%, which were insignificantly different. To investigate the selectivity of carbon gas products, the temperature was increased from 300-600 °C for ESR. At 300 °C, all catalysts revealed a large amount of acetaldehyde (CH_3CHO), which is an intermediate reactant from ethanol dehydrogenation, as mentioned in Eq. (2.16). At 500 °C, CH3CHO was still detected by in-situ catalysts; Ni/Z-NS-IN and Ni/Z-CON-IN because the Ni could not properly interact with ethanol or steam because the majority of Ni are encapsulated inside the pores of ZSM-5 support. However, CH_3CHO would be further converted to other carbon gas products and would be absent at high temperatures. After the temperature increased to 600 °C, there were only three main carbon gas products, which were CO, CH_4, and CO_2.
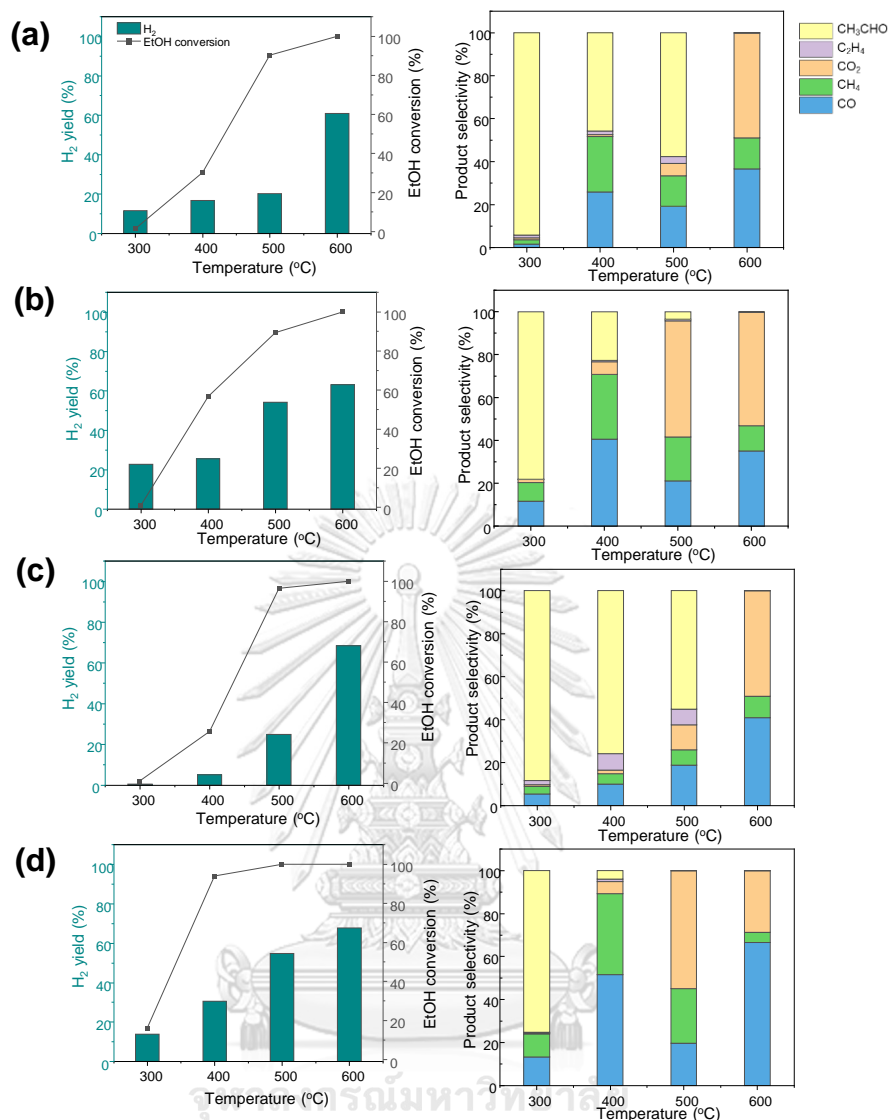
Figure 4.21 Influence of temperature on catalytic performances of ESR at 300-600 °C over (a) Ni/Z-NS-IN, (b) Ni/Z-NS-IMP, (c) Ni/Z-CON-IN, and (d) Ni/Z-CON-IMP.

4.2.2.2 The influence of acidic catalyst

As mentioned before regarding the effect of acidic catalysts on ESR. In the supplementary work, the acidic catalyst was prepared by loading the same amount of nickel on commercial ZSM-5 (Si/Al ratio at 25) by the wet impregnation method. The catalyst was defined as Ni/Z-COM25. Some characterization of Z-COM25 and its nickel catalyst can be found in Figure B2 (Appendix B). The Ni/Z-COM25 catalyst indicated both weak and strong acid sites with a total acid amount of 0.829 mmol/g, which ascribed to Brønsted acid sites according to a large amount of Al content as

shown in Table. 4.3 The ESR catalytic performance of Ni/Z-COM25 showed that the main gas product was ethylene (C_2H_4) due to the acid sites favour dehydration of the ethanol process and C_2H_4 basically leads to carbon formation as seen in Figure 4.22b. Furthermore, the stability test exhibited that hydrogen yield dramatically decreased from 60% to 20% after 24 h of ESR catalysis, while ethylene gas gradually reached 60%, as seen in Figure 4.22c and 4.22d. The TGA of spent Ni/Z-COM25 in Figure B3 (Appendix B) presented the amount of coke at 47wt%, which was approximately three times higher than that of Ni/Z-NS-IN. Hence, the strong acid sites are disadvantageous to producing hydrogen via ESR because it also produces a lot of carbon formation.
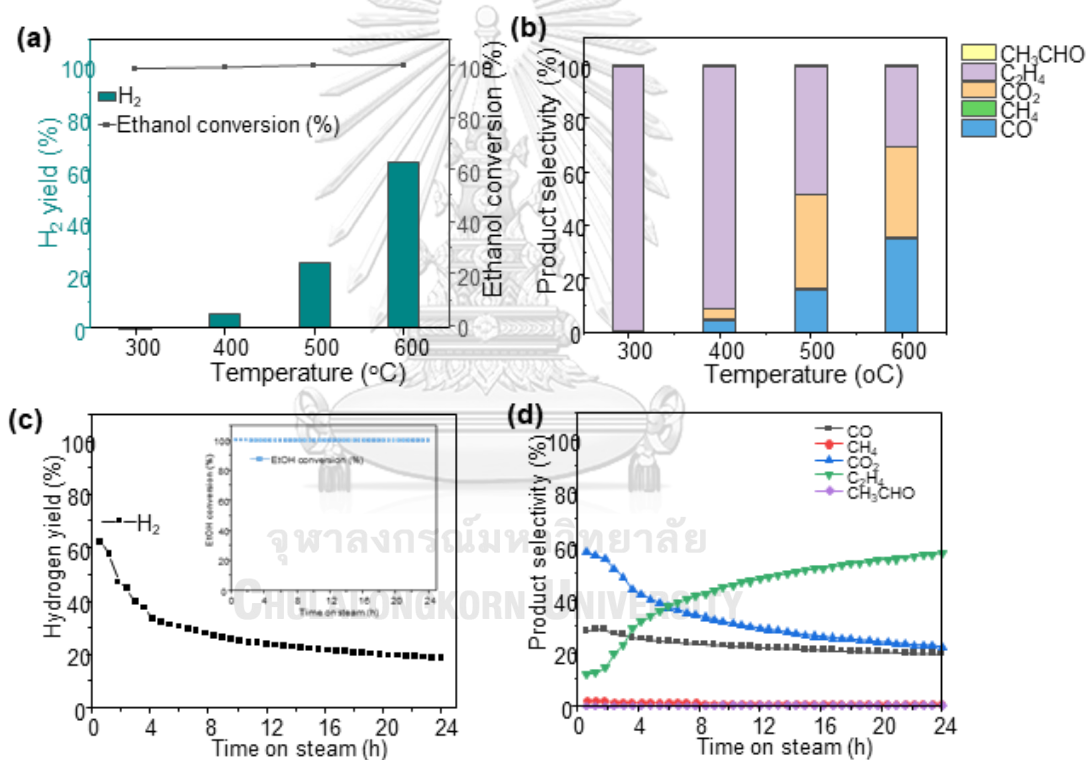
Figure 4.22 (a) EtOH conversion and H_2 yield, and (b) selectivity of gas products on ESR catalytic performance at 300-600 °C, and (c) H_2 yield, and (d) selectivity of gas products on stability test at 550 °C for 48 h.

4.2.2.3 Study of possible surface species (*in-situ* DRIFTS)

To study insight into the possible surface species responsible for the activity and selectivity of ESR, the *in-situ* DRIFTS spectra were collected from the Ni/Z-NS-IN under ESR (Steam/Carbon ratio of 8) at 350 °C. The peaks are stack-plotted at 3 min, 5 min, 10 min, and 15 min as shown in Figure 4.23a. The peaks are insignificantly different, it could be assumed that the ESR over Ni/Z-NS-IN has remained stable. The negative broad hump from 3745 to 3000 cm^{-1} indicated the OH group from the adsorbed water molecules. The CH stretching bands were assigned between 2800 and 3000 cm^{-1}, with the CH stretching (ν), symmetric (s) and asymmetric (as) modes, found at 2950, and 2900 cm^{-1} ($CH_3\nu_{as}$, and $CH_3\nu_s$). The characteristic peak at 2345 cm^{-1} was indicted to CO_2. The species between CO and Ni are assumed in three forms. The hollow structure between CO and Ni was observed at 2100 cm^{-1}, while the bridge structure was at 1950 cm^{-1}. Further, the linear form of CO and Ni was displayed at 1845 cm^{-1}. The shoulder peak at 1750 cm^{-1} was assigned to C=O stretching, confirming the existence of CHO species from acetaldehyde. The shoulder around 1590 cm^{-1} could be assigned to the CO stretching of acetaldehyde, which is rapidly oxidized to form acetate species (HCOO). These results are in agreement with the catalytic performance obtained at low temperatures in the range of 300-400 °C, where the intermediate was acetaldehyde as shown in Figure 4.21. The peak at 1300 cm^{-1} was assumed to be CH bending band from the acetate and the shoulder peaks at 1190 and 1120 were assigned to the ethoxy CO band. Figure 23b exhibited the comparison of *in-situ* DRIFTS spectra between Ni/Z-NS-IN and Ni/Z-CON-IN at 5 min of ESR at 350 °C with a steam/carbon ratio of 8. It could be seen that the DRIFTS spectra revealed similar species under the same condition. The resulting DRIFTS spectra were interpreted on the basis of the relevant works of literature for band assignments, reported by Lui *et al*, 2022 [84] and Xu *et al*, 2013 [85].
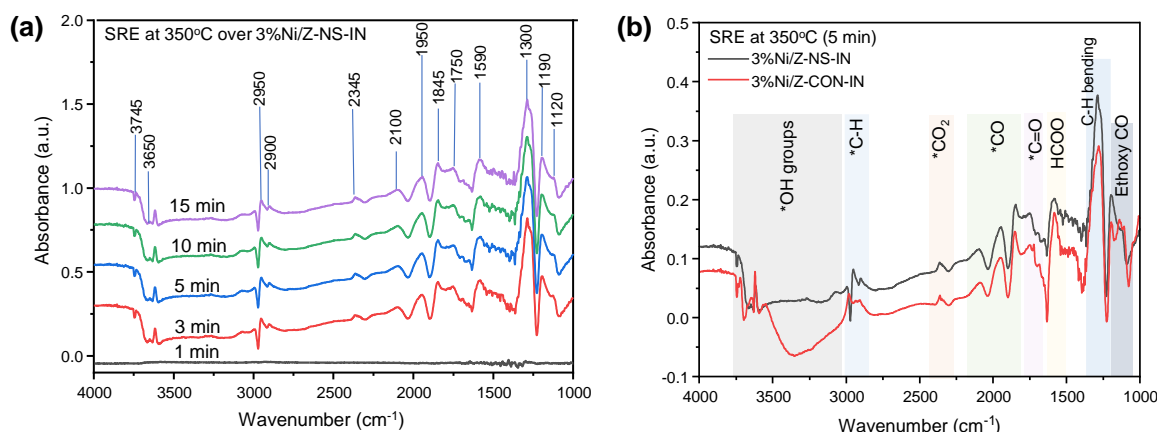
Figure 4.23 *In-situ* DRIFTS spectra of Ni/Z-NS-IN under ESR at 350 °C Steam/Carbon of 8).

4.2.2.4 Kinetic study

The kinetic study, having a low conversion of ethanol (<15%), was further used to calculate the activation energy (Ea) of ESR to compare reaction rates between *in-situ* and impregnation catalysts. The activation energy of the ESR in Figure 4.24 was obtained from the Arrhenius equation as presented in Eq. (4.2). The activation energy of *in-situ* catalysts, Ni/Z-NS-IN and Ni/Z-CON-IN, displayed the lower activation energy at 66 and 88 kJ/mol, compared to those of impregnation catalysts, Ni/Z-NS-IMP and Ni/Z-CON-IMP at 105 and 93 kJ/mol. The lower activation energy of the *in-situ* catalyst results in a higher reaction rate because there is a smaller energy barrier to starting the reaction. This can be assumed that the *in-situ* catalysts were more active than impregnation catalysts due to the smaller Ni particle sizes that could be initially activated to perform ESR at low temperatures. However, the kinetic study needs to be carefully considered at much higher EtOH conversion along with higher reaction temperature, it could be different from the low temperature. Increasing the temperature of ESR has the effect of increasing the number of reactant molecules, which are EtOH and water, and they have more energy than the activation energy. Likewise, incremental temperature increases initial catalytic performance but decreases catalyst life due to the catalyst's deactivation, caused by carbon formation at high temperatures. These results further support the experimental work, performed by Zhurka *et al*, 2018 [86].

$$lnk = lnA - Ea/RT \qquad (4.2)$$

where k is the rate constant, T is the absolute temperature (Kelvin), A is the pre-exponential factor, Ea is the activation energy for the reaction, and R is the universal gas constant.
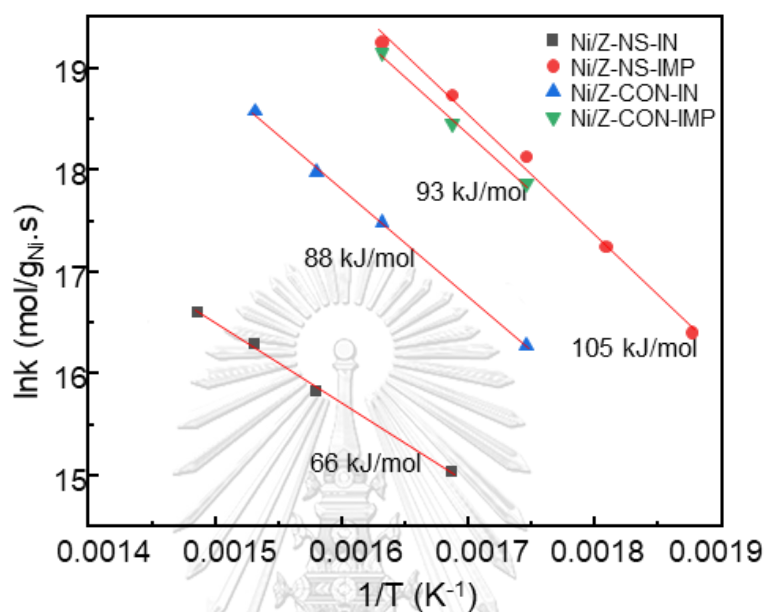
Figure 4.24 Arrhenius plots to determine activation energy of the catalytic ESR (<15% of ethanol conversion).

4.2.2.5 Stability test

The stability test was studied from ESR at 550 °C for 48 h over different types of Ni/ZSM-5 catalysts as shown in Figure 4.25. Figure 4.25a showed the percentage of H_2 yield. The H_2 yield of Ni/Z-NS-IN remained at 64% for 48 h of the longevity test, while that of Ni/Z-NS-IMP slightly decreased from 65% to 60% due to the carbon formation easily blocking external Ni particles on the outer catalyst surfaces. Although the H_2 yield of Ni/Z-CON-IN continued the same all along the ESR, it was only around 50%. The H_2 yield of Ni/Z-CON-IMP significantly went down from 65% to 50% because the coking was simply formed.

Figure 4.25b revealed the percentage of EtOH conversion. The EtOH conversion of Ni/Z-NS-IN presented slightly dropped from 99% to 88% and remained stable over 48 h, while those of Ni/Z-NS-IMP and Ni/Z-CON-IMP dramatically reduced to 70% and 50%, respectively. The carbon gas products of all catalysts

mainly were CO_2 and CO and were unstable at the first 10 h but constantly remained the same for the rest of the time. However, the EtOH conversion of Ni/Z-CON-IN was noticeably almost 100% for 48 h because the carbon gas products remained CH_3CHO. This could be assumed that Ni/Z-CON-IN catalysts were prepared by *in-situ* method and the ZSM-5 support was a three-dimension zeolite with a spherical shape and a thickness of one unit (shown in Figure 4.18e), thus the accessibility of active centers was suppressed. Hence, the catalysis occurred on the ZSM-5 surfaces instead of nickel active sites. ZSM-5 favors the hydration of alcohol reaction, and the majority of gas product is acetaldehyde as confirmed by Atchimarungsri et al [87].
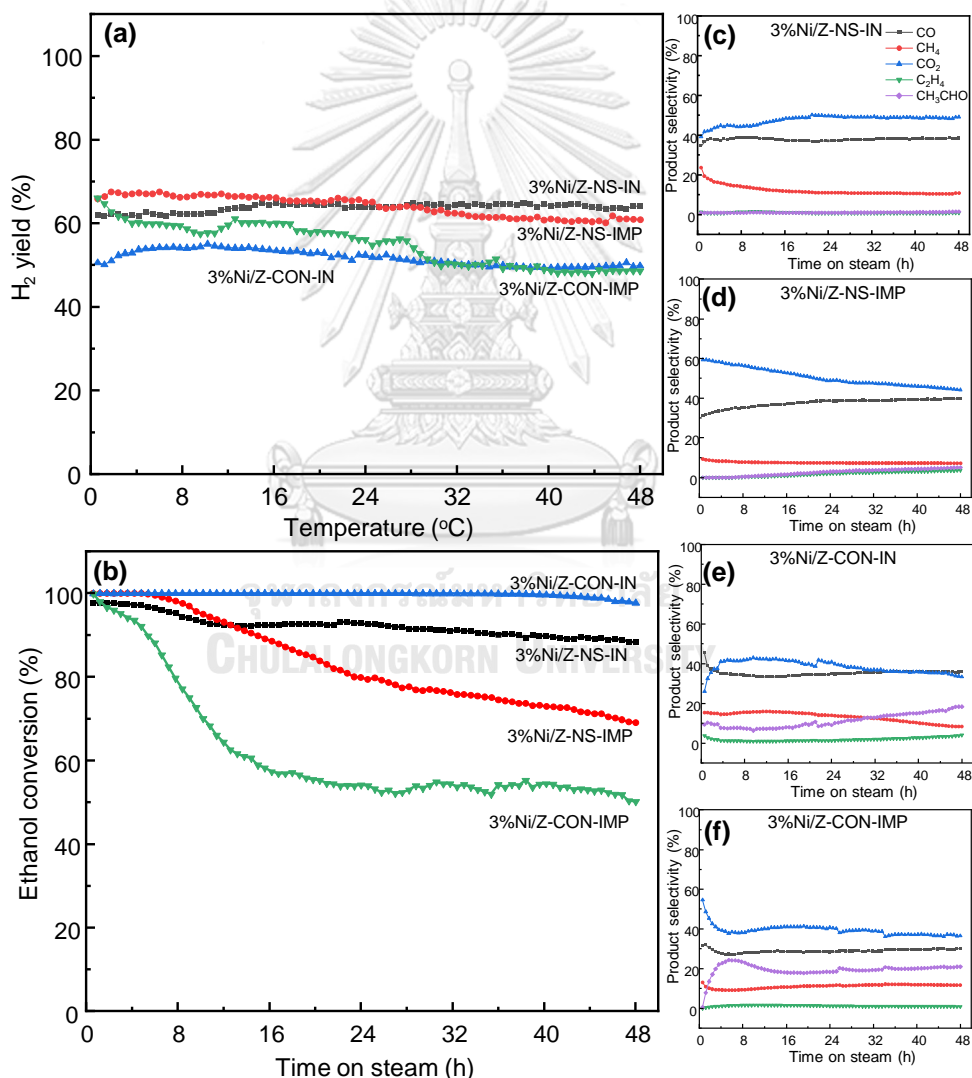
Figure 4.25 Stability test of catalysts over ESR at 550 °C for 48 h (S/C=8) regarding (a) EtOH conversion, (b) H_2 yield, and carbon gas product selectivity of (c) Ni/Z-NS-IN, (d) Ni/Z-NS-IMP, (e) Ni/Z-CON-IN and (f) Ni/Z-CON-IMP.

4.2.3 Characterization of spent catalysts

4.2.3.1 Morphology

The TEM images from Figure 4.26 illustrated the morphology of spent catalysts after 48 h of the ESR stability test at 550°C. Figure 4.26a showed small spots of Ni particles because the particles were trapped into the interconnected lamellar layers of Z-NS, suggesting nickel sintering was suppressed during catalysis. Ismaila *et al*, 2022 [88] have suggested that the encapsulated catalyst method is an effective strategy for preparing highly dispersed metal into supports, hence, it prevents metal particles from sintering and coke formation. On the other hand, the other spent catalysts showed larger nickel particle sizes of nickel sintering due to the weak metal-support interaction as it can refer to earlier research studied by Yang *et al*, 2016 [89]. The TEM images of spent catalysts also exhibited filamentous carbon or carbon nanotubes (CNTs) as they are the carbon formation.
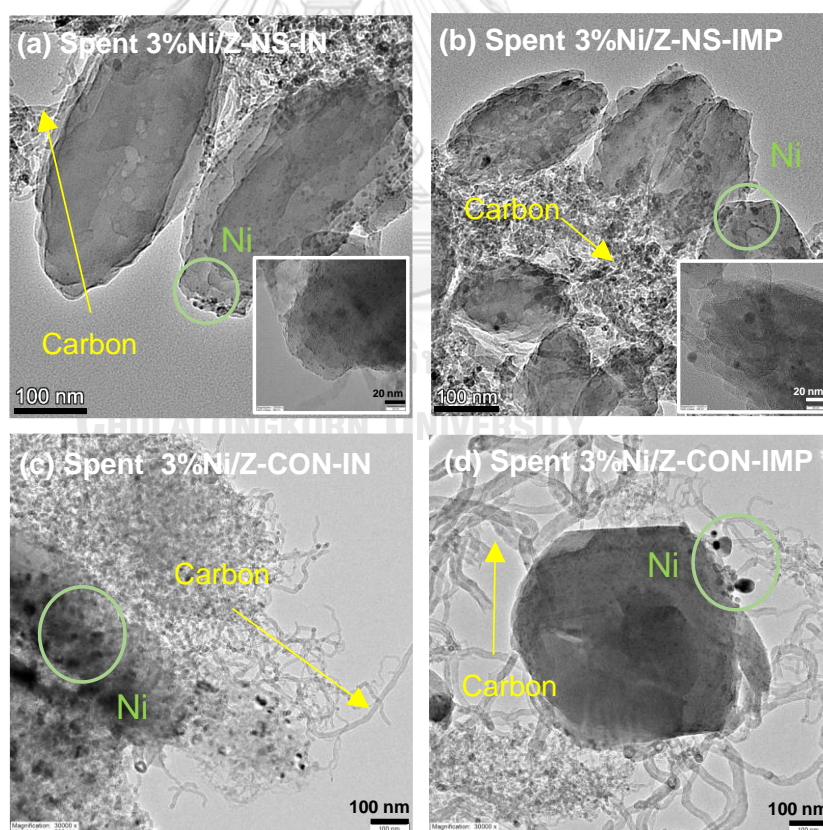
Figure 4.26 TEM images of spent catalysts after 48 h of ESR stability at 550 °C: (a) Ni/Z-NS-IN, (b) Ni/Z-NS-IMP, (c) Ni/Z-CON-IN, and (d) Ni/Z-CON-IMP.

4.2.3.2 Chemical properties

The XRD patterns of spent catalysts are presented in Figure 4.27. The 2θ peaks located at 44.5° and 52° were assigned to metallic Ni, while the peak at 26° was detected to carbon. A similar XRD pattern was reported by Prasongthum *et al*, 2017 [57].
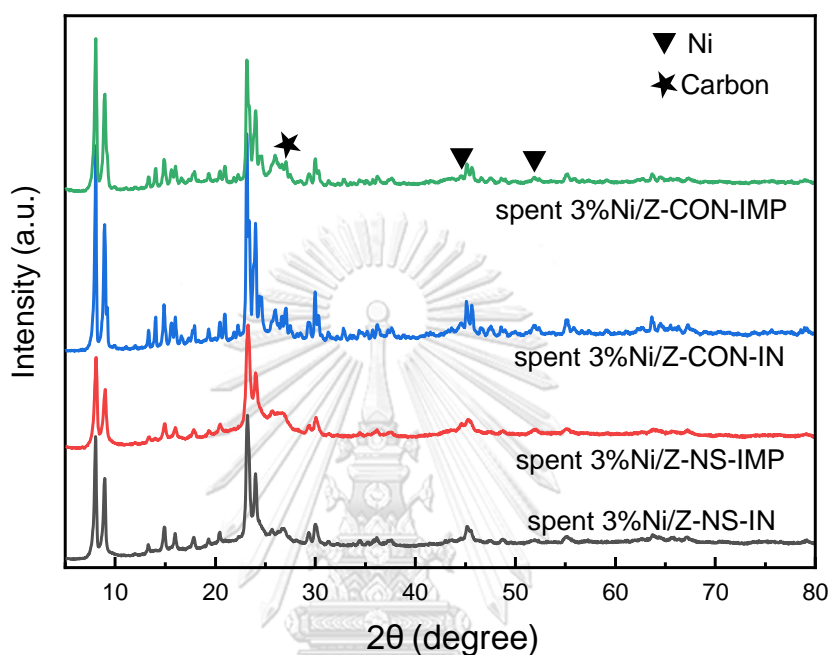
Figure 4.27 XRD patterns of spent catalysts after stability test.

4.2.3.3 Carbon deposition

The TGA profiles of the spent catalysts after 48 h, running ESR, presented in Figure 4.28, could confirm the amount of coke deposition according to the percentage of weight loss. The decomposition temperature of TGA between 450-650 °C was ascribed to CNTs. Bannov et al, 2020 [90] also observed that the TGA of CNTs showed decreases in the mass loss within the same thermal region. The spent Ni/Z-NS-IN presented 17 wt%, the smallest amount of coke according to the smallest weight loss. The Ni-catalysts on Z-NS supports have high accessibility of active centres on the surface with reduced diffusion resistance and the thin layers of Z-NS support the heat transfer. Moreover, when nickel particles form and grow inside the pores, they would be well encapsulated due to their small sizes and be not easy to escape from between lamellar layers of Z-NS. These properties could suppress carbon formation on nickel active sites during catalysis. The spent Ni/Z-CON-IN presented

25 wt% of carbon amounts. Although it was three-dimension Z-CON catalyst support, the in-situ preparation method flourished coking decrement due to nickel active sites formed intramolecular in Z-CON structures. However, the amount of coking of the spent Ni/Z-NS-IMP and spent Ni/Z-CON-IMP were the same percentage of weight loss, which were about 33 wt%. The impregnated catalysts, showing a larger amount of coke, consisted of Ni active sites, mostly located on the outer catalyst surfaces. Thus, the carbon deposition was continuously grown further from the Ni particles after ESR until they finally became CNTs.
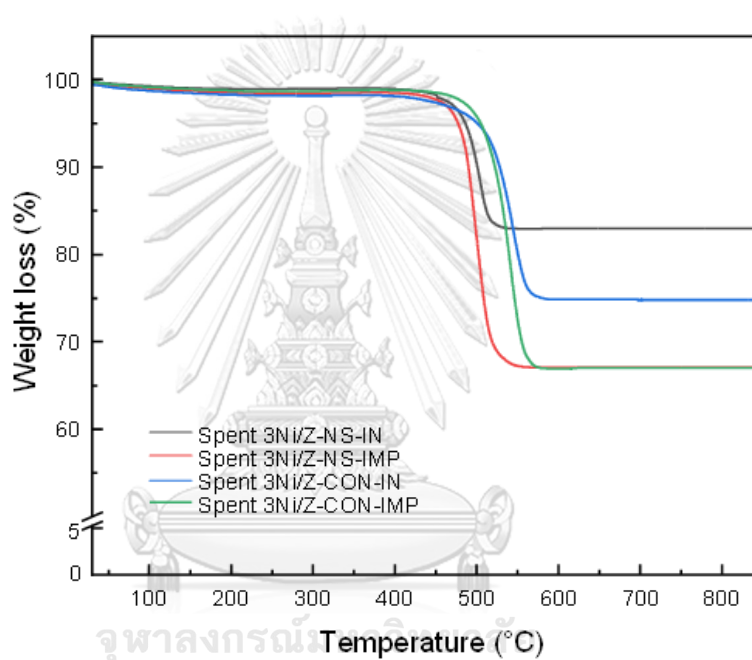
Figure 4.28 TGA results of spent catalysts after 48 h on stability of ESR at 550 °C.

CHAPTER 5
CONCLUSIONS AND SUGGESTION

5.1 Conclusions

5.1.1 Hydrogen production by steam reforming of fusel oil over Ni/SiC

We have successfully synthesized the SiC from rice husk by pyrolysis at high temperatures. The FESEM and XRD analyses demonstrated that pyrolyzed SiC consisted of β-SiC and α-SiC phases. Pyrolysis of RH at 1300°C was not properly formed SiC, while at 1500 °C and 1700 °C, β-SiC and α-SiC phases were formed, and rod structures were obtained with a diameter of 80-200 nm. The prepared SiC from pyrolysis of rice husk possessed a markedly larger than that of the SiC-com. When applied as a support for a 10wt%Ni catalyst in steam reforming of fusel oil at 700 °C, S/C of 9, W/F of 15 $g_{catalyst}.h.mol^{-1}$, the Ni/SiC1500 exhibited the highest catalytic performance in terms of giving the stable fusel oil gas conversion of 90% during a 300 min of reaction and the highest hydrogen yield of 29%. The larger surface area of the pyrolyzed rice husk support enhanced the dispersion of nickel to achieve smaller nickel particle sizes, while the presence of unique rod structure and β-SiC phase in the Ni/SiC1500 catalyst could be beneficial to reduce the carbon formation due to the property of thermal conductivity, hence presenting a superior performance, and maintaining higher stability in the steam reforming test.

5.1.2 Hydrogen production by steam reforming of bioethanol over Ni/ZSM-5 nanosheet

The synthesis of a two-dimension ZSM-5 nanosheet (Z-NS) was successfully performed. The Z-NS supports were formed by several thin sheets, grown in one direction and the size of the entire particle was about 200 nm. The thickness of each lamellar stacking, composed of ZSM-5 framework, was in the range of 10-20 nm. The Z-NS was used as the support for preparing nickel catalysts because it shows high accessibility of active centers on the surface with reduced diffusion resistance, which enhances catalytic performances. Two different methods were prepared for nickel catalyst synthesis, that is, *in-situ* (IN) and wet impregnation method (IMP). The Ni/Z-

NS-IN catalyst exhibited a more uniform nickel particle size of 5.6 nm, while that of Ni/Z-NS-IMP showed 7.8 nm with some agglomerated nickel particles. The three-dimension Z-CON, which is a spherical shape with a large particle of 500-700 nm, was also used for nickel catalyst supports and to compare the catalytic performance with nickel catalysts of Z-NS. The prepared nickel catalysts were applied for ESR to produce hydrogen. The stability test of the catalysts was investigated at 550 °C for 48 h (S/C of 8). The Ni/Z-NS-IN presented excellent catalytic performance, showing 65% of H_2 yield, 88% of ethanol conversion, and only 17wt% of coke deposition, compared to those of other catalysts. Therefore, two-dimension Z-NS could be beneficial to reduce carbon formation due to the reduction of surface diffusion barriers. Moreover, the *in-situ* method presented well-encapsulated small sizes of nickel particles in the interconnected lamellar layers of Z-NS for preventing nickel sinter and coke, hence giving a good performance, and maintaining longevity in the steam reforming test.

5.2 Suggestion and recommendation

Hydrogen production of fusel oil over Ni/SiC

To reduce carbon deposition, silicon carbide (SiC) from rice husk could be developed into foam structures that can prevent carbon deposition. The SiC could be efficiently employed as a foam support for controlling the dispersion of the active phase. It also decreases a pressure drop during the reaction proceeding with thermal stability. The metal can also be coated on the SiC foam supports with a thin and uniform layer, prepared by an impregnation method. The foam catalysts also improve mass and heat transfer, and catalytic reaction as well as hydrogen yield [91, 92].

Hydrogen production of bioethanol over Ni/ZSM-5 nanosheet

Although the Ni/Z-NS-IN exhibited the improvement of catalytic activities with the encapsulated nickel particles as well as enhanced the longevity test, some aspects of the ESR and Ni catalysts need further investigation to improve hydrogen yield. Therefore, catalyst development with high hydrogen yield is required for further research. A fusion of a small amount of the noble metals (Pd, Pt, Rh, and Ru) to Ni catalysts have been suggested as a promising way to improve the hydrogen yield

as well as catalytic stability. In this work, the steam/carbon ratio is 8, hence varying the proper ratio could enrich more hydrogen yield products with low amounts of coke.

Due to an excellent thermal property of Ni/ZSM-5 nanosheet catalyst, this research would further study the catalyst regeneration, which is process of regenerating spent catalysts to make them reusable. This process also involves recovering the chemical characteristics of spent catalysts and restoring their effectiveness in catalytic performances.

The Ni on ZSM-5 nanosheet catalysts presented good catalytic performances of ESR according to the two-dimension structures giving the reduction of surface diffusion barriers. The use of a two-dimension ZSM-5 nanosheet as catalyst support could be one of the most attractive choices for other catalytic reactions.

Appendix A

Hydrogen production of FSR over Ni/SiC

Component and chemical formulation of fusel oil

Chemical	Density (g/cm³)	Peak area (pure)	Peak area (real fusel oil)	Mw
Ethanol	0.789	126231	4579.41	46
Propan-1-ol	0.803	176557	12217.6	60
Iso butanol	0.802	184065	31898.5	74
Isoamyl alcohol	0.8104	195143	113019	88

The weight percentage component of fusel oil was calculated based on the peak area of pure each chemical, compared with real fusel oil. It was found that there are four components in real fusel oil. (iso-amyl alcohol, iso-butanol, propanol, and ethanol). The GC was conducted by Tham Le.

Weight of injection (g) = 0.001 x 0.789 = 0.000789 g

Mol of ethanol (pure) = 0.000789/46 = 1.71522E-05

Mol of ethanol (real fusel oil) = (Peak area of real fusel x mol of pure ethanol)/peak area of pure ethanol = (4579.41 x 1.71522E-05)/126231 = 0.000000622 mol

In case of iso amyl-alcohol, iso butanol, and propanol were 0.000005334, 0.000001878, and 0.000000926, respectively.

Weight of each component in fusel oil:

$m_{Ethanol}$ = 0.000000622 x 46 = 0.0000286 g

$m_{propanol}$ = 0.000000926 x 60 = 0.0000556 g

$m_{isobutanol}$ = 0.000001878 x 74 = 0.0001390 g

$m_{isoamyl}$ = 0.000005334 x 88 = 0.0004694 g

Total of weight = 0.0000286 + 0.0000556 + 0.0001390 + 0.0004694 = 0.0006925 g

%wt of each component in real fusel oil:

% Ethanol = (0.0000286/0.0006925) x 100 = 4.13%

% Propanol = (0.0000556/0.0006925) x 100 = 8.02%

%Iso-butanol = (0.0001390/0.0006925) x 100 = 20.06%

%Iso-amyl = (0.0004694/0.0006925) x 100 = 67.7%

To calculate the general formulation in fusel oil using this equation:

$$\bar{M}_W = \frac{\sum wt\%}{\sum \dfrac{wt\%}{M_{wi}}}$$

$\bar{M}_w$: Average molecular weight

$\sum$ wt%: total of weight percentage

M_{wi} : weight molecular of each component

Hence,

$\sum$ wt% = 4.13% + 8.02% + 20.06% + 67.7% = 1

$\sum$ (wt%/M_{wi}) = $\sum$ ((4.13%/46) + (8.02%/60) + (20.06%/74) + (67.7%/88)) = 0.0126

M_w = $\sum$ wt% / $\sum$ (wt%/M_{wi}) = 1/0.0126 = 79.36

The general formula for the representation of an alcohol is

$C_nH_{2n+2}O$
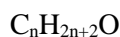
Where n refers to the number of carbon atoms in the chain. Put down the values of molecular mass of C, H and O.

12n + (2n + 2) + 16

The general formulation as $C_nH_{2n+1}OH$

14n + 18 = 79.36; n = 4.36

Therefore, the general formulation was $C_{4.36}H_{10.72}O$

The determination of water content in fusel oil

The water content was detected by Karl Fischer Titration from Thailand Institute of Scientific and Technological Research. The result reported there was 0.01% of water content, assuming that no water in fusel oil.
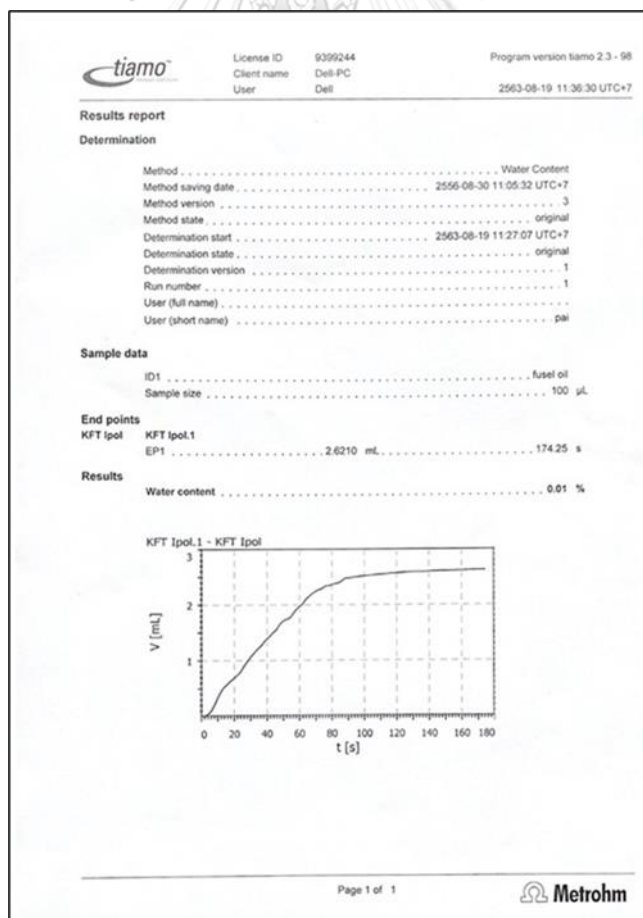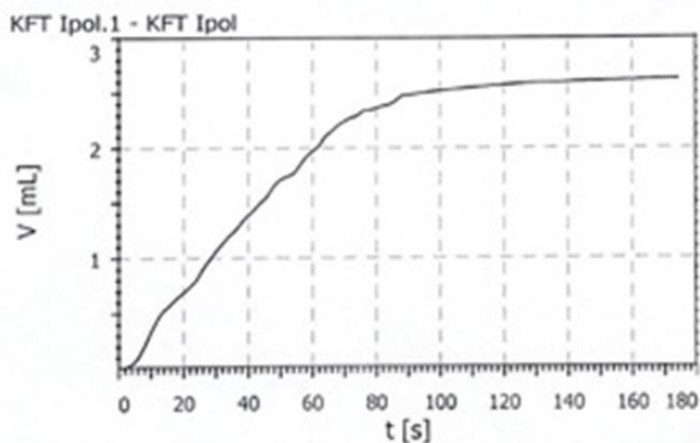
Hydrogen production of ESR over Ni/ZSM-5 nanosheet

The calculation of Ar flow rate for ethanol and water, measuring by vapor pressure.

Ethanol Vapour Pressure			Total Flow	100		
			a =	-5341.1	Y = ln (P)	
			b =	19.955	X = (1/T (K))	C1 (ppm)	20000
Saturator Temperature	ln (P)	P (kPa)	Dilution factor	He Flow (ml/min)	C2 (ppm)	10000
(°C)	K					C2 (%)	1
0	273	0.39053114	1.477765479	1.47776548	67.6697361	

H2O Concentration (Vol%)			5	←	Change the concentr
Water, H2O			Total Flow	100	←	Change
			a =	-5206.67	Y = ln (P)
Y = -5206.6x+18.607			b =	18.607	X = (1/T (K))
Saturator Temperature	ln (P)	P (kPa)	Dilution factor	Ar Flow (ml/min)	
(°C)	K				
55	328	2.7330061	15.37904852	3.0758097	27.51176425	H2O (g, sccm)	5

The hydrogen standard calibration and the calculation.

H2 feed rate (ml/min)	H2 peak area	Propene feed rate (ml/min)	Propene peak area
0	0	4	73882
0.5	218531.5	4	73843.5
1	459809	4	73734
2	920751	4	73806.5
3	1350662	4	73945.5
4	1761308	4	73841
5	2151262	4	73913

H₂/Propene Cppm	H₂/Propene Peak area
0	0
1.25	2.959387082
2.5	6.236051211
5	12.47520205
7.5	18.26564159
10	23.85271055
12.5	29.10532653

H_2 std calibration

$y = 2.3776x$
$R^2 = 0.9995$
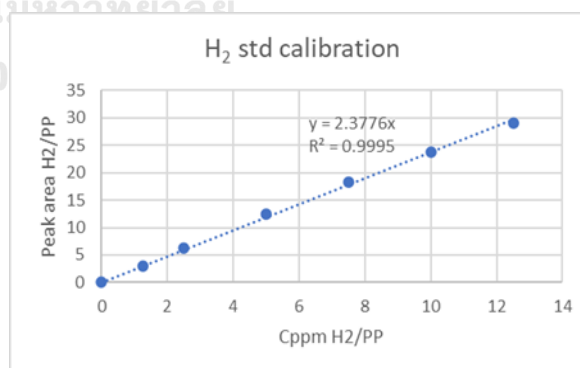
ZSM-5 calculation

Calculation of ZSM-5 nanosheet (Si/Al = 100)

$$\frac{SiO2}{Al2O3} = 200, = \frac{Si}{Al} = 100$$

chemical	TEOS	Al isopropoxide	TBAOH	NaOH	DI
Mole ratio	0.042	0.00021	0.01	0.0017	0.58
Mw	208.33	204.24	259.5	40	18
g	8.4	0.086	8.1	0.02	2.32

gSiO2 = 0.042 x 60g/1mol = 2.5 g SiO2

g Al2O3 = 0.00021 x 102g/1mol = 0.02 g Al2O3

To prepare 3%Ni/Z-CON-IN

$$\text{g of Ni(NO3)2} = \frac{3 \text{ g Ni}}{97 \text{ gSupport}} \, x \, \frac{1 \text{ mol Ni}}{58.69 \text{ gNi}} \, x \, \frac{1 \text{mol Ni(NO3)2}}{1 \text{ molNi}} \, x \, \frac{290.81 \text{ gNi(NO3)2}}{1 \text{ mol Ni(NO3)2}} \, x \, 2.52$$

= 0.38 g

chemical	EDA	DI water	Ni(NO3)2
Mole ratio	3.25	50	1
Mole of use	0.004225	0.065	0.0013
Mw	60.1	18.0	290.8
g of use	0.25	1.17	0.38

Calculation of ZSM-5 conventional (Si/Al = 100)

chemical	TEOS	NaAlO3	TPAOH	NaOH	DI
Mole ratio	0.02	0.0002	0.01	0.0017	0.58
Mw	208.33	81.97	203.36	40	18
g	3.5	0.0164	2.02	0.0693	10.47

g SiO2 = 0.02 x 60g/1mol = 1.2 g SiO2

To prepare 3%Ni/Z-CON-IN

$$\text{g of Ni(NO3)2} = \frac{3\text{ g Ni}}{97\text{ gSupport}} \, x \, \frac{1\text{ mol Ni}}{58.69\text{ gNi}} \, x \, \frac{1\text{mol Ni(NO3)2}}{1\text{ molNi}} \, x \, \frac{290.81\text{ gNi(NO3)2}}{1\text{ mol Ni(NO3)2}} \, x \, 1.2$$

$$= 0.184\text{ g} = 0.0006\text{ mole Ni(NO3)2}$$

The mole ratio of the stabilizing agent mixture is 3.25EDA : 50DI water : 1 Ni(NO3)2

chemical	EDA	DI water	Ni(NO3)2
Mole ratio	3.25	50	1
Mole of use	0.00195	0.03	0.00063
Mw	60.1	18.0	290.8
g of use	0.12	0.54	0.18

Calculation of 3wt%Ni/ZSM-5 impregnation

Basis 1 g of ZSM-5 support

97 g ZSM-5 loaded 3 g Ni

1 g ZSM-5 loaded (3x1)/97 = 0.03 g

58.69 g Ni use 290.81 g Ni(NO3)2.6H2O

0.03 g Ni use (290.81 x 0.03)/58.69 = 0.15 g Ni(NO3)2.6H2O

Appendix B
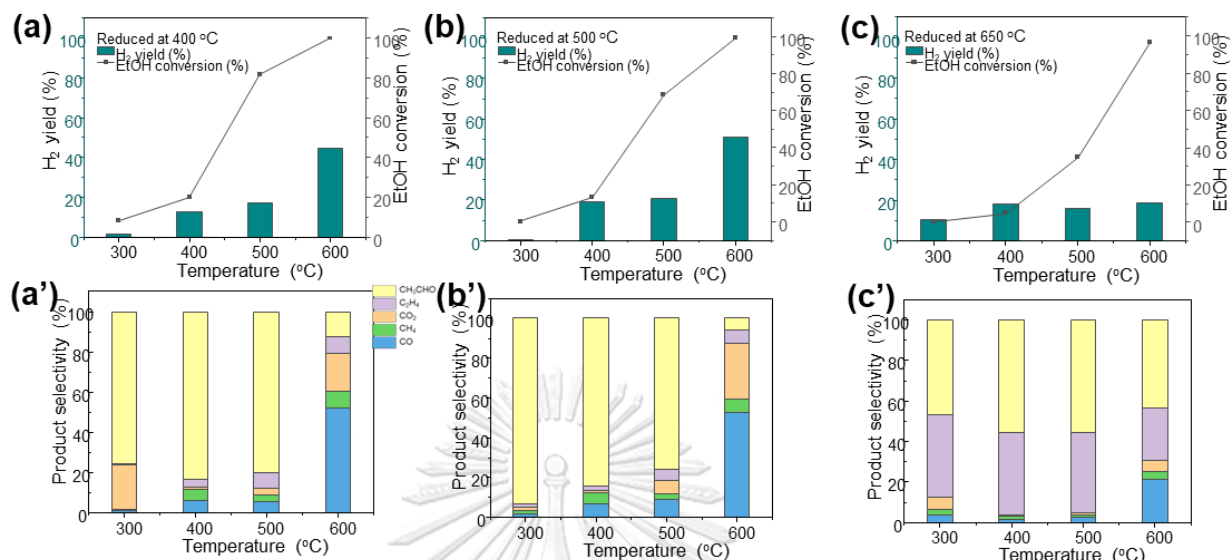
Figure B1. Influence of reduction temperature on the catalytic performances of SRE at (a, a') 400 °C, (b, b') 500 °C, and (c, c') 650 °C on 1%Ni/Z-NS-IN catalyst.
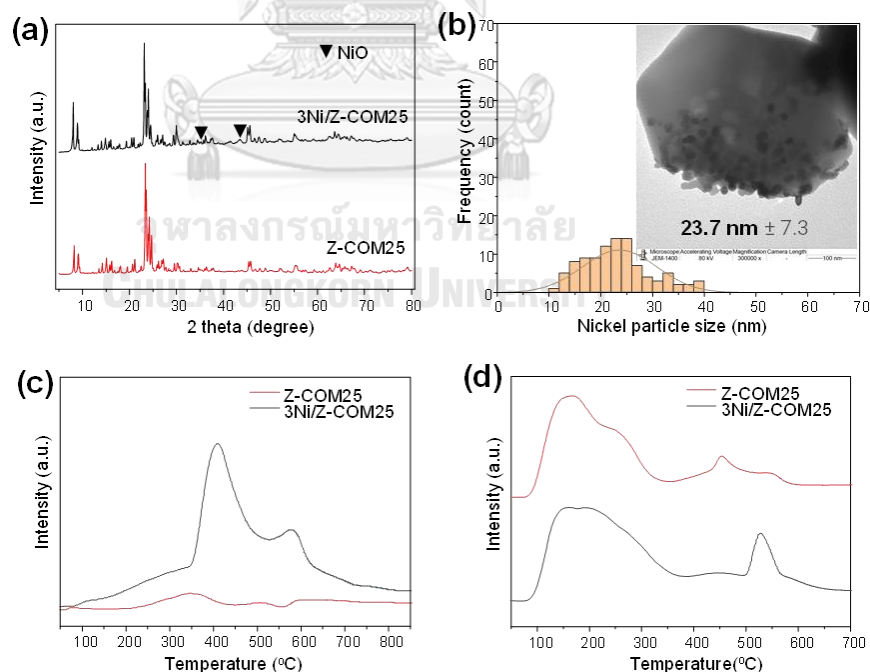

Figure B2. Catalyst characterization of Z-COM25 and 3%Ni/Z-COM25 regarding (a) XRD pattern, (b) TEM image and Ni size distribution, (c) H_2-TPR and (d) NH_3-TPD.
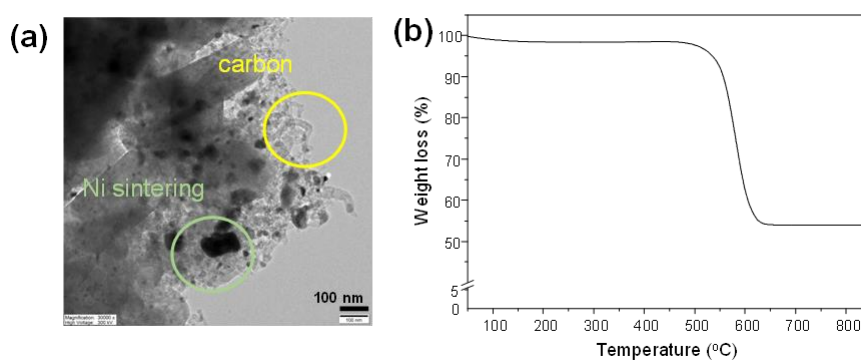
Figure B3. (a) FETEM images, and (b) TGA profile of spent 3%Ni/Z-COM25 catalysts after 48 h of ESR stability test at 550 °C.

REFERENCES

[1] Dufour, J.; Serrano, D. P.; Gálvez, J. L.; Moreno, J.; González, A. Hydrogen Production from Fossil Fuels: Life Cycle Assessment of Technologies with Low Greenhouse Gas Emissions. *Energy & Fuels* **2011**, *25* (5), 2194-2202.

[2] Navarro, R. M.; Peña, M. A.; Fierro, J. L. G. Hydrogen Production Reactions from Carbon Feedstocks: Fossil Fuels and Biomass. *Chemical Reviews* **2007**, *107* (10), 3952-3991.

[3] Shinoki, T.; Kamizono, M.; Katagiri, K.; Kusumi, M.; Takeda, Y.; Tanigawa, H.; Hirata, K. Hydrogen Production From Petroleum Hydrocarbons. *Journal of Electrochemical Energy Conversion and Storage* **2020**, *18* (1).

[4] Bušić, A.; Marđetko, N.; Kundas, S.; Morzak, G.; Belskaya, H.; Ivančić Šantek, M.; Komes, D.; Novak, S.; Šantek, B. Bioethanol Production from Renewable Raw Materials and Its Separation and Purification: A Review. *Food Technol Biotechnol* **2018**, *56* (3), 289-311.

[5] Tse, T. J.; Wiens, D. J.; Reaney, M. J. T. Production of Bioethanol—A Review of Factors Affecting Ethanol Yield. In *Fermentation*, 2021; Vol. 7.

[6] Cifuentes, A.; Torres, R.; Llorca, J. Modelling of the ethanol steam reforming over Rh-Pd/CeO2 catalytic wall reactors. *International Journal of Hydrogen Energy* **2020**, *45* (49), 26265-26273.

[7] Kourtelesis, M.; Moraes, T. S.; Mattos, L. V.; Niakolas, D. K.; Noronha, F. B.; Verykios, X. The effects of support morphology on the performance of Pt/CeO2 catalysts for the low temperature steam reforming of ethanol. *Applied Catalysis B: Environmental* **2021**, *284*, 119757.

[8] Moraes, T. S.; Borges, L. E. P.; Farrauto, R.; Noronha, F. B. Steam reforming of ethanol on Rh/SiCeO2 washcoated monolith catalyst: Stable catalyst performance. *International Journal of Hydrogen Energy* **2018**, *43* (1), 115-126.

[9] Nejat, T.; Jalalinezhad, P.; Hormozi, F.; Bahrami, Z. Hydrogen production from steam reforming of ethanol over Ni-Co bimetallic catalysts and MCM-41 as support. *Journal of the Taiwan Institute of Chemical Engineers* **2019**, *97*, 216-226.

[10] Niazi, Z.; Irankhah, A.; Wang, Y.; Arandiyan, H. Cu, Mg and Co effect on nickel-ceria supported catalysts for ethanol steam reforming reaction. *International Journal of Hydrogen Energy* **2020**, *45* (41), 21512-21522.

[11] Yoo, S.; Park, S.; Song, J. H.; Kim, D. H. Hydrogen production by the steam reforming of ethanol over K-promoted Co/Al2O3–CaO xerogel catalysts. *Molecular Catalysis* **2020**, *491*, 110980.

[12] Di Michele, A.; Dell'Angelo, A.; Tripodi, A.; Bahadori, E.; Sànchez, F.; Motta, D.; Dimitratos, N.; Rossetti, I.; Ramis, G. Steam reforming of ethanol over Ni/MgAl2O4 catalysts. *International Journal of Hydrogen Energy* **2019**, *44* (2), 952-964.

[13] Alweendo, S. T.; Johnson, O. T.; Shongwe, M. B.; Kavishe, F. P. L.; Borode, J. O. Synthesis, Optimization and Characterization of Silicon Carbide (SiC) from Rice Husk. *Procedia Manufacturing* **2019**, *35*, 962-967.

[14] Singh, B. Rice husk ash. In *Waste and Supplementary Cementitious Materials in Concrete*, 2018; pp 417-460.

[15] Pereira, M. L. G.; Figueira, D. S. S.; Girolamo, B. R.; Vernilli, F. Synthesis of silicon carbide from rice husk. *Cerâmica* **2020**, *66* (379), 256-261.

[16] Chiew, Y. L.; Cheong, K. Y. A review on the synthesis of SiC from plant-based

biomasses. *Materials Science and Engineering: B* **2011**, *176* (13), 951-964.

[17] Gao, X.; Liu, G.; Wei, Q.; Yang, G.; Masaki, M.; Peng, X.; Yang, R.; Tsubaki, N. Carbon nanofibers decorated SiC foam monoliths as the support of anti-sintering Ni catalyst for methane dry reforming. *International Journal of Hydrogen Energy* **2017**, *42* (26), 16547-16556.

[18] Le, T. A.; Kang, J. K.; Park, E. D. CO and CO2 Methanation Over Ni/SiC and Ni/SiO2 Catalysts. *Topics in Catalysis* **2018**, *61* (15), 1537-1544.

[19] Liao, M.; Wang, C.; Bu, E.; Chen, Y.; Cheng, Z.; Luo, X.; Shu, R.; Wu, J. Efficient hydrogen production from partial oxidation of propane over SiC doped Ni/Al2O3 catalyst. *Energy Procedia* **2019**, *158*, 1772-1779.

[20] Wei, Q.; Yang, G.; Gao, X.; Yamane, N.; Zhang, P.; Liu, G.; Tsubaki, N. Ni/Silicalite-1 coating being coated on SiC foam: A tailor-made monolith catalyst for syngas production using a combined methane reforming process. *Chemical Engineering Journal* **2017**, *327*, 465-473.

[21] Abusuek, D. A.; Tkachenko, O. P.; Bykov, A. V.; Sidorov, A. I.; Matveeva, V. G.; Sulman, M. G.; Nikoshvili, L. Z. ZSM-5 as a support for Ru-containing catalysts of levulinic acid hydrogenation: Influence of the reaction conditions and the zeolite acidity. *Catalysis Today* **2022**.

[22] Sridhar, A.; Rahman, M.; Infantes-Molina, A.; Wylie, B. J.; Borcik, C. G.; Khatib, S. J. Bimetallic Mo-Co/ZSM-5 and Mo-Ni/ZSM-5 catalysts for methane dehydroaromatization: A study of the effect of pretreatment and metal loadings on the catalytic behavior. *Applied Catalysis A: General* **2020**, *589*, 117247.

[23] Sun, Y.; Ma, T.; Zhang, L.; Song, Y.; Shang, Y.; Zhai, Y.; Gong, Y.; Duan, A. The influence of zoned Al distribution of ZSM-5 zeolite on the reactivity of hexane cracking. *Molecular Catalysis* **2020**, *484*, 110770.

[24] Kore, R.; Srivastava, R.; Satpati, B. ZSM-5 zeolite nanosheets with improved catalytic activity synthesized using a new class of structure-directing agents. *Chemistry* **2014**, *20* (36), 11511-11521.

[25] Wetchasat, P.; Salakhum, S.; Imyen, T.; Suttipat, D.; Wannapakdee, W.; Ketkaew, M.; Prasertsab, A.; Kidkhunthod, P.; Witoon, T.; Wattanakit, C. One-Pot Synthesis of Ultra-Small Pt Dispersed on Hierarchical Zeolite Nanosheet Surfaces for Mild Hydrodeoxygenation of 4-Propylphenol. *Catalysts* **2021**, *11* (3).

[26] Idriss, H.; Scott, M.; Subramani, V. 1 - Introduction to hydrogen and its properties. In *Compendium of Hydrogen Energy*, Subramani, V., Basile, A., Veziroğlu, T. N. Eds.; Woodhead Publishing, 2015; pp 3-19.

[27] Sumrunronnasak, S.; Reubroycharoen, P.; Pimpha, N.; Chanlek, N.; Tantayanon, S. Hydrogen Production by Steam Reforming of Fusel Oil Using a CeCoOx Mixed-Oxide Catalyst. *Chemical Engineering & Technology* **2020**, *43* (4), 689-697.

[28] Marzoughi, T.; Rahimpour, E.; Rahimpour, M. R. 14 - Sustainable and green bio-ethanol purification for biofuel production via membrane engineering. In *Membrane Engineering in the Circular Economy*, Iulianelli, A., Cassano, A., Conidi, C., Petrotos, K. Eds.; Elsevier, 2022; pp 375-392.

[29] Cifuentes, B.; Gómez, J.; Sánchez, N.; Proaño, L.; Bustamante, F.; Cobo, M. Bioethanol steam reforming over monoliths washcoated with RhPt/CeO2–SiO2: The use of residual biomass to stably produce syngas. *International Journal of Hydrogen Energy* **2021**, *46* (5), 4007-4018.

[30] Sanchez, N.; Ruiz, R.; Hacker, V.; Cobo, M. Impact of bioethanol impurities on

steam reforming for hydrogen production: A review. *International Journal of Hydrogen Energy* **2020**, *45* (21), 11923-11942.

[31] Trane, R.; Dahl, S.; Skjøth-Rasmussen, M. S.; Jensen, A. D. Catalytic steam reforming of bio-oil. *International Journal of Hydrogen Energy* **2012**, *37* (8), 6447-6472.

[32] Frusteri, F.; Bonura, G. 5 - Hydrogen production by reforming of bio-alcohols. In *Compendium of Hydrogen Energy*, Subramani, V., Basile, A., Veziroğlu, T. N. Eds.; Woodhead Publishing, 2015; pp 109-136.

[33] Llorca, J.; Corberán, V. C.; Divins, N. J.; Fraile, Raquel O.; Taboada, E. Hydrogen from Bioethanol. In *Renewable Hydrogen Technologies*, 2013; pp 135-169.

[34] Valecillos, J.; Iglesias-Vázquez, S.; Landa, L.; Remiro, A.; Bilbao, J.; Gayubo, A. G. Insights into the Reaction Routes for H2 Formation in the Ethanol Steam Reforming on a Catalyst Derived from NiAl2O4 Spinel. *Energy & Fuels* **2021**, *35* (21), 17197-17211.

[35] Haynes, D. J.; Shekhawat, D. Chapter 6 - Oxidative Steam Reforming. In *Fuel Cells: Technologies for Fuel Processing*, Shekhawat, D., Spivey, J. J., Berry, D. A. Eds.; Elsevier, 2011; pp 129-190.

[36] Mattos, L. V.; Jacobs, G.; Davis, B. H.; Noronha, F. B. Production of Hydrogen from Ethanol: Review of Reaction Mechanism and Catalyst Deactivation. *Chemical Reviews* **2012**, *112* (7), 4094-4123.

[37] Ochoa, A.; Arregi, A.; Amutio, M.; Gayubo, A. G.; Olazar, M.; Bilbao, J.; Castaño, P. Coking and sintering progress of a Ni supported catalyst in the steam reforming of biomass pyrolysis volatiles. *Applied Catalysis B: Environmental* **2018**, *233*, 289-300.

[38] Xu, D.; Lv, H.; Liu, B. Encapsulation of Metal Nanoparticle Catalysts Within Mesoporous Zeolites and Their Enhanced Catalytic Performances: A Review. *Frontiers in Chemistry* **2018**, *6*, Review.

[39] Pérez-Ramírez, J.; Christensen, C. H.; Egeblad, K.; Christensen, C. H.; Groen, J. C. Hierarchical zeolites: enhanced utilisation of microporous crystals in catalysis by advances in materials design. *Chemical Society Reviews* **2008**, *37* (11), 2530-2542, 10.1039/B809030K.

[40] Liu, L.; Díaz, U.; Arenal, R.; Agostini, G.; Concepción, P.; Corma, A. Generation of subnanometric platinum with high stability during transformation of a 2D zeolite into 3D. *Nature Materials* **2017**, *16* (1), 132-138.

[41] Contreras, J. L.; Salmones, J.; Colín-Luna, J. A.; Nuño, L.; Quintana, B.; Córdova, I.; Zeifert, B.; Tapia, C.; Fuentes, G. A. Catalysts for H2 production using the ethanol steam reforming (a review). *International Journal of Hydrogen Energy* **2014**, *39* (33), 18835-18853.

[42] D'Souza, L.; Barnes, S.; Regalbuto, J. The Simple, Effective Synthesis of Highly Dispersed Pd/C and CoPd/C Heterogeneous Catalysts via Charge-Enhanced Dry Impregnation. *Catalysts* **2016**, *6* (5).

[43] Munnik, P.; de Jongh, P. E.; de Jong, K. P. Recent Developments in the Synthesis of Supported Catalysts. *Chemical Reviews* **2015**, *115* (14), 6687-6718.

[44] Alshammari, A. S. Heterogeneous Gold Catalysis: From Discovery to Applications. In *Catalysts*, 2019; Vol. 9.

[45] Ponnusamy, S. K.; Ramakrishnan, K.; Kirupha, S.; Sivanesan, S. Thermodynamic and kinetic studies of cadmium adsorption from aqueous solution onto rice husk. *Brazilian Journal of Chemical Engineering - BRAZ J CHEM ENG* **2010**, *27*.

[46] Casady, J. B.; Johnson, R. W. Status of silicon carbide (SiC) as a wide-bandgap semiconductor for high-temperature applications: A review. *Solid-State Electronics* **1996**, *39* (10), 1409-1422.

[47] Acheson, E. G. Carborundum: Its history, manufacture and uses. *Journal of the Franklin Institute* **1893**, *136* (3), 194-203.

[48] Ji, Y.; Yang, H.; Yan, W. Strategies to Enhance the Catalytic Performance of ZSM-5 Zeolite in Hydrocarbon Cracking: A Review. In *Catalysts*, 2017; Vol. 7.

[49] Liang, G.; Cheng, H.; Li, W.; He, L.; Yu, Y.; Zhao, F. Selective conversion of microcrystalline cellulose into hexitols on nickel particles encapsulated within ZSM-5 zeolite. *Green Chemistry* **2012**, *14* (8), 2146-2149, 10.1039/C2GC35685F.

[50] Meng, L.; Zhu, X.; Hensen, E. J. M. Stable Fe/ZSM-5 Nanosheet Zeolite Catalysts for the Oxidation of Benzene to Phenol. *ACS Catalysis* **2017**, *7* (4), 2709-2719.

[51] Zhang, X.; Liu, D.; Xu, D.; Asahina, S.; Cychosz, K.; Agrawal, K. V.; Alwahedi, Y.; Bhan, A.; Hashimi, S.; Terasaki, O.; et al. Synthesis of Self-Pillared Zeolite Nanosheets by Repetitive Branching. *Science (New York, N.Y.)* **2012**, *336*, 1684-1687.

[52] Kumar, A.; Prasad, R.; Sharma, Y. C. Ethanol steam reforming study over ZSM-5 supported cobalt versus nickel catalyst for renewable hydrogen generation. *Chinese Journal of Chemical Engineering* **2019**, *27* (3), 677-684.

[53] Cimenler, U.; Joseph, B.; Kuhn, J. N. Hydrocarbon steam reforming using Silicalite-1 zeolite encapsulated Ni-based catalyst. *AIChE Journal* **2017**, *63* (1), 200-207, https://doi.org/10.1002/aic.15521.

[54] Davidson, S. D.; Zhang, H.; Sun, J.; Wang, Y. Supported metal catalysts for alcohol/sugar alcohol steam reforming. *Dalton Trans* **2014**, *43* (31), 11782-11802.

[55] Jiang, L.; Fu, H.; Wang, L.; Zhou, W.; Jiang, B.; Wang, R. Pt loaded onto silicon carbide/porous carbon hybrids as an electrocatalyst in the methanol oxidation reaction. *RSC Adv.* **2014**, *4* (93), 51272-51279.

[56] Wang, M.; Au, C.-T.; Lai, S.-Y. H2 production from catalytic steam reforming of n-propanol over ruthenium and ruthenium-nickel bimetallic catalysts supported on ceria-alumina oxides with different ceria loadings. *International Journal of Hydrogen Energy* **2015**, *40* (40), 13926-13935.

[57] Prasongthum, N.; Xiao, R.; Zhang, H.; Tsubaki, N.; Natewong, P.; Reubroycharoen, P. Highly active and stable Ni supported on CNTs-SiO2 fiber catalysts for steam reforming of ethanol. *Fuel Processing Technology* **2017**, *160*, 185-195.

[58] Mhadmhan, S.; Natewong, P.; Prasongthum, N.; Samart, C.; Reubroycharoen, P. Investigation of Ni/SiO2 Fiber Catalysts Prepared by Different Methods on Hydrogen production from Ethanol Steam Reforming. *Catalysts* **2018**, *8* (8).

[59] Sumrunronnasak, S.; Reubroycharoen, P.; Pimpha, N.; Chanlek, N.; Tantayanon, S. Hydrogen Production by Steam Reforming of Fuel Oil Using a CeCoO$_x$Mixed-Oxide Catalyst. *Chemical Engineering & Technology* **2020**, *43* (4), 689-697.

[60] Olivares, A. C. V.; Gomez, M. F.; Barroso, M. N.; Abello, M. C. Ni-supported catalysts for ethanol steam reforming: effect of the solvent and metallic precursor in catalyst preparation. *International Journal of Industrial Chemistry* **2018**, *9* (1), 61-73.

[61] Ogo, S.; Sekine, Y. Recent progress in ethanol steam reforming using non-noble transition metal catalysts: A review. *Fuel Processing Technology* **2020**, *199*, 106238.

[62] Makornpan, C.; Mongkolkachit, C.; Wanakitti, S.; Wasanapiarnpong, T. Fabrication of Silicon Carbide from Rice Husk by Carbothermal-Reduction and In Situ Reaction Bonding Technique. *Key Engineering Materials* **2014**, *608*, 235-240.

[63] Krishnarao, R. V.; Mahajan, Y. R.; Kumar, T. J. Conversion of raw rice husks to SiC by pyrolysis in nitrogen atmosphere. *Journal of the European Ceramic Society* **1998**, *18* (2), 147-152.

[64] Yi, J.; Xue, W. J.; Xie, Z. P.; Liu, W.; Cheng, L. X.; Chen, J.; Wang, L.; Cheng, H.; Gao, Y. X.; Wang, H. B. The dependence of interlocking and laminated microstructure on toughness and hardness of β-SiC ceramics sintered at low temperature. *Materials Science and Engineering: A* **2013**, *586*, 338-341.

[65] Stein, R. A.; Lanig, P. Control of polytype formation by surface energy effects during the growth of SiC monocrystals by the sublimation method. *Journal of Crystal Growth* **1993**, *131* (1), 71-74.

[66] Hu, X.; Lu, G. Investigation of steam reforming of acetic acid to hydrogen over Ni–Co metal catalyst. *Journal of Molecular Catalysis A: Chemical* **2007**, *261* (1), 43-48.

[67] Reubroycharoen, P.; Tangkanaporn, N.; Chaiya, C. Ni/SiO2 fiber catalyst prepared by electrospinning technique for glycerol reforming to synthesis gas. In *Studies in Surface Science and Catalysis*, Gaigneaux, E. M., Devillers, M., Hermans, S., Jacobs, P. A., Martens, J. A., Ruiz, P. Eds.; Vol. 175; Elsevier, 2010; pp 689-693.

[68] Touhami, D.; Zhu, Z.; Balan, W. S.; Janaun, J.; Haywood, S.; Zein, S. Characterization of rice husk-based catalyst prepared via conventional and microwave carbonisation. *Journal of Environmental Chemical Engineering* **2017**, *5* (3), 2388-2394.

[69] Kim, S. M.; Woo, S. I. Sustainable Production of Syngas from Biomass-Derived Glycerol by Steam Reforming over Highly Stable Ni/SiC. *ChemSusChem* **2012**, *5* (8), 1513-1522.

[70] Noh, Y. S.; Lee, K.-Y.; Moon, D. J. Hydrogen production by steam reforming of methane over nickel based structured catalysts supported on calcium aluminate modified SiC. *International Journal of Hydrogen Energy* **2019**, *44* (38), 21010-21019.

[71] Le-Mai, T. H.; Mhadmhan, S.; Trieu, T. Q.; Prasongthum, N.; Suriya, P.; Reubroycharoen, P. Hydrogen production by steam reforming of fusel oil over Ni-based fiber catalyst. *Materials Today: Proceedings* **2021**.

[72] Łamacz, A.; Jagódka, P.; Stawowy, M.; Matus, K. Dry Reforming of Methane over CNT-Supported CeZrO2, Ni and Ni-CeZrO2 Catalysts. *Catalysts* **2020**, *10* (7).

[73] Pérez-Page, M.; Makel, J.; Guan, K.; Zhang, S.; Tringe, J.; Castro, R. H. R.; Stroeve, P. Gas adsorption properties of ZSM-5 zeolites heated to extreme temperatures. *Ceramics International* **2016**, *42* (14), 15423-15431.

[74] Tang, M.; Xu, L.; Fan, M. Effect of Ce on 5 wt% Ni/ZSM-5 catalysts in the CO2 reforming of CH4 reaction. *International Journal of Hydrogen Energy* **2014**, *39* (28), 15482-15496.

[75] Cui, Y.; Qiu, J.; Chen, B.; Xu, L.; Chen, M.; Wu, C.-e.; Cheng, G.; Yang, B.; Wang, N.; Hu, X. CO2 methanation over Ni/ZSM-5 catalysts: The effects of support morphology and La2O3 modification. *Fuel* **2022**, *324*, 124679.

[76] Hu, Z.-P.; Weng, C.-C.; Chen, C.; Yuan, Z.-Y. Catalytic decomposition of ammonia to COx-free hydrogen over Ni/ZSM-5 catalysts: A comparative study of the preparation methods. *Applied Catalysis A: General* **2018**, *562*, 49-57.

[77] Sarkar, B.; Tiwari, R.; Singha, R. K.; Suman, S.; Ghosh, S.; Acharyya, S. S.; Mantri, K.; Konathala, L. N. S.; Pendem, C.; Bal, R. Reforming of methane with CO2 over Ni nanoparticle supported on mesoporous ZSM-5. *Catalysis Today* **2012**, *198* (1), 209-214.

[78] Saini, B.; Tathod, A. P.; Diwakar, J.; Arumugam, S.; Viswanadham, N. Nickel

nano-particles confined in ZSM-5 framework as an efficient catalyst for selective hydrodeoxygenation of lignin-derived monomers. *Biomass and Bioenergy* **2022**, *157*, 106350.

[79] Shetsiri, S.; Thivasasith, A.; Saenluang, K.; Wannapakdee, W.; Salakhum, S.; Wetchasat, P.; Nokbin, S.; Limtrakul, J.; Wattanakit, C. Sustainable production of ethylene from bioethanol over hierarchical ZSM-5 nanosheets. *Sustainable Energy & Fuels* **2019**, *3* (1), 115-126.

[80] Ayodele, O. B. Influence of oxalate ligand functionalization on Co/ZSM-5 activity in Fischer Tropsch synthesis and hydrodeoxygenation of oleic acid into hydrocarbon fuels. *Sci Rep* **2017**, *7* (1), 10008.

[81] Feng, F.; Wang, L.; Zhang, X.; Wang, Q. Self-Pillared ZSM-5-Supported Ni Nanoparticles as an Efficient Catalyst for Upgrading Oleic Acid to Aviation-Fuel-Range-Alkanes. *Industrial & Engineering Chemistry Research* **2019**, *58* (29), 13112-13121.

[82] Kore, R.; Srivastava, R.; Satpati, B. ZSM-5 Zeolite Nanosheets with Improved Catalytic Activity Synthesized Using a New Class of Structure-Directing Agents. *Chemistry – A European Journal* **2014**, *20* (36), 11511-11521, https://doi.org/10.1002/chem.201402665.

[83] Feng, F.; Niu, X.; Wang, L.; Zhang, X.; Wang, Q. TEOS-modified Ni/ZSM-5 nanosheet catalysts for hydroconversion of oleic acid to high-performance aviation fuel: Effect of acid spatial distribution. *Microporous and Mesoporous Materials* **2020**, *291*, 109705.

[84] Liu, Y.-L.; Huang, X.; Ren, J.; Zhao, X.-Y.; Cao, J.-P. Low-Temperature Reforming of Biomass Tar over Ni/ZSM-5 Catalysts: Unraveling the H2-Rich Gas Production Pathways Using In Situ and Ex Situ Techniques. *Industrial & Engineering Chemistry Research* **2022**, *61* (17), 5734-5746.

[85] Xu, W.; Liu, Z.; Johnston-Peck, A. C.; Senanayake, S. D.; Zhou, G.; Stacchiola, D.; Stach, E. A.; Rodriguez, J. A. Steam Reforming of Ethanol on Ni/CeO2: Reaction Pathway and Interaction between Ni and the CeO2 Support. *ACS Catalysis* **2013**, *3* (5), 975-984.

[86] Zhurka, M. D.; Lemonidou, A. A.; Anderson, J. A.; Kechagiopoulos, P. N. Kinetic analysis of the steam reforming of ethanol over Ni/SiO2 for the elucidation of metal-dominated reaction pathways. *Reaction Chemistry & Engineering* **2018**, *3* (6), 883-897, 10.1039/C8RE00145F.

[87] Atchimarungsri, T.; Gao, X.; Ma, Q.; Zhang, J.; Fan, S.-B.; He, F.; Tian, J.; Reubroycharoen, P.; Zhao, T. Highly Efficient Conversion of Glycerol to Acetaldehyde Over In2O3/HZSM-5 Catalysts. *ACS Sustainable Chemistry & Engineering* **2022**, *10* (34), 11078-11087.

[88] Ismaila, A.; Chen, H.; Fan, X. Nickel encapsulated in silicalite-1 zeolite catalysts for steam reforming of glycerol (SRG) towards renewable hydrogen production. *Fuel Processing Technology* **2022**, *233*, 107306.

[89] Yang, W.; Liu, H.; Li, Y.; Wu, H.; He, D. CO2 reforming of methane to syngas over highly-stable Ni/SBA-15 catalysts prepared by P123-assisted method. *International Journal of Hydrogen Energy* **2016**, *41* (3), 1513-1523.

[90] Bannov, A. G.; Popov, M. V.; Kurmashov, P. B. Thermal analysis of carbon nanomaterials: advantages and problems of interpretation. *Journal of Thermal Analysis and Calorimetry* **2020**, *142* (1), 349-370.

[91] Tian, C.; Zhang, J.; Cao, X.; Liu, Q.; Hu, W. High strength silicon carbide foams and their deformation behavior. *Journal of Materials Science and Technology* **2006**, *22* (2), 269-272, Article.

[92] Duong-Viet, C.; Ba, H.; El-Berrichi, Z.; Nhut, J.-M.; Ledoux, M. J.; Liu, Y.; Pham-Huu, C. Silicon carbide foam as a porous support platform for catalytic applications. *New Journal of Chemistry* **2016**, *40* (5), 4285-4299.

VITA

NAME   Porapak Suriya

DATE OF BIRTH   3 September 1993

PLACE OF BIRTH   Thailand

**INSTITUTIONS
ATTENDED**   M.Sc (2016-2018): Department of Petrochemistry and
                        Polymer Science, Faculty of Science, Chulalongkorn
                        University, Thailand
                        B.Sc (2012-2016): Department of Chemistry, Faculty
                        of Science and Technology, Thammasat University,
                        Thailand

HOME ADDRESS   Angthong, Bangkok